# THÈSE

**En vue de l'obtention du**

# DOCTORAT DE L'UNIVERSITÉ DE TOULOUSE

**Délivré par :**

Institut National Polytechnique de Toulouse (Toulouse INP)

**Discipline ou spécialité :**

Electromagnétisme et Systèmes Haute Fréquence

---

**Présentée et soutenue par :**

M. WENCONG ZHANG

le dimanche 26 mai 2019

**Titre :**

Recherche numérique et expérimentale sur les propriétés de décharge et les caractéristiques de propagation électromagnétique dans les torches à plasma micro-ondes

---

**Ecole doctorale :**

Génie Electrique, Electronique, Télécommunications (GEET)

**Unité de recherche :**

Laboratoire Plasma et Conversion d'Energie ( LAPLACE)

**Directeur(s) de Thèse :**

M. JUNWU TAO

M. KAMA HUANG

**Rapporteurs :**

M. JUNHONG WANG, UNIVERSITE DE BEIJING

Mme ANA LACOSTE, UNIVERSITE GRENOBLE ALPES

**Membre(s) du jury :**

M. SHAOQIU XIAO, UNIV OF ELECTRONIC SC & TECH OF CHINA, Président

M. HAIJING ZHOU, ACADEMIE SCES DE CHINE BEIJING, Membre

M. JUNWU TAO, TOULOUSE INP, Membre

M. KAMA HUANG, SICHUAN UNIVERSITY, Membre

Mme LI WU, SICHUAN UNIVERSITY, Invité


# Research on Gas Discharges and Wave Propagations in Microwave Plasma Torches

**Wencong ZHANG**

**Supervised by Prof. Junwu TAO**

**and Prof. Kama HUANG**

Université fédérale de Toulouse Midi-Pyrénées

INPT-ENSEEIHT-LAPLACE

# Table of contents

**Abstract** ..... **1**

**Résumé** ..... **4**

**Chapter 1 Introduction and objectives** ..... **7**

1.1 Introduction of the microwave plasma torches ..... 7

1.2 Problems in the applications of microwave plasma torches ..... 10

1.3 Objectives of this dissertation ..... 12

1.4 Organization of this dissertation ..... 12

**Chapter 2 Electromagnetic modes of the travelling wave in the waveguide-based MPTs with metallic enclosure** ..... **14**

2.1 Introduction of the travelling wave in the MPT ..... 14

2.2 Waveguide structure change of the metal-enclosed discharge tube with plasma column ..... 17

2.2.1 Electromagnetic properties of a plasma ..... 17

2.2.2 Microwave penetration depth (skin depth) of a plasma ..... 18

2.2.3 Formation of a two-conductor-like coaxial waveguide structure of the discharge tube ..... 19

2.3 Electromagnetic propagating modes of the plasma travelling wave ..... 22

2.3.1 Conditions for the existence of the TEM propagating mode and other higher-order propagating modes ..... 22

2.3.2 Effects of the energy-input ways on the electromagnetic propagating modes of the travelling wave ..... 24

2.4 Full-wave numerical validation ..... 25

2.4.1 Implementation of the numerical calculation ..... 25

2.4.2 Propagating TEM mode ..... 26

2.4.3 Hybrid propagating TEM and TE11 modes ..... 28

2.4.4 Suppression of TE11 mode in the two-port MPT ..... 30

2.4 Conclusions ..... 31

**Chapter 3 Role of the glass tube in improving the power coupling efficiency of a waveguide-based MPT** ..... **33**

3.1 Background and hypothesis of the “waveguide-to-coaxial mode adaptor” ..... 33

3.2 Experiment design ..... 34

3.2.1 Experiment system ..... 34

3.2.2 Experiment procedure ..... 36
3.3 Results and analysis ..... 37
3.3.1 Effects of the glass tube on improving the power coupling efficiency ..... 37
3.3.2 Mechanism of the efficiency-improving method ..... 38
3.4 Dependence of the efficiency-improving method on operation conditions ..... 39
3.4.1 Different input microwave powers ..... 39
3.4.2 Different pressures ..... 41
3.5 Conclusion ..... 43
**Chapter 4 Two-dimensional axisymmetric fluid model of the argon plasma in MPTs under atmospheric pressure ..... 45**
4.1 A brief Introduction of the plasma modelling methods ..... 45
4.2 Simplification of the calculation domain ..... 46
4.2.1 Geometrical model and calculation domain ..... 46
4.2.2 Validity and limitation of the two-dimensional axisymmetric simplification 47
4.3 Two-fluid model of the microwave argon plasma under atmospheric pressure with ambipolar diffusion approximation ..... 49
4.3.1 Chemical reactions of the atmospheric argon plasma ..... 49
4.3.2 Microwave field - Helmholtz equation ..... 51
4.3.3 Number densities of different species - Continuity equations based on the mass conservation law ..... 52
4.3.4 Temperatures of electrons and heavy species mixture - Heat transfer equation based on the energy conservation law ..... 52
4.3.5 Gas flow - Navier-Stockes equations based on mass and momentum conservation laws ..... 54
4.3.6 Ambipolar diffusion approximation based on the electric neutrality. ..... 54
4.3.7 Transport properties of each species ..... 57
4.3.8 Boundary conditions ..... 57
4.4 Numerical implementation and calculation procedure ..... 59
4.4.1 Numerical implementation ..... 59
4.4.2 Calculation procedure ..... 59
4.5 Conclusion ..... 60
**Chapter 5 Wave propagation and discharge maintenance in a MPT under different operation conditions ..... 61**
5.1 Background ..... 61

5.2 Mechanism of plasma column extension and discharge maintenance..... 62

5.2.1 Numerical modelling of the plasma column extension with the increase of microwave power..... 63

5.2.2 Formation of the two-conductor-like waveguide structure..... 64

5.2.3 Wave dissipation and discharge maintenance..... 68

5.3 Mechanism of plasma column shortening and glass overheating..... 71

5.3.1 Numerical modelling of the plasma column shortening with the increase of gas inflow rate ..... 71

5.3.2 Wave propagation with the increase of gas inflow rate..... 72

5.3.3 Glass overheating problem ..... 75

5.4 Conclusion..... 78

**Chapter 6 Three-dimensional fluid modelling based on plane-symmetric simplification ..... 80**

6.1 Mathematical model ..... 80

6.1.1 Geometrical model and computation domain..... 80

6.1.2 Governing equations and boundary conditions..... 81

6.1.3 Implementation of the numerical calculations..... 83

6.2 Results and discussion..... 83

6.2.1 Non-axisymmetric discharge properties and wave propagation in the one-port MPT ..... 83

6.2.2 Axisymmetric discharge properties and wave propagation in the one-port MPT ..... 86

6.2.3 Discharge properties and wave propagation in the two-port MPT with microwave excitations from both ports..... 89

6.2.4 Comparison of the results from two-dimensional axisymmetric modelling and three-dimensional plane-symmetric calculation ..... 91

6.3 Conclusions ..... 96

**Chapter 7 Conclusions and future works..... 97**

7.1 Conclusions ..... 97

7.2 Future works..... 100

**Reference..... 102**

**List of publications..... 109**

**Acknowledgements..... 110**

**Vingtaine page de résumé français ..... 112**

# Abstract

Over the past several decades, the microwave plasma torch becomes increasingly popular as one of the plasma sources, because of their advantages of simple structure, high flexibility in different working environment and electrodeless working ability. It has been demonstrated to have great potential in both scientific researches and industrial applications. However, microwave discharges in the plasma torches involve microwave propagation, reflection and dissipation in different situations, complex energy exchange and transfer, dynamic excitation, ionization and recombination reactions, transport of massive particles and different types of gas flow. There are still some phenomena and problems in the microwave plasma torches that remain unclear or unsolved, for example, the mechanism of the discharge maintenance, the changes of wave propagation characteristics and discharge properties in different operational conditions. Besides, it is lack of a fast, efficient and accurate mathematical model to describe the discharges in the microwave plasma torches in different circumstances.

This thesis aims to better understand the discharges in the microwave plasma torches. More specifically, it is to investigate the microwave propagation characteristics and the discharge properties in the microwave plasma torches based on rectangular waveguide under different operational conditions.

To achieve this goal, we have firstly investigated the waveguide structure change of the cylindrical discharge tube shielded by a metallic enclosure in the microwave plasma torches, when the discharge occurs. The electromagnetic mode of the microwave in the discharge tube and their existence conditions have been theoretically studied and numerically validated by the full-wave analysis, with the assumption of constant plasma properties.

Secondly, based on our assumption that the microwave plasma torch will become a waveguide-coaxial mode adapter when the discharge occurs in some situations. Experiments are carried out to investigate the effects of the glass tube on the efficiency of power coupling from the input microwave to the discharge in a microwave plasma torch under different input powers, pressures and gas inflow rates. It aims to explore the possibility to improve the microwave coupling efficiency by simply choosing a proper glass tube without using any external tuning measures.

Thirdly, a two-dimensional fluid model is proposed to simulate the argon discharges in the microwave plasma torch under atmospheric pressure, which makes use of the ambipolar diffusion approximation and an axisymmetric simplification of the calculation domain of the discharge tube. With this model, we have numerically investigated the mechanism of the plasma column length change under different microwave powers and gas inflow rates, the mechanism of the glass tube overheating problem, the discharge properties and the microwave propagation characteristics.

Finally, a three-dimensional model based on the previous two-dimensional model is further proposed to investigate the discharges in the microwave plasma torches. With this model, we have modelled the argon discharges under atmospheric pressure in two types of microwave plasma torches with different glass tubes. Besides, we have compared the results from both the two-dimensional simulation and the three-dimensional modelling.

In these above works, we have found that the discharge tube with metallic enclosure in the microwave plasma torches is able to become a two-conductor-like coaxial waveguide, when the discharge properties meet some requirements. With this waveguide structure transition, the cylindrical discharge tube allows the input microwave to enter the discharge tube and propagate along the plasma column towards both ends of the glass tube without the limitation of cut-off frequency.

Furthermore, it has been proved that the microwave in the discharge tube is able to propagate in TEM mode. The well-known $m = 0$ mode is not always a TM mode and it can be the TEM mode as well. The wall thickness and dielectric property of the glass tube are able to affect the electromagnetic mode of the microwave in the discharge tube and the microwave power coupling efficiency of the plasma torch. A power coupling efficiency around 90% can be achieved by simply choosing a proper glass tube with its wall thickness in particular range.

Numerical and experimental results in this thesis demonstrated that the argon plasma column under atmospheric pressure can act as another conductor besides the metallic enclosure, changing the discharge tube to a two-conductor like coaxial waveguide. The plasma column length extension with the increase of the microwave power is actually driven by the travelling microwave in the discharge tube. The length of the plasma column is determined by the propagation distance. Apart from the particle loss

introduced by the increasingly strong gas flow convection, the shortening of plasma column length with an increase in the gas inflow rate is reinforced by the consequent decrease of the surface wave propagation distance. Regarding the glass overheating problem, it is found that the increasing the gas inflow rate can not solve the glass overheating problem for the microwave plasma torch operated with only axial gas flow, because of the shielding capability of the plasma column. In our numerical simulations, it is found that the two-dimensional axisymmetric simplification of the calculation domain of the discharge tube is valid, when the microwave in the discharge tube of the microwave plasma torch propagates in azimuthally symmetric TEM mode.

These conclusions may help to better understand the discharge properties and microwave propagation characteristics in the microwave plasma torches. It also may contribute to the optimization of current microwave plasma torches or the design of new types of microwave plasma torches.

**Key words**: Microwave plasma torch, gas discharge, argon plasma, numerical modelling, fluid model, gas flow, discharge maintenance.

# Résumé

Au cours des dernières décennies, la torche de plasma à micro-ondes devient de plus en plus populaire comme l'une des sources des plasmas, en raison de leurs avantages de la structure simple, une grande flexibilité dans un environnement de travail différent et la capacité de travail sans électrode. Il a été démontré qu'il avait un grand potentiel dans les recherches scientifiques et les applications industrielles. Cependant, les décharges de micro-ondes dans les torches de plasma impliquent la propagation, la réflexion et la dissipation de micro-ondes dans différentes situations, l'échange et le transfert d'énergie complexes, l'excitation dynamique, l'ionisation et les réactions de recombinaison, le transport des particules et différents types de flux de gaz. Il y a encore des phénomènes et des problèmes dans les torches à plasma micro-ondes qui restent flous ou non résolus, par exemple, le mécanisme de l'entretien des décharges, les changements des caractéristiques de propagation des ondes et les propriétés de décharge dans différents conditions opérationnelles. En outre, il est l'absence d'un modèle mathématique rapide, efficace et précis pour décrire les décharges dans les torches de plasma micro-ondes dans différentes circonstances.

Cette thèse vise à mieux comprendre les décharges dans les torches de plasma à micro-ondes. Plus précisément, il s'agit d'étudier les caractéristiques de propagation des micro-ondes et les propriétés de décharge dans les torches de plasma à micro-ondes basées sur le guide rectangulaire des ondes dans différentes conditions opérationnelles.

Pour atteindre cet objectif, nous avons d'abord étudié le changement de structure du guide d'ondes du tube de décharge cylindrique protégé par un boîtier métallique dans les torches de plasma à micro-ondes, lorsque la décharge se produit. Le mode électromagnétique du micro-ondes dans le tube de décharge et leurs conditions d'existence ont été théoriquement étudiés et validés numériquement par l'analyse des ondes complètes, avec l'hypothèse de propriétés plasmatiques constantes.

Deuxièmement, sur la base de notre hypothèse que la torche de plasma à micro-ondes deviendra un adaptateur de mode lorsque la décharge se produit dans certaines situations. Des expériences sont menées pour étudier les effets du tube de quartz sur l'efficacité du couplage de puissance du micro-ondes à la décharge dans une torche de plasma à micro-ondes sous différents pouvoirs d'entrée, pressions et taux d'entrée de

gaz. Il vise à explorer la possibilité d'améliorer l'efficacité de couplage micro-ondes en choisissant simplement un tube en verre approprié sans utiliser de mesures de tuning externe.

Troisièmement, un modèle de fluide bidimensionnel est proposé pour simuler les décharges d'argon dans la torche à micro-ondes sous pression atmosphérique, ce qui utilise l'approximation de diffusion et une simplification axisymétrique du domaine de calcul du tube de décharge. Avec ce modèle, nous avons examiné numériquement le mécanisme du changement de longueur de colonne de plasma sous différents pouvoirs de micro-ondes et taux d'entrée de gaz, le mécanisme du problème de surchauffe de tube de verre, les propriétés de décharge et la propagation de micro-ondes caractéristiques.

Enfin, un modèle tridimensionnel basé sur le modèle bidimensionnel précédent est également proposé pour étudier les décharges dans les torches de plasma à micro-ondes. Avec ce modèle, nous avons modélisé les décharges d'argon sous pression atmosphérique dans deux types de torches de plasma à micro-ondes avec différents tubes de quartz. En outre, nous avons comparé les résultats de la simulation bidimensionnelle et de la modélisation tridimensionnelle.

Dans ces travaux ci-dessus, nous avons constaté que le tube de décharge avec boîtier métallique dans les torches de plasma à micro-ondes est capable de devenir un guide d'onde coaxial à deux conducteurs, lorsque les propriétés de décharge répondent à certaines exigences. Avec cette transition de structure de guide d'onde, le tube cylindrique de décharge permet au micro-onde d'entrée d'entrer dans le tube de décharge et de se propager le long de la colonne de plasma vers les deux extrémités du tube de quartz sans la limitation de la fréquence de coupure.

En outre, il a été prouvé que le micro-ondes dans le tube de décharge est capable de se propager en mode TEM. Le mode $m = 0$ bien connu n'est pas toujours un mode TM et il peut être le mode TEM ainsi. L'épaisseur du mur et la propriété diélectrique du tube de verre sont en mesure d'affecter le mode électromagnétique du micro-ondes dans le tube de décharge et l'efficacité de couplage de puissance micro-ondes de la torche de plasma. Une efficacité de couplage de puissance autour de 90% peut être réalisée en choisissant simplement un tube en verre approprié avec son épaisseur de mur dans la gamme particulière.

Les résultats numériques et expérimentaux dans cette thèse ont démontré que la colonne de plasma d'argon sous pression atmosphérique peut agir comme un autre conducteur en plus de l'enceinte métallique, changeant le tube de décharge en un guide d'onde coaxial à deux conducteurs. L'extension de longueur de colonne de plasma avec l'augmentation de la puissance de micro-ondes est réellement entraînée par le micro-ondes de déplacement dans le tube de décharge. La longueur de la colonne de plasma est déterminée par la distance de propagation de micro-ondes. Outre la perte de particules introduite par la convection de flux de gaz de plus en plus forte, le raccourcissement de la longueur de la colonne de plasma avec une augmentation du taux d'entrée de gaz est renforcé par la diminution conséquente de la distance de propagation de micro-ondes. En ce qui concerne le problème de surchauffe du verre, il est constaté que l'augmentation du taux d'entrée de gaz ne peut pas résoudre le problème de surchauffe du verre pour la torche de plasma à micro-ondes fonctionné avec seulement le flux de gaz axial, en raison de la capacité de blindage de micro-ondes de la colonne de plasma. Dans nos simulations numériques, il est constaté que la simplification axisymmétrique bidimensionnelle du domaine de calcul du tube de décharge est valide, lorsque le micro-ondes dans le tube de décharge se propage dans tem azimuthally symétrique mode.

Ces conclusions peuvent aider à mieux comprendre les propriétés de décharge et les caractéristiques de propagation des micro-ondes dans les torches de plasma à micro-ondes. Il peut également contribuer à l'optimisation des torches actuelles de plasma à micro-ondes ou à la conception de nouveaux types de torches à plasma micro-ondes.

**Mots-clés**: Torche de plasma à micro-ondes, Décharge de gaz, Plasma d'argon, Modélisation numérique, Modèle fluide, Flux de gaz.

# Chapter 1 Introduction and objectives

## 1.1 Introduction of the microwave plasma torches

Plasma, known as the fourth state of matter, is defined as a quasi-neutral particle mixture containing many charged and neutral particles (electrons, ions and neutral atoms or molecules), which exhibits collective behaviours [1]. In fact, most of the matters (99%) in universe are plasmas [2], for example, the stars, solar corona, ionosphere of earth, and so on. In addition to these natural plasmas, they can be found in our daily life directly or indirectly, such as in lighting devices and in semiconductors manufacturing. Although plasmas can be produced in a variety of ways, electric discharge is the most common approach in laboratory, which can be generally induced by direct current, alternating current, laser or electromagnetic waves in radio frequency and microwave frequency ranges.

Microwave plasma torches (MPTs) are one of the most popular plasma sources [3], which have simple structures, inexpensive domestic magnetron sources [4], electrodeless working ability [5] and high flexibility in different working environments (different operating pressures [6, 7] and numerous types of working gases [8, 9, 10]).

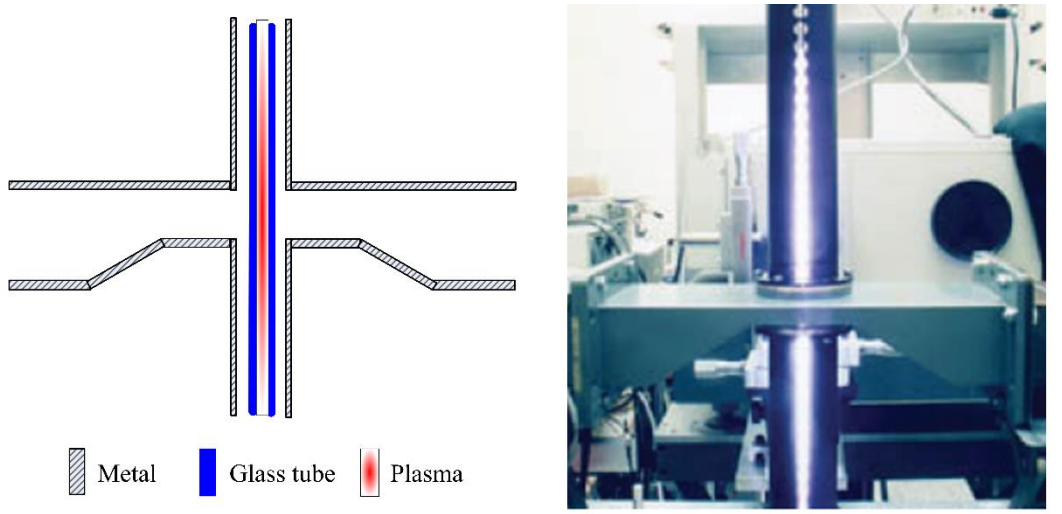


(a) Schematic of the surfaguide plasma torch (b) Photo of the surfaguide plasma torch

**Figure 1.1** Surfaguide microwave plasma torch.

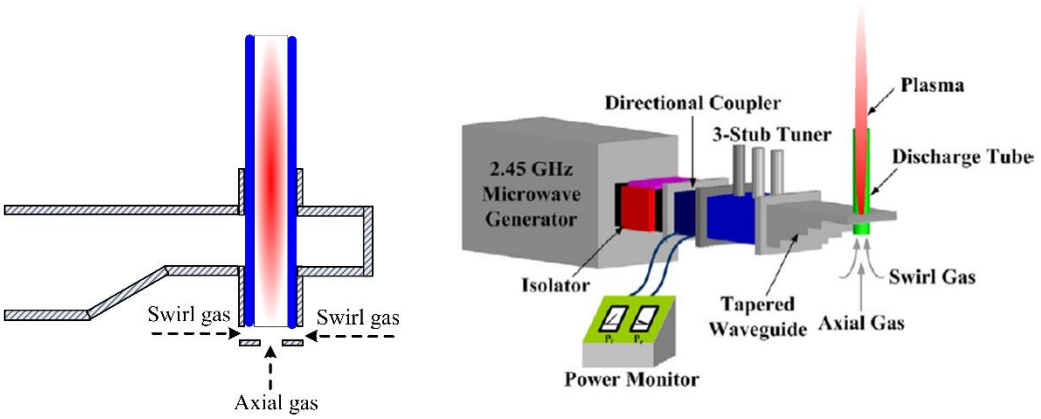


**Figure 1.2** Uhm-type microwave plasma torch.

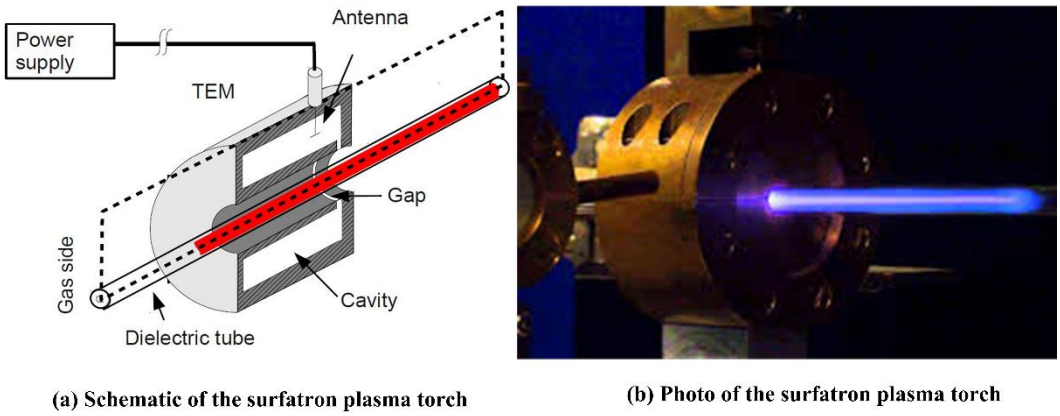


**(a) Schematic of the surfatron plasma torch** **(b) Photo of the surfatron plasma torch**

**Figure 1.3** Surfatron microwave plasma torch.

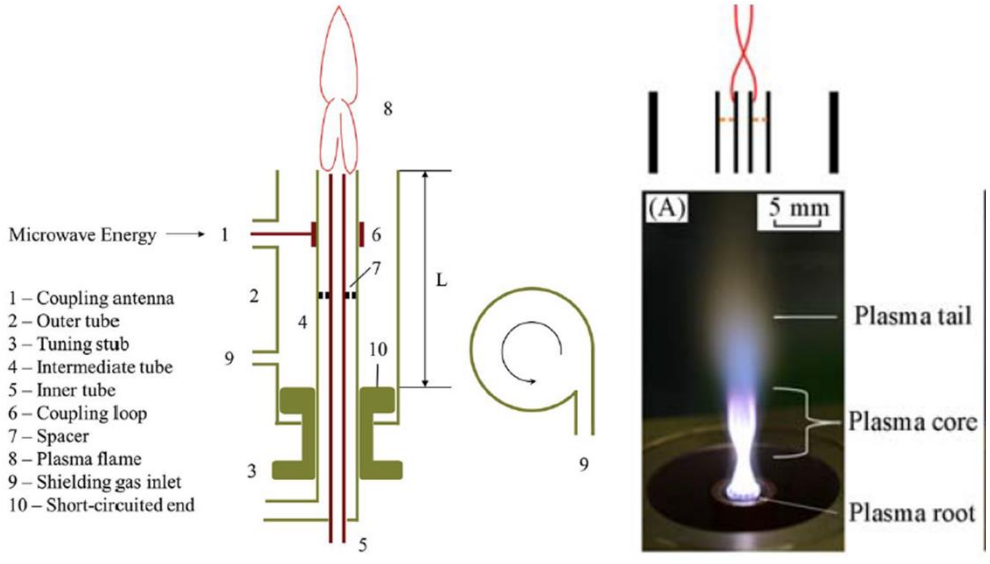


**(a) Schematic of the coaxial plasma torch** **(b) Discharge in the coaxial plasma torch**

**Figure 1.4** Coaxial microwave plasma torch.

Over the past several decades, numerous kinds of microwave plasma torches have been developed for different purposes, to name a few typical ones, the classic

surfaguide plasma source based on rectangular waveguide [11], the Uhm-type plasma torch [12], the surfatron plasma source [13] and the coaxial plasma torch [14]. The above figures (Figure 1.1-1.4) show the structures of these typical microwave plasma torches.

The surfatron and surfaguide microwave plasma torches, shown in Figure 1.1 and Figure 1.3, were developed by M. Moisan in 1975 and 1984 respectively. For these two types of microwave plasma torches, the discharges occur within the glass tube and are sustained by the travelling electromagnetic wave propagating along the plasma column. The Uhm-type microwave plasma torch was proposed by H. S. Uhm, which is similar to the surfaguide plasma source but has a much simpler structure. The coaxial microwave plasma torch was proposed for the spectroscopy research by Q. H. Jin in about 1991, in which the discharge is exposed in air and has a jet-like plasma shape. Limited by the power capacity of the coaxial cable that connects the microwave source to the plasma torch, the surfatron and coaxial plasma torches are generally operated with an input microwave power lower than 1 kW [15, 16]. However, the rectangular-waveguide-based plasma torches are able to work with an input microwave power up to 6 kW [16]. Except the coaxial plasma torch in Figure 1.4, the other microwave plasma torches are capable to sustain the discharges both in low pressures and atmospheric pressure. Due to their high flexibility in different pressures and high-power capacity, the waveguide-based surfaguide and Uhm-type MPTs are much more popular in industrial applications.

Currently, the MPTs have been demonstrated to have great potential in both scientific researches and industrial applications. In material processing, the MPTs can be used in cutting, welding, quartz/ceramic processing [6], diamond synthesis [ 17 ], oxide nanoparticle synthesis [18], nitrogen oxide formation [19] and surface nitriding [20]. In environmental protection, the MPTs can be applied in decontamination of chemical and biological warfare agents [21] and abatement of perfluorinated compounds [22] by decomposing the macromolecules. Regarding the solid waste processing, the MPT can be applied to gasify the biomass waste transforming it into syngas and generating energy [23]. Besides, researchers have successfully applied the waveguide-based MPTs to carbon dioxide elimination and producing valuable syngas at the same time [24, 25, 26, 27]. In energy conversion area, MPT has been proved to be an efficient device in hydrogen production [9, 28, 29, 30, 31, 32, 33] from methane or alcohol reforming.

Another important application of MPT is the lamp for spectroscopy research [14]. Actually, a lot of related publications can be easily found about the optical emission spectroscopy and the detection of different objects [34, 35]. All these applications demonstrate that MPT is a plasma source that is efficient, economical, electrodeless, simple in form and easy to operate [36, 37].

## 1.2 Problems in the applications of microwave plasma torches

Due to the popularity of MPTs, they have been extensively studied both theoretically and experimentally, resulting in numerous publications. However, some problems in the applications of the MPTs still remain unsolved, which are listed as follows:

(1) Wave propagation and discharge maintenance mechanism in MPTs are unclear

Before the discharge occurs, it is easy to figure out how the microwave propagates in the plasma torch either by numerical simulation or theoretical analysis. However, after the discharge is successfully triggered, the high densities of charged electrons and ions are able to shield the microwave from penetrating the plasma, resulting a high power reflection. In this case, how the discharge is maintained and how the input microwave propagates in the MPT become considerably complicated and remain unclear in some MPTs.

(2) Low power coupling efficiency

In industrial applications, a high power coupling efficiency, which indicates the efficiency of power transferring from the input microwave to the discharge**,** is a general requirement for all kinds of MPTs. However, when the gas discharge occurs, the microwave shielding capability of plasma prevents the input microwave from being absorbed and causes power reflection, resulted in energy waste and low power coupling efficiency. Actually, from the birth of MPTs, maximizing the power coupling efficiency is always one of the main tasks in their development history.

(3) Unstable discharge under high gas inflow rates

Large-scale industrial applications of MPTs generally require a high gas disposal rate. However, it was observed in experiments that the discharge in a

rectangular-waveguide-based MPT became unstable with an increase in the gas inflow rate, and even became extinct when the gas inflow rate was sufficiently high [23]. The instability of the discharges in the MPT under high gas inflow rates greatly limits its industrial applications.

(4) Glass tube overheating problem under high input microwave powers

Unlike the surfatron and the coaxial MPTs whose power capacities are limited by the small power capacity of the coaxial cable, the power capacity limitations of the waveguide-based MPTs are mainly due to the glass overheating problem under high input microwave powers. For example, the temperature of the argon plasma column under atmospheric pressure can be higher than 4000 K under an input microwave power of 1 KW [7]. However, the melting point of the quartz glass tube is generally around 2000 K. Therefore, the glass tube cooling is one of the main concerns for the MPTs with glass tube to confine the discharges [15, 37].

(5) Difficulties in multi-dimensional numerical modelling of MPTs

Microwave plasma involves numerous reactions, motions of massive particles and strongly nonlinear interactions between microwave and plasma, resulting in great difficulty in the numerical modelling of MPTs especially in multiple dimensions. To be specific, the mathematical model describing the discharges in MPTs involves a large and strongly nonlinear equation system to model microwave propagation, transport of different species, energy and momentum conservations. The high nonlinearity of the equation system will limit the iteration steps in solving the equations. Moreover, because of the large gradients of the particle number densities in plasma, modeling the MPT in two or three dimensions requires a dense mesh structure with a considerably large number of mesh cells, resulted in a huge matrix. Therefore, multi-dimensional modelling of the MPT is extremely time-consuming and demands a large amount of calculation resources. In fact, limited numerical studies have been conducted to investigate the MPT in two or three dimensions up to now.

## 1.3 Objectives of this dissertation

The problems above require further studies on the MPTs both theoretically and experimentally. Therefore, the aim of this dissertation is to better understand the microwave plasmas in the MPTs under different conditions. Specifically, the objectives of this dissertation are to:

A. Investigate electromagnetic modes of the travelling wave that propagates along the plasma column in waveguide-based MPTs with a cylindrical metal wall that encloses the glass tube and discharge.

B. Figure out the effects of the glass tube on the power coupling efficiency of a waveguide-based MPT. Explore the possibility of improving the power coupling efficiency without using external tuning measures like the movable short-circuited ending plunger or the three-stub tuner.

C. Propose a two-dimensional and a three-dimensional multi-physics model to characterize the discharges in MPTs under atmospheric pressure.

D. Investigate the discharge properties and the wave propagation in MPTs under different microwave powers, gas inflow rates, and energy-input ways with our proposed mathematical models.

## 1.4 Organization of this dissertation

This dissertation is organized as follows:

Chapter 1: Briefly introduce the background of MPTs including their typical types, applications and unsolved problems. Present the objectives and organization of this dissertation.

Chapter 2: Theoretically deduce the analytic expression of the skin depth of a collisional plasma under microwave radiations. Investigate the electromagnetic modes of the travelling wave in the discharge tube and their existence conditions.

Chapter 3: Experimentally investigate the effects of the glass tube on the power coupling efficiency of a waveguide-based MPT under different pressures, input powers and gas inflow rates. Explore the possibility of improving the power coupling efficiency by simply choosing a proper glass tube.

Chapter 4: Propose a two-dimensional plasma fluid model to simulate the atmospheric discharges in waveguide-based MPTs with a metallic shielding wall.

Chapter 5: Investigate wave propagation and discharge charaterisitcs in MPTs with the proposed model in two dimensions under different microwave powers and gas inflow rates.

Chapter 6: Propose a three-dimensional fluid model to characterize the discharges in MPTs based on the two-dimensional model in Chapter 4. Investigate the influence of energy-input ways on the microwave propagation and discharge properties with the proposed three-dimensional model. Compare the results from two-dimensional and three-dimensional models.

Chapter 7: Conclude this dissertation and list the main contributions and prospective works.

# Chapter 2 Electromagnetic modes of the travelling wave in the waveguide-based MPTs with metallic enclosure

## 2.1 Introduction of the travelling wave in the MPT

The fact that electromagnetic wave can propagate along a cylindrical plasma column or a beam excited by other means was recognized in a very early time [38, 39]. After several decades, researchers started to realize that the travelling electromagnetic wave can be used for the generation of plasma as well. The first travelling-wave-sustained discharge was identified by Tuma in 1970. In the following decade, a large number of publications emerged which are related to the design of the travelling-wave plasma setups. Among them, the surfaguide, the surfatron and the one-port MPTs are the most popular and typical ones [11, 13, 24]. In these MPTs, the discharges occur in a glass tube and are sustained by the travelling electromagnetic wave that propagates along the plasma column. Therefore, the wave propagation characteristics of the travelling wave (attenuation, dispersion, wave number, electromagnetic modes and so on) become of great importance to the discharge maintenance and stability.

For the electromagnetic modes of the travelling wave particularly, Moisan and his cooperators [40, 41, 37], Benova and Zhelyazkov [42,43,44,45], Sola [46], Ferreira [47], Kortshagen [48] and Li [49], to name just a few, contributed a lot in setting up a systematic theory to describe them. According to the theory, the electromagnetic mode of the travelling wave is characterized by the azimuthal wavenumber *m*, which comes from the azimuthal electric field term $e^{jm\varphi}$ ($\varphi$ is the azimuthal angle when using the cylindrical coordinate). For example, the $m = 0$ mode indicates a mode whose electric field is azimuthally symmetric. It is clearly pointed out that the $m = 0$ mode is a pure transverse magnetic (TM) wave [41, 37, 46, 50] and it is the lowest mode of the travelling wave [41]. The field components of each mode are obtained by solving Maxwell's equations, under an assumption of the existence of either $\overline{E_z}$ or $\overline{H_z}$ (z-axis is chosen as the wave propagation direction). Detailed derivations can be found in

references [40, 37, 42-49]. On the experimental research aspect, Moisan's research group [50] experimentally investigated the conditions of the $m = 0$ and $m = 1$ modes of the travelling wave, with respect to different discharge tube diameters.

In a certain number of published works, the plasma column bounded by the glass tube is enclosed with a cylindrical metallic wall with an initial purpose of preventing the electromagnetic wave from radiating to the free space. However, the metallic enclosure plays a much more important role in the propagation of the travelling wave and the discharge properties, besides the well-known electromagnetic shielding function. For example, it helps to enhance the plasma column length, which has been already observed in experiments [37]. In the above mentioned researches, most of them were carried out without presence of the metallic enclosure [40, 45, 47, 49, 50] or without consideration of the metallic enclosure's influence [42, 44, 46]. Benova and Zhelyazkov noticed the influence of the metallic enclosure on the wave propagation characteristics and the plasma column [44, 42]. In their studies, the Maxwell's equations were solved and the electromagnetic field of the azimuthally symmetric mode ($m = 0$ mode) was obtained with an assumption that the electric field of the travelling wave has a component $\overline{E_z}$ in its wave propagation direction. The same theoretical derivation method can be found in other studies [48] in the same case with the presence of the metallic enclosure.

In our work [51], it is found that the argon plasma column under atmospheric pressure is able to shield the input microwave from penetrating itself and behaves like a metal conductor. Combined with another conductor the metallic enclosure, the discharge tube turned to be a two-conductor-like coaxial waveguide. For a two-conductor waveguide, its first-order mode is the TEM mode, which has neither the electric component nor the magnetic component in the wave propagation direction ($\overline{E_z} = 0$ and $\overline{H_z} = 0$). It is reasonable to infer that the travelling wave is able to propagate in TEM mode, when the discharge tube with metallic enclosure becomes a two-conductor-like coaxial waveguide. If so, the field components of the travelling wave in this case can not be obtained by solving Maxwell's equations with $\overline{E_z}$ or $\overline{H_z}$ as the researches above, because $\overline{E_z} = 0$ and $\overline{H_z} = 0$ for TEM mode. Furthermore, it will indicate the $m = 0$ mode is not always a TM mode in any cases and it can be the TEM mode as well.

Except the commonly used azimuthally symmetric mode ($m = 0$ mode), different applications require other higher-order modes, such as the $m = 1$ mode sustained plasma [50, 52, 37] and the electron density determination [53]. For the higher-order propagating modes, previous studies have revealed that the glass tube has a great influence on the propagating modes of the travelling wave and the discharge maintenance [45, 50]. However, these researches were done for the case that the discharge tube was exposed to air. Therefore, it is significant to investigate the conditions for the excitation of higher-order propagating modes considering the effects of the glass tube particularly for the case with presence of the metallic enclosure.

In this chapter, two waveguide-based MPTs, with metallic enclosure bounding the glass tube and discharge, are taken as examples to investigate the electromagnetic modes of the travelling wave, propagating along the plasma column and sustaining the discharge.

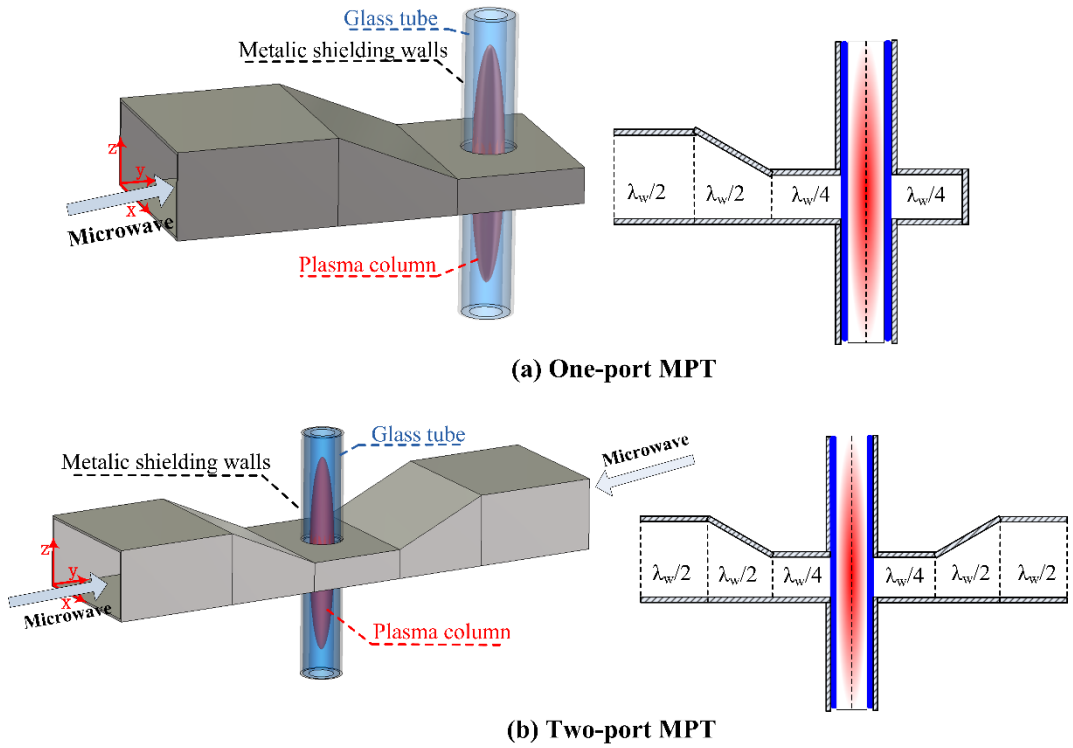


**Figure 2.1** The waveguide-based one-port and two-port MPTs with metallic enclosure to bound the glass tube and discharge.

Figure 2.1 shows the schematics of the two MPTs, which are similar to the surfaguide and the Uhm-type MPTs. Compared the Uhm-type MPT, the two MPTs in Figure 2.1 have a cylindrical metal wall bonding the glass tube and the discharge. Besides, it is worth noting that there is no air gap between the metal wall and the outer wall of the

glass tube, which is different from the surfaguide MPT. These two MPTs are based on the standard rectangular waveguide WR430 and work at the microwave frequency of 2.45 GHz. The metal cylindrical enclosures in both MPTs in Figure 2.1 have an inner diameter of 30 mm.

This chapter begins with the electromagnetic properties of the collisional plasma and its microwave penetration depth. Secondly, it discusses the waveguide structure change of the discharge tube. A much stricter criterion is proposed to determine the formation of the two-conductor-like waveguide structure of the discharge tube. Thirdly, existence conditions of the TEM propagating mode and other higher-order propagating modes are investigated, when the discharge tube becomes a two-conductor-like coaxial waveguide. Fourthly, effects of the energy-input ways are theoretically analysed. Finally, relevant full-wave numerical calculations are carried out to validate the theoretical analysis above.

## 2.2 Waveguide structure change of the metal-enclosed discharge tube with plasma column

### 2.2.1 Electromagnetic properties of a plasma

A collisional plasma can be regarded as either a conductor with the electric conductivity $\sigma_p$ given in equation (2.1), or equivalently, a dielectric with the relative permittivity of $\varepsilon_{rp}$ given in equation (2.2) [54].

$$\sigma_p = \frac{\varepsilon_0 \omega_p^2}{\nu_m + j\omega} = \frac{\varepsilon_0 \omega_p^2 \nu_m}{\nu_m{}^2 + \omega^2} - j\frac{\varepsilon_0 \omega_p^2 \omega}{\nu_m{}^2 + \omega^2} \tag{2.1}$$

$$\varepsilon_{rp} = 1 - j\frac{\sigma_p}{\omega\varepsilon_0} = 1 - \frac{\omega_p{}^2}{\omega^2 + \nu_m{}^2} - j\frac{\omega_p{}^2 \nu_m}{\omega\left(\omega^2 + \nu_m{}^2\right)} \tag{2.2}$$

With:

$\nu_m$ the electron elastic collision frequency with the neutral particles

$\varepsilon_0 = 8.854 \times 10^{-12}$ farad $\cdot\, m^{-1}$ the permittivity of free space

$\omega$ the angular frequency of the input microwave

$\omega_p$ the plasma frequency

$$\omega_p = \sqrt{\frac{n_e q^2}{m_e \varepsilon_0}} \tag{2.3}$$

where $n_e$ is the electron number density. $m_e$ and $q$ are respectively the elementary mass weight and electric charge of the electron.

### 2.2.2 Microwave penetration depth (skin depth) of a plasma

In electromagnetic theory, the microwave shielding capability of a plasma can be characterized by its skin depth. It is defined as the distance from its surface through which the amplitude of the electromagnetic wave is reduced by a factor of $1/e$ (about 37%). Below gives the derivation of the plasma skin depth equation. Assuming an electromagnetic wave with an arbitrary frequency propagates inside a plasma medium, its wave fields can be characterized by the Maxwell's equations as follows:

$$\nabla \times \vec{H} = \vec{J} + j\omega\vec{D} \tag{2.4}$$

$$\nabla \times \vec{E} = -j\omega\mu_0\vec{H} \tag{2.5}$$

where $\vec{E}$ and $\vec{H}$ are electric and magnetic fields respectively. $\vec{J}$ is the electric current density corresponding to the conductive current in conductor. $\vec{D}$ is the electric flux density indicating the displacement current. $\mu_0 = 4\pi \times 10^{-7}\ \mathrm{H} \cdot m^{-1}$ is the magnetic permeability of free space. If the plasma is regarded as a conductor, equation (2.4) can be reduced to:

$$\nabla \times \vec{H} = \sigma_p \vec{E} \tag{2.6}$$

Taking the rotation of equation (2.5), the following equation can be obtained.

$$\nabla \times \nabla \times \vec{E} = \nabla\left(\nabla \bullet \vec{E}\right) - \nabla^2\vec{E} = -j\omega\mu_0 \nabla \times \vec{H} \tag{2.7}$$

Substituting equation (2.6) into equation (2.7), the Helmholtz equation in the plasma medium can be given as follows:

$$\nabla^2\vec{E} = j\omega\mu_0\sigma_p\vec{E} \tag{2.8}$$

Assuming $\gamma^2 = (\alpha + j\beta)^2 = j\omega\mu_0\sigma_p$, $\gamma$ is the wave propagation constant (or wave number) of the electromagnetic wave in a plasma, $\alpha$ is the attenuation constant and $\beta$ is the phase constant. The plasma skin depth $\delta_p$ can be obtained with the following equation [55]:

$$\delta_p = \frac{1}{\alpha} = \frac{1}{\mathrm{Re}\sqrt{j\omega\mu_0\sigma_p}} \tag{2.9}$$

Re indicates the real part of a complex number. The formula (2.9) can be rewritten as follows by substituting relevant parameters into it [56, 57].

$$\delta_p = \frac{c}{\omega_p \cos(\theta)}\left(1+\frac{\nu_m{}^2}{\omega^2}\right)^{\frac{1}{4}} \tag{2.10}$$

where $\theta = 0.5\arctan(\nu_m/\omega)$. If the plasma is treated equivalently as a dielectric with the relative permittivity as shown in equation (2.2), the same results of $\delta_p$ can be obtained in a similar way [58]. It is worth noting that the plasma skin depth is only determined by its electromagnetic property and the frequency of electromagnetic wave.

### 2.2.3 Formation of a two-conductor-like coaxial waveguide structure of the discharge tube

TEM mode can only exist in a waveguide structure with two or more conductors. Structures with only one conductor, such as the circular waveguide and rectangular waveguide, are not able to support propagating TEM mode [55]. Therefore, it is of significance to discuss the conditions in which the discharge tube with metallic enclosure forms a two-conductor-like waveguide structure. Equivalently, it is to discuss when the plasma column can be regarded as a conductor with similar behavior of metal conductor under microwave radiation. It is the precondition to further discuss whether the travelling wave can propagate in TEM mode.

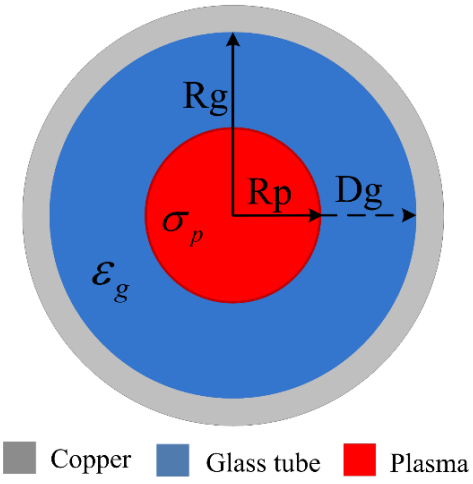


**Figure 2.2** Cross section of the cylindrical discharge tube in the regions out of the rectangular waveguide.

Figure. 2.2 shows the cross section of the cylindrical discharge tube in the regions out of the rectangular waveguide. $R_g$ is the outer radius of the glass tube, which is fixed at 15 mm in our laboratory. $R_P$ is the radius of the plasma column as well as the inner radius of the glass tube. $D_g$ is the thickness of the glass tube wall. The glass tube has a relative permittivity $\varepsilon_g$, which is generally in the range of 3.5 to 10 depending on its chemical composition.

Traditionally, plasma under microwave radiation is regarded to begin to behave like a metal conductor and shield the microwave from penetrating itself, once the real part of the plasma relative permittivity becomes negative with the increase of $\nu_m$ and $n_e$. The transition occurs when $\omega_p^2 = \omega^2 + \nu_m^2$. With this transition relation, a critical electron number density $n_c$ can be obtained as follows.

$$n_c = \frac{m_e \varepsilon_0 \left(\omega^2 + \nu_m^2\right)}{q^2} \tag{2.11}$$

When $n_e > n_c$ but $\delta_p > 2R_p$, it indicates the microwave is still able to penetrate the plasma column in its radial direction. The plasma column does not have the similar function of shielding the microwave from penetrating itself as the metal conductor. From the perspective of wave propagation, the plasma column can not be approximated as a conductor, since it is not able to behave similarly as the metal conductor in guiding the microwave propagation without the wave-shielding capability.

It only acts as a lossy medium and the discharge tube remains to be a one-conductor circular waveguide filled with a multiple-layer medium. Therefore, in present case, the above condition ($n_e > n_c$) is not enough to determine the transition of the discharge tube from a one-conductor circular waveguide to a two-conductor-like coaxial waveguide.

However, when $\delta_p < R_p$ is fulfilled, the high-frequency wave at the angular frequency of $\omega$ is not able to penetrate the plasma column and it will dissipate in the plasma within the skin depth $\delta_p$. A “hollow” will appear in the center of the plasma column, where the high-frequency wave can not reach. As a result, the plasma column will behave like a metal conductor being able to shield the microwave from penetrating it. In this case, the plasma column, together with the metallic enclosure, becomes a two-

conductor-like coaxial waveguide structure. The glass tube turns to be the dielectric of this coaxial waveguide.

Substituting relevant parameters to the relation $\delta_p < R_p$, it can be rewritten as follows:

$$n_e > \frac{c^2 m_e \varepsilon_0}{R_p{}^2 q^2 \cos^2(\theta)} \left(1 + \frac{\nu_m{}^2}{\omega^2}\right)^{\frac{1}{2}} \tag{2.12}$$

If the glass tube is chosen, for example $D_g = 12\ mm$ and $R_p = 3\ mm$, a map can be drawn to show the formation of the two-conductor-like coaxial waveguide structure of the discharge tube under different kinds of conditions (different $n_e$ and $\nu_m$).

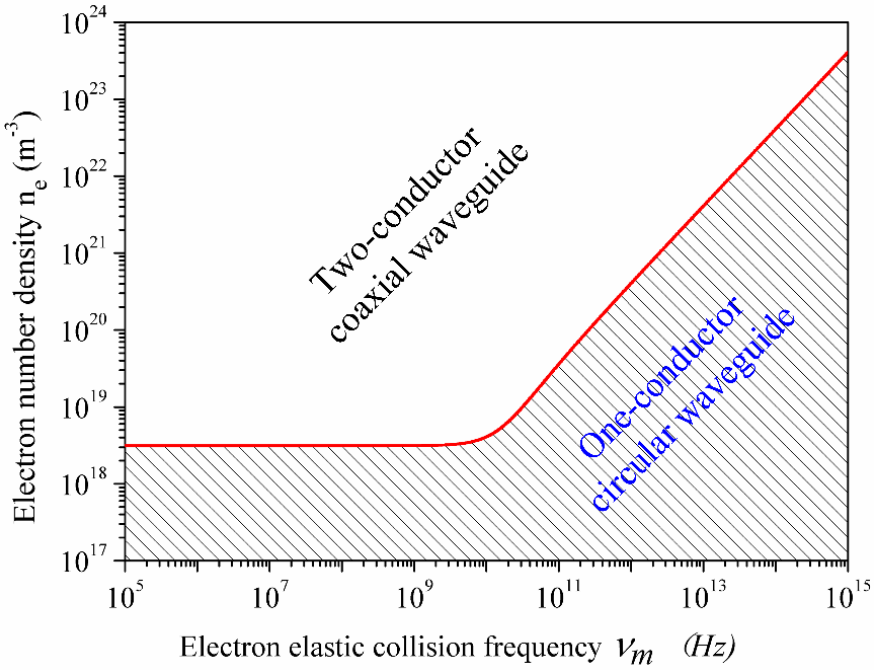


**Figure 2.3** Electromagnetic waveguide structure of the discharge tube under different $n_e$ and $\nu_m$ ($R_p = 3\ mm\ and\ \omega = 2\pi \times 2.45 \times 10^9\ rad/s$).

Since the microwave angular frequency $\omega$ and the plasma column radius $R_p$ are generally constant in most cases, equation (2.12) indicates that the formation of the two-conductor-like waveguide structure finally depends on the plasma parameters $n_e$ and $\nu_m$.

Compared with the conventional metal coaxial waveguide, the two-conductor-like discharge tube has a plasma column as its inner conductor with a plasma skin depth. The smaller the skin depth is, the similar the discharge tube and the conventional metal coaxial waveguide are.

In this paper, we only discuss the simplest case ($\delta_p \ll R_p$), in which a two-conductor-like coaxial waveguide structure can be ensured for the discharge tube.

## 2.3 Electromagnetic propagating modes of the plasma travelling wave

### 2.3.1 Conditions for the existence of the TEM propagating mode and other higher-order propagating modes

For a two-conductor coaxial waveguide, its first-order electromagnetic mode is the TEM mode. Once the discharge tube becomes a two-conductor-like coaxial waveguide, it allows the input microwave to propagate in TEM mode between the plasma column and the outer metallic enclosure without the limitation of cut-off frequency [55].

Besides, just like other waveguide structures, the coaxial waveguide also allows other higher-order modes to propagate and carry energy, providing that the wavelength of working frequency is smaller than the cut-off wavelengths of the higher-order modes.

The following Figure. 2.4 shows the field distribution characteristics of the TEM mode and the first higher-order $TE_{11}$ mode at the cross section of a coaxial waveguide, which helps us to identify the travelling wave propagating modes in the following section 2.4.

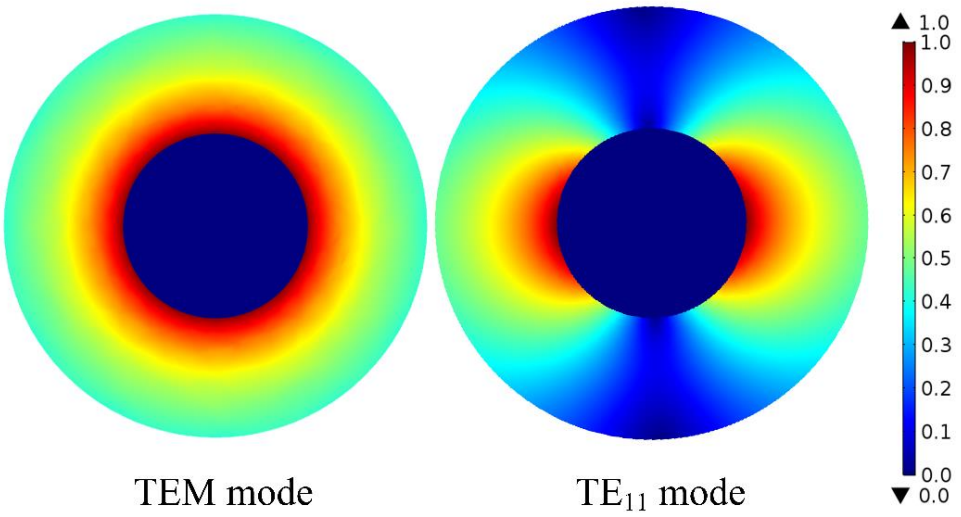


**Figure 2.4** Electric field distribution characteristics of TEM and $TE_{11}$ modes with normalized electric field intensity.

Below is the approximate cutoff wavelength $\lambda_c$ of the first higher-order mode $TE_{11}$ (Transverse electric mode) of the coaxial waveguide [59].

$$\lambda_c = \pi\left(R_g + R_p\right)\sqrt{\varepsilon_g} \tag{2.13}$$

When $\lambda > \lambda_c$, only the TEM mode can propagate in the coaxial waveguide. When $\lambda < \lambda_c$, the higher-order $TE_{11}$ mode is able to propagate and carry the microwave energy. Expression (2.14) gives the condition for the existence of a pure TEM mode in the cylindrical discharge tube.

$$D_g > 2R_g - \frac{c}{\pi f \sqrt{\varepsilon_g}} \tag{2.14}$$

$f$ is the frequency of the input microwave. Taking the size and the working frequency of the plasma source in our laboratory as an example ($R_g = 15\,mm$ and $f = 2.45\,GHz$), a propagating mode distribution map of the travelling wave can be drawn with respect to the thickness and permittivity of the glass tube wall, which is shown in Figure 2.5.

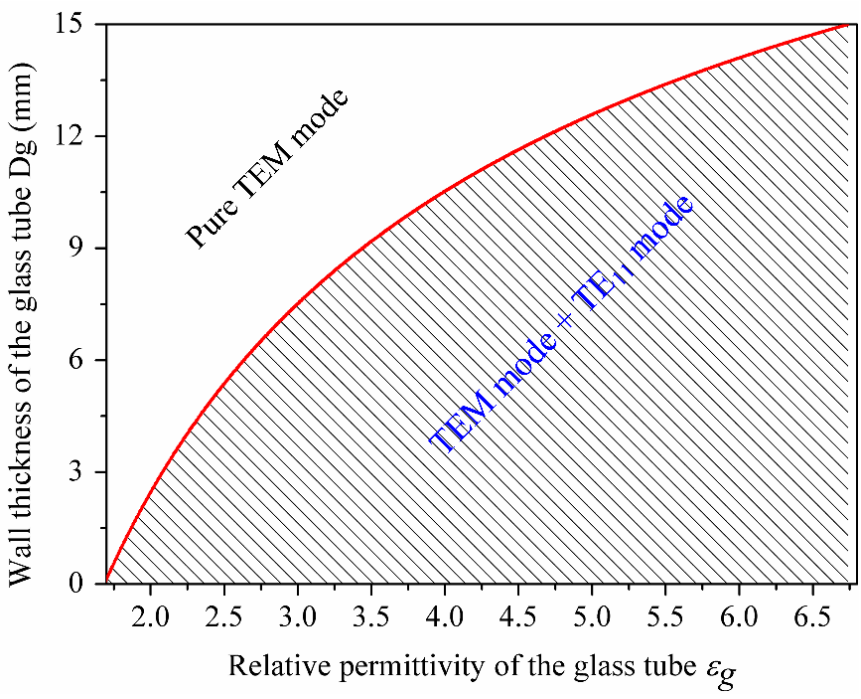


**Figure 2.5** Mode distribution map of the travelling wave in the two-conductor-like discharge tube in our study.

It provides us an indication to select the propagating modes of the travelling wave by using a proper glass tube with particular wall thickness and permittivity.

If the TEM mode ($m = 0$, azimuthally symmetric mode) of the travelling wave is preferable in the waveguide-based plasma source [60, 61], it is better to choose a glass tube with a large wall thickness and a low permittivity.

If the $TE_{11}$ mode ($m = 1$, dipolar mode) is preferable [62], it is better to choose a glass tube with a small wall thickness and a high permittivity. What's more, when the permittivity of the glass tube is approximately larger than 6.75, pure TEM mode in the cylindrical discharge tube can not be maintained and the higher-order $TE_{11}$ mode will be able to exist and propagate when the outer radius of the glass tube remains to be 15 mm in our study.

Restricted by the conditions ( $f = 2.45\ GHz, R_g = 15\ mm\ and\ \varepsilon_g \leq 10$ ) corresponding to the plasma sources in our laboratory as shown in Figure. 2.1, other higher-order propagating modes can hardly be excited.

### 2.3.2 Effects of the energy-input ways on the electromagnetic propagating modes of the travelling wave

The above analysis gives the existence conditions of different electromagnetic propagating modes of the plasma travelling wave in the MPTs with metal enclosure as shown in Figure 2.1. However, it just indicates that these modes are allowed to exist. It does not mean that all these electromagnetic modes will definitely exist in the discharge tube.

In reality, the electromagnetic modes in waveguides or cavities can be selectively excited, if the wave excitation is in an appropriate way [55]. This method is commonly used in the design of mode adapters and resonant cavities for dielectric properties measurements [63].

For the one-port MPT in Figure 2.1, the microwave electric field is not axisymmetric around the plasma column in the rectangular waveguide (in cylindrical coordinates). The intensity of the microwave electric field is much higher on the side near the tapered waveguide in the microwave incoming direction, compared with that on the other side close to the short-circuited end. If a quartz glass tube (relative permittivity is generally 3.5-4) is chosen and its wall thickness is small (< 6 mm), the discharge tube with a diameter of 30 mm allows both TEM and $TE_{11}$ modes to propagate within it. The non-axisymmetric wave excitation in the interaction part between the rectangular waveguide

and the discharge tube will be benefit of excitation of the non-axisymmetric $TE_{11}$ mode. As a consequence, the travelling wave in the discharge tube with such a glass tube in the one-port MPT will have two propagating electromagnetic modes (TEM plus $TE_{11}$). If the one-port MPT only allows pure TEM mode to exist, the size and relative permittivity of the glass tube must meet the requirements as shown in Figure 2.5.

For the two-port MPT in Figure 2.1, if the microwaves come from both ports and have the same frequency, phase and power, the microwave electric field will be approximately axisymmetric around the plasma column in the rectangular waveguide (in cylindrical coordinates). The axial symmetry of the wave excitation will restrain the excitation of the non-axisymmetric $TE_{11}$ mode. In this case, pure axisymmetric TEM mode is much easier to be maintained in the two-port MPT compared with the one-port MPT with the same glass tube.

## 2.4 Full-wave numerical validation

### 2.4.1 Implementation of the numerical calculation

In order to validate the theoretical analysis above, a set of full-wave numerical simulations are implemented in HFSS, a commercial electromagnetics suite based on the finite element method. The calculations are carried out by solving only the Maxwell's equations in MPTs as shown in Figure 2.1, without considering the plasma chemistry and the transport of each species. In order to obtain the electromagnetic properties of the plasma column for the numerical calculations, $n_e$ and $\nu_m$ are assumed to be respectively $1 \times 10^{20} m^{-3}$ and $1 \times 10^{10} Hz$ corresponding to a plasma skin depth of 0.6 mm. In this case, the formation of a two-conductor-like waveguide structure of the discharge tube can be ensured ($\delta_p < R_p$). Other values for $n_e$ and $\nu_m$ are also allowed providing that $\delta_p < R_p$.

The microwave excitations at the ports of the MPTs in Figure 2.1 are defined by the wave port boundary with a preset total input power of 500W (250W for each port of the two-port MPT). Other walls of the MPTs are imposed with PEC (perfect conductor) boundaries. The total number of mesh elements for each calculation is validated by the adaptive meshing skill in HFSS with the convergence criterion of 0.001 for the reflection coefficient.

It should be clarified that our numerical calculations have neglected the following facts for simplicity.

(1) The plasma parameters $n_e$ and $\nu_m$ are assumed to be constant. In fact, these two parameters are inhomogeneous and spatially distributed. They change with the microwave input power, gas inflow rate, pressure, gas type and so on. Besides the limited experimental measurements [ 64 ], it requires an extremely computation-demanding and time-consuming calculation to obtain the spatially-distributed $n_e$ and $\nu_m$, with the popular self-consistent fluid modeling [51, 65, 66, 67, 68].

(2) The plasma column length is assumed to be a constant length of 0.25 m, which does not fit the reality. Actually, it increases with the rise of the input microwave power but decreases with the growth of the gas inflow rate [51, 69].

Despite the limitations above, the numerical calculations in this study are capable to validate the theoretical analysis above, because it requires not the accurate microwave field intensity but the field distribution characteristics to identify the electromagnetic mode of the travelling wave under different conditions.

### 2.4.2 Propagating TEM mode

According to the expression (2.14) and the mode distribution map Figure 2.5 above, if a quartz glass tube with $\varepsilon_g = 3.5$ is employed in the MPTs, pure TEM mode can be maintained in the cylindrical discharge tube, when $D_g > 9.18\ mm$. Figure 2.6 presents the distribution of the microwave electric field norm in the one-port MPT with a glass tube whose relative permittivity is 3.5 and wall thickness is 12 mm ($\varepsilon_g = 3.5$ and $D_g = 12\ mm$). The radial electric field at the cross section of the cylindrical discharge tube shows a good azimuthal symmetry along the plasma column (in cylindrical coordinates), which demonstrates that the travelling wave propagates in TEM mode.

Besides the azimuthally symmetric electric field distribution, the TEM mode is featured by having neither the electric field component nor the magnetic component in the wave propagation direction ($|\overline{E_z}| \approx 0$ and $|\overline{H_z}| \approx 0$ in our case), which differs from other azimuthally symmetric modes. Figure. 7 presents the intensity of $\overline{E_z}$ along a line in the middle of the glass tube wall, which is parallel to the plasma column. The data are from the same calculation as that in Figure 2.6 ($\varepsilon_g = 3.5$ and $D_g = 12\ mm$).

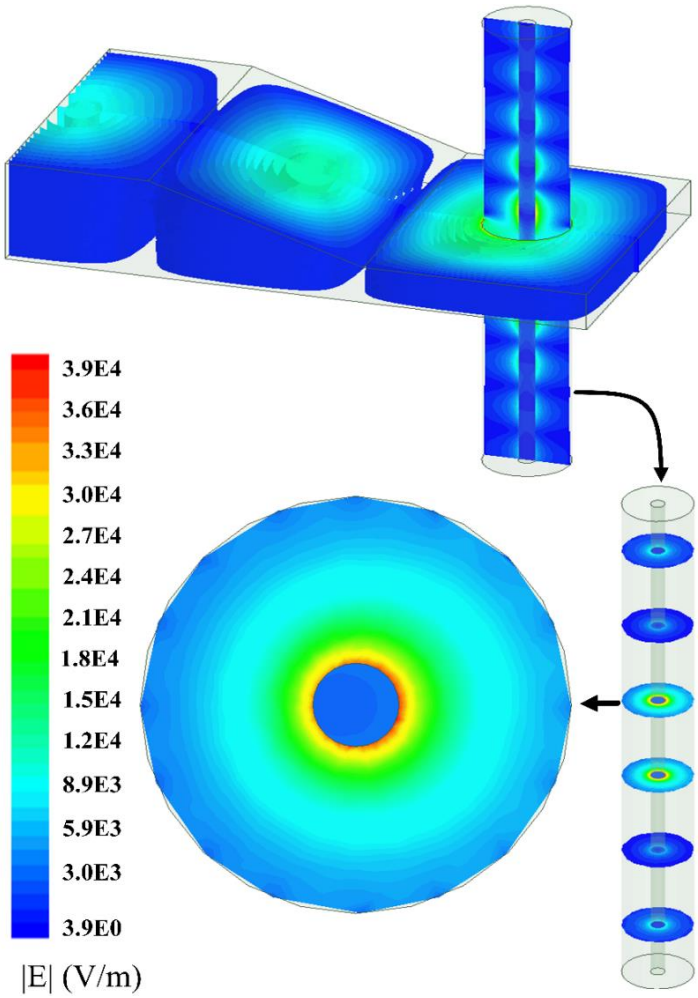


**Figure 2.6** The distribution of microwave electric field norm under the conditions of $\varepsilon_g = 3.5$ and $D_g = 12\ mm$.

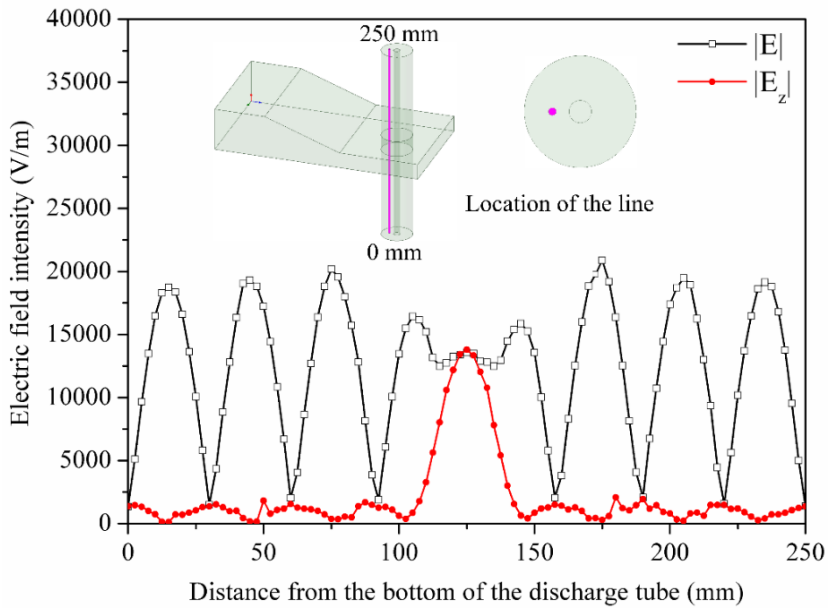


**Figure 2.7** Comparison of the intensities of the microwave electric field with its component in the travelling wave propagation direction $|\overline{E_z}|$ across a line in the middle of the glass tube wall parallel to the plasma column.

Figure 2.7 shows that the intensity of the electric field component in the travelling wave propagation direction $|\overline{E_z}|$ is negligibly small in the discharge tube part which is out of the rectangular waveguide and shielded with the metallic enclosure. Compared with the intensity of the electric field norm $|\bar{E}|$, it is approximately equal to zero ($|\overline{E_z}| \approx 0$).

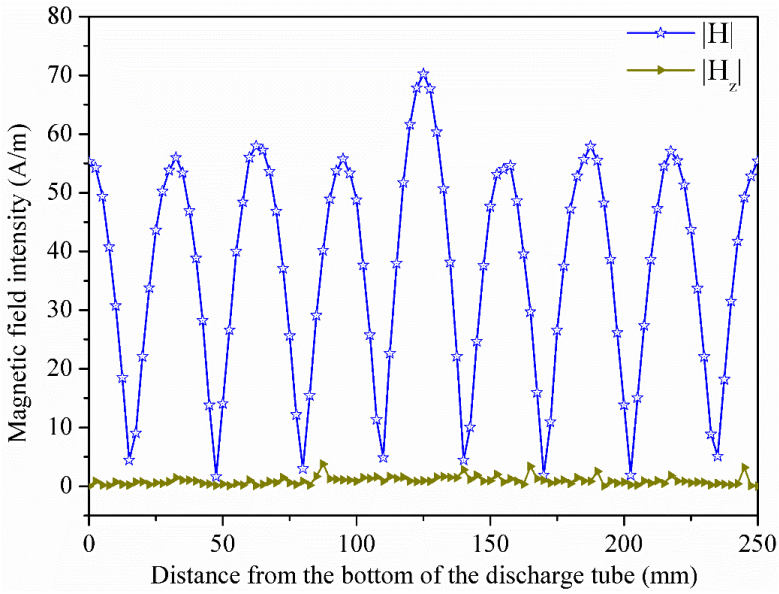


**Figure 2.8** Comparison of the intensities of the microwave magnetic field with its component in the travelling wave propagation direction $|\overline{H_z}|$ across the same line as shown in Figure 2.7.

Figure 2.8 shows the corresponding $|\overline{H_z}|$ along the same line as shown in Figure 2.7. It demonstrates that the intensity of the magnetic field component in the travelling wave propagation direction is indeed close to zero ($|\overline{H_z}| \approx 0$), especially compared with the intensity of the magnetic field norm $|\bar{H}|$. The facts that $|\overline{E_z}| \approx 0$ and $|\overline{H_z}| \approx 0$ shown in Figure 2.7 and Figure 2.8 verify again that the electromagnetic mode of travelling wave in Figure 2.6 is the TEM mode. Furthermore, it demonstrates that the discharge tube parts with metallic enclosure have turned to be two-conductor-like coaxial waveguides, because only the waveguide with two or more conductors can support the propagating TEM mode.

### 2.4.3 Hybrid propagating TEM and $\mathrm{TE}_{11}$ modes

The theoretical analysis in section 2.3.1 shows that the high-order $\mathrm{TE}_{11}$ mode is able to exist and propagate along the plasma column, when the thickness of the glass tube wall is smaller than 9.18 mm with a constant glass permittivity $\varepsilon_g = 3.5$. In this case, there will exist two propagating electromagnetic modes in the cylindrical discharge tube

and both of them will carry the energy from the microwave source. The travelling wave will propagate no longer in a pure TEM mode but in hybrid TEM and $TE_{11}$ modes.

Figure 2.9 presents the distribution of the microwave electric field norm in the one-port MPT with a glass tube having smaller thickness of the glass tube wall ($D_g = 8\,mm$) and the same glass dielectric property as the case shown in Figure 2.6 ($\varepsilon_g = 3.5$). The electric field distributions of the travelling wave at the cross section of the cylindrical discharge tube demonstrate that the azimuthal symmetry is no longer fulfilled. Comparing the electric field distribution characteristics in Figure 2.9 and Figure 2.4, we can conclude that the higher-order $TE_{11}$ mode is indeed excited and the travelling wave propagates in hybrid TEM and $TE_{11}$ modes.

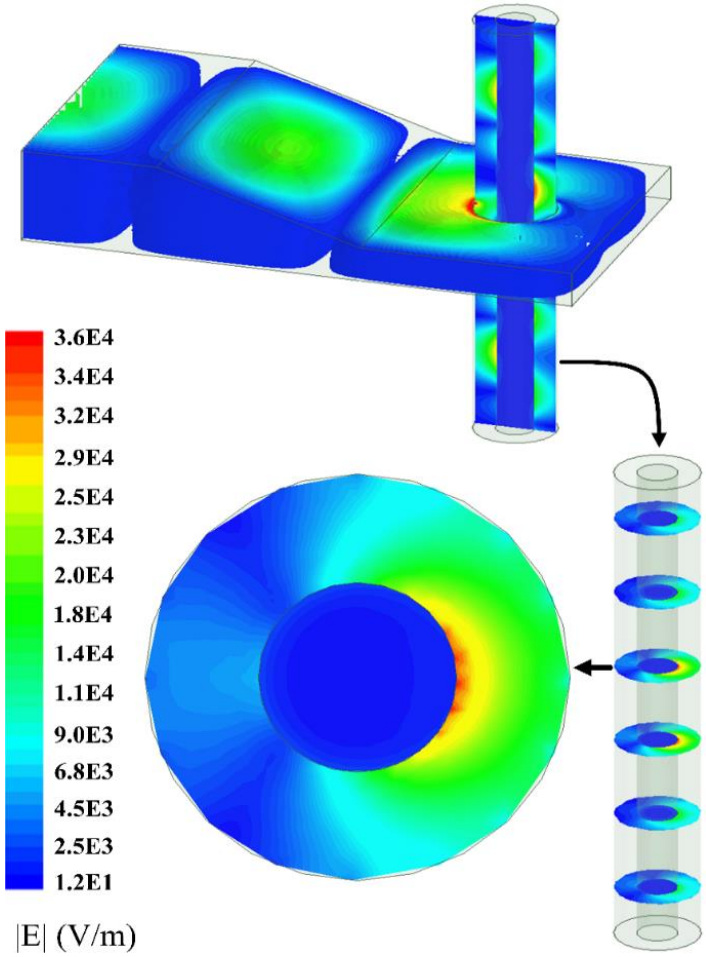


**Figure 2.9** The distribution of microwave electric field norm under the conditions of $\varepsilon_g = 3.5$ and $D_g = 8\,mm$.

As shown in the electromagnetic mode distribution map in Figure 2.5, increasing the permittivity of the glass tube is also able to introduce higher-order propagating modes in the two-conductor-like "coaxial waveguide", even if the thickness of glass tube wall

remains constant. Figure 2.10 shows the microwave electric field norm distribution in the microwave plasma torch, when the relative permittivity of the glass tube wall becomes 6.5 and the thickness of glass tube wall remains the same as the case in Figure 2.6 ($D_g = 12\ mm$). It demonstrates that the travelling wave propagates in hybrid TEM and $TE_{11}$ modes.

In conclusion, the numerical results (Figure 2.6-2.10) prove that the glass tube participates the guidance of the travelling wave as a part of the wave-guiding structure (dielectric of the coaxial waveguide), besides acting as the discharge confining material. The travelling wave can be designed to propagate in pure TEM mode or hybrid TEM and $TE_{11}$ modes by choosing an appropriate glass tube with particular wall thickness and dielectric property.

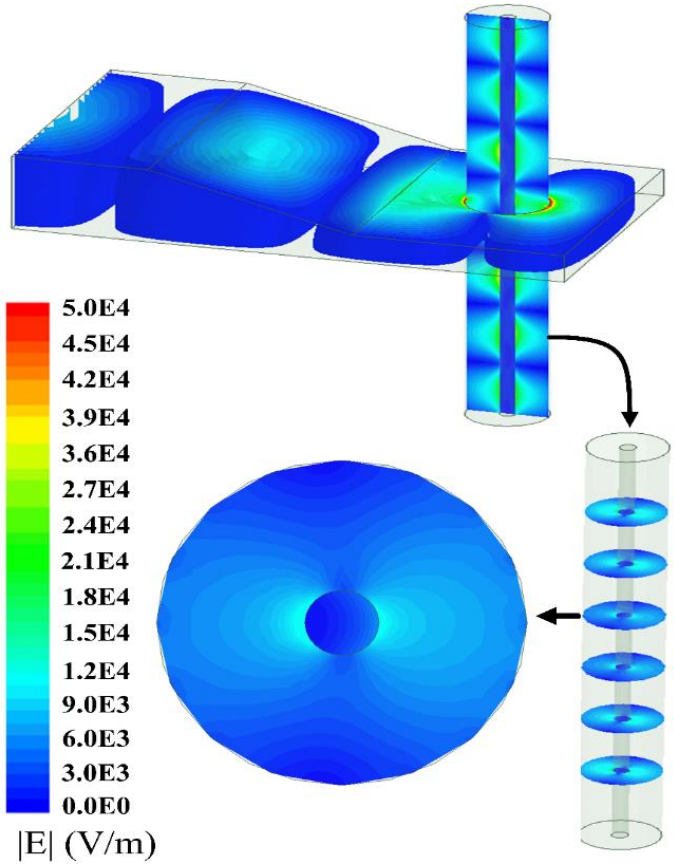


**Figure 2.10** The distribution of microwave electric field norm under the conditions of $\varepsilon_g = 6.5$ and $D_g = 12\ mm$.

## 2.4.4 Suppression of $TE_{11}$ mode in the two-port MPT

Figure 2.11 illustrates the microwave electric field distribution in the two-port MPT with the same glass tube as in figure 2.9 ($\varepsilon_g = 3.5$ and $D_g = 8\ mm$) for the one-port

MPT, when the microwaves come from both ports with the same frequency, phase and power of 250 W. Compared with the field distribution in the one-port MPT with the same glass tube as shown in Figure 2.9, the microwave electric field in the two-port MPT shows a good azimuthal symmetry. The non-axisymmetric $TE_{11}$ has been successfully restrained, when it is allowed to exist as a propagating mode.

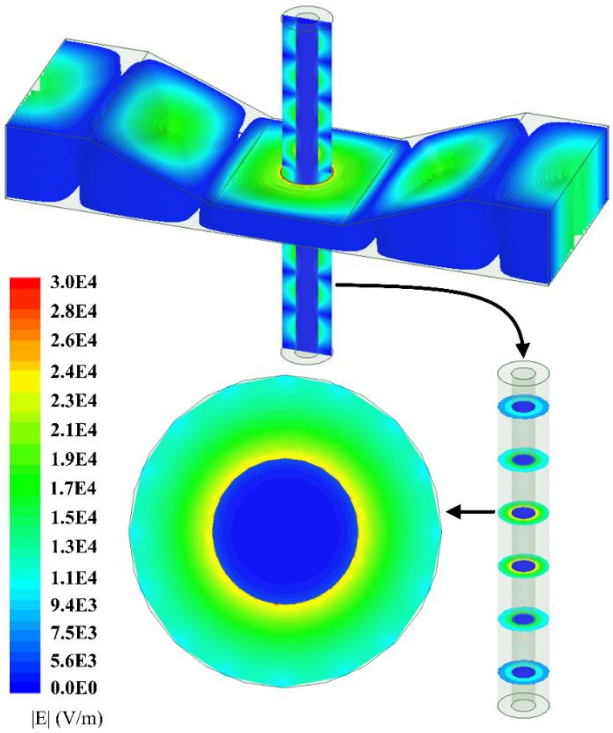


**Figure 2.11** The distribution of microwave electric field norm under the conditions of $\varepsilon_g = 3.5$ and $D_g = 8\ mm$ in the two-port MPT.

## 2.4 Conclusions

This chapter has theoretically investigated and numerically validated the electromagnetic propagating modes of the travelling wave in a cylindrical discharge tube bounded by a metallic enclosure in the one-port and two-port MPTs operating at 2.45 GHz. A new criterion is proposed to determine the transition of the discharge tube from a one-conductor circular waveguide to a two-conductor-like waveguide. The main conclusions can be drawn as follows:

(1) When the plasma skin depth is larger than the diameter of the plasma column ( $\delta_p > 2R_p$ ), the discharge tube remains to be a one-conductor circular waveguide filled with a multiple-layer medium even the electron number density is larger than the critical number density ($n_e > n_c$), in which the TEM

mode is not possible to exist. While $\delta_p < R_p$, the plasma column, the discharge confining glass tube and together with the metallic shielding enclosure form a two-conductor-like coaxial waveguide, allowing the travelling wave to propagate in TEM mode without the limitation of cutoff frequency.

(2) In a travelling-wave plasma torch with metallic enclosure, the $m = 0$ mode is not always the TM mode. It can be the TEM mode as well, when the discharge tube becomes a two-conductor-like coaxial waveguide.

(3) The wall thickness and the dielectric permittivity of the glass tube are able to determine the microwave propagating modes allowed to exist in the two-conductor-like discharge tube. For the one-port MPT in this chapter, the glass tube is even able to determine whether the travelling wave propagates in a pure TEM mode or in hybrid modes in the discharge tube. It indicates the possibility to control the propagating modes of the travelling wave for different purposes by choosing a proper glass tube with particular wall thickness and dielectric property.

(4) The non-axisymmetric $\mathrm{TE}_{11}$ can be restrained in the two-port MPT, when the microwaves come from both ports with the same frequency, phase and power.

However, it is worth to note that this chapter only discussed the propagating modes of the travelling wave in the discharge tube with metallic enclosure in the simplest case $\delta_p \ll R_p$. Therefore, further investigations are required to explore other cases. For example, when the skin depth is large and comparable to the radius of the plasma column even if $\delta_p < R_p$ is fulfilled, the discharge tube should be treated as a coaxial waveguide filled with a multiple-layer medium (glass and the skin depth area of the plasma column). In this case, it is necessary to consider the effects of the large skin depth in determining the conditions of the electromagnetic propagating modes of the travelling wave. Besides, an in-depth investigation is required to explore the one-conductor circular waveguide case when $\delta_p > R_p$.

# Chapter 3 Role of the glass tube in improving the power coupling efficiency of a waveguide-based MPT

## 3.1 Background and hypothesis of the "waveguide-to-coaxial mode adaptor"

A high power coupling efficiency, which is the efficiency of power transferring from the input microwave to the discharge, is a general requirement for large-scale industrial applications of MPTs. However, when the gas discharge occurs, the high density of the charged species enables the plasma column to shield the incident microwave from penetrating it, thereby causing the power reflection and energy waste [54]. Actually, from the birth of MPTs, maximizing the power coupling efficiency is always one of the main tasks [11, 13, 70]. Researchers developed a lot of skills to decrease the microwave reflection and to improve the power coupling efficiency of the MPT for different applications [71, 72, 73, 74]. It is generally achieved by adjusting the movable short-circuit ending plunger or the three-stub tuner under the monitoring of the microwave power meters [12, 70, 71, 72, 73, 74]. However, in industrial applications, the MPTs are often expected to achieve an acceptable microwave power coupling efficiency naturally without using any external tuning measures (For example, 90% is a generally acceptable efficiency in microwave energy industrial applications). It helps to simplify the system and save the cost of the tuning devices, enhancing the advantage of the MPT in economy.

In previous chapter, it is found that the discharge tube with metallic enclosure can act as a two-conductor like coaxial waveguide supporting the input microwave to propagate along the plasma column in coaxial waveguide modes under some conditions. In this case, the MPT, as shown in Figure 3.1, can be regarded as a "waveguide-to-coaxial mode adapter" from the perspective of microwave components. For a waveguide-to-coaxial mode adapter, it is able to improve its conversion efficiency by optimizing the dielectric thickness of the coaxial waveguide according to the

transmission line theory. Besides, previous publications have reported that the thickness and dielectric properties of the glass tube wall have a great influence on the propagation of the plasma-sustaining wave and the discharge properties [50, 45, 43, 46]. Considering the fact that the plasma-sustaining travelling wave in the discharge tube is from the input microwave in the rectangular waveguide in our case, it is reasonable to infer that changing the wall thickness or the material of the glass tube will affect the power coupling efficiency of the plasma torch.

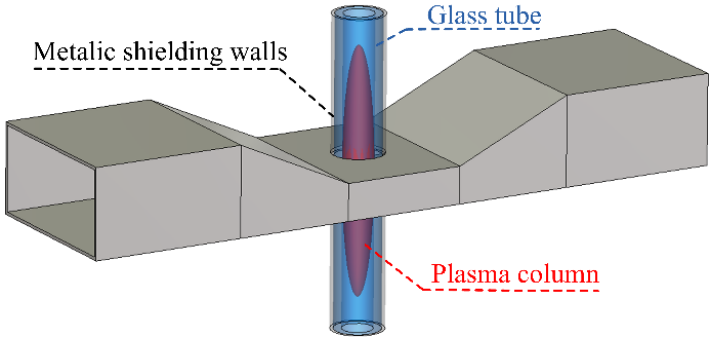


**Figure 3.1** Schematic diagram of one type of MPTs in our laboratory.

This chapter aims to experimentally investigate the effects of the glass tube on the power coupling efficiency of a MPT with metallic enclosure. It explores the possibility of improving the power coupling efficiency by simply choosing a proper glass tube without using any external tuning devices like the movable short-circuit ending plunger or the three-stub tuner. Besides, validity of this efficiency-improving method in different operation conditions of the MPT will be investigated as well.

## 3.2 Experiment design

### 3.2.1 Experiment system

In order to achieve these goals mentioned above, an experimental system was set up in our laboratory to measure the power coupling efficiencies of the MPT under different conditions. Figure 3.2 is a photo of the experimental system for low pressures and Figure 3.3 shows the corresponding schematic diagram. This system consists of a magnetron (Panasonic 2M244-M11) microwave source powered by a high-voltage electric supply, a circulator, two directional couplers connected to two microwave power meters (AV2433) respectively, a MPT and a movable short-circuited ending

plunger. The MPT has been shown in Figure 3.1 above, which is similar to the classic surfaguide plasma source. The minor difference is that there is no air gap between the glass tube outer walls and the metallic shielding walls for our MPT. The discharge occurs in the glass tube and it is sustained by the travelling wave propagating along the plasma column. Detailed description regarding this plasma torch can refer to reference [37].

The system works at the microwave frequency of 2.45 GHz and under low pressures (100-2666 Pa). The output power of the magnetron source, as well as the input microwave power of the plasma torch, can change from 100 W up to 1000 W by adjusting the high-voltage electric supply, which was measured by the power meter 1 as shown in Figure 3.2 and 3.3. The reflected microwave power from the plasma torch was separated by the circulator, measured by the power meter 2 and finally absorbed by the impedance-matched load with water cooling. It is worth noting that the waveguide-based MPT in present study has a metallic enclosure that bounds the glass tube and the discharge preventing the plasma-sustaining microwave from radiating to the space. Therefore, the input microwave only can be either reflected or absorbed by the plasma column. In this case, the power coupling efficiency $\eta$ equals to $1 - P_{re}/P_{in}$ where $P_{re}$ is the reflected microwave power and $P_{in}$ is the input microwave power.

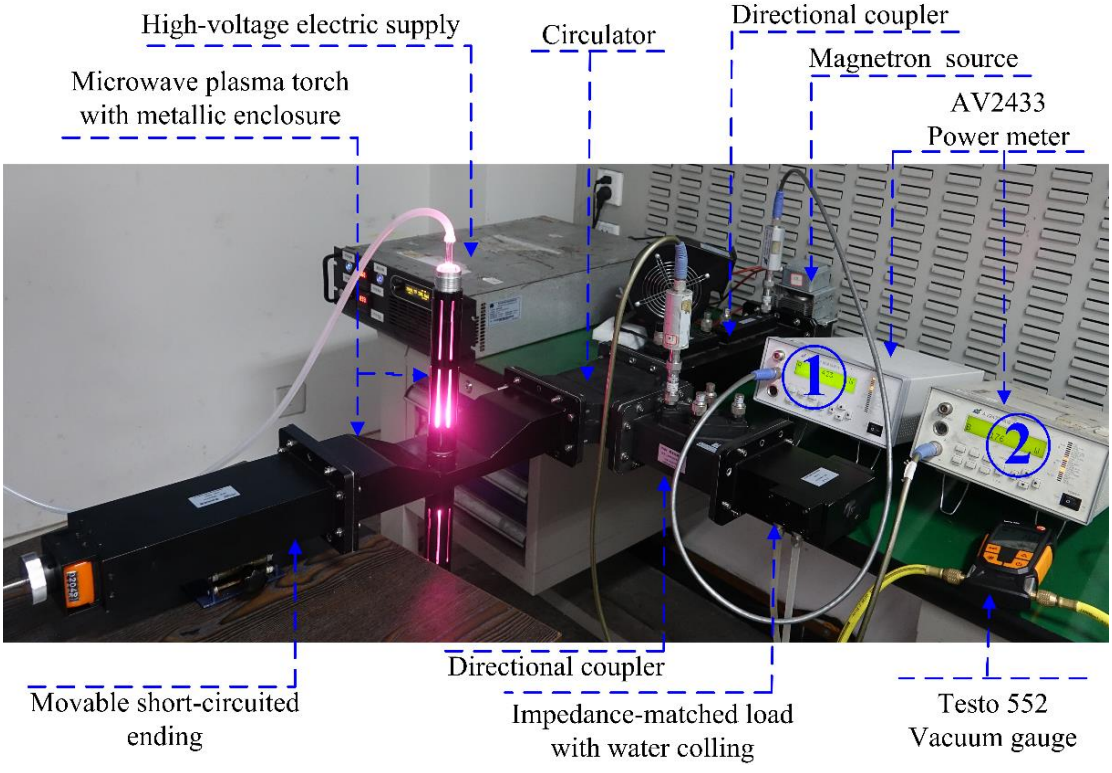


**Figure 3.2** Photo of the experimental system at low pressures.

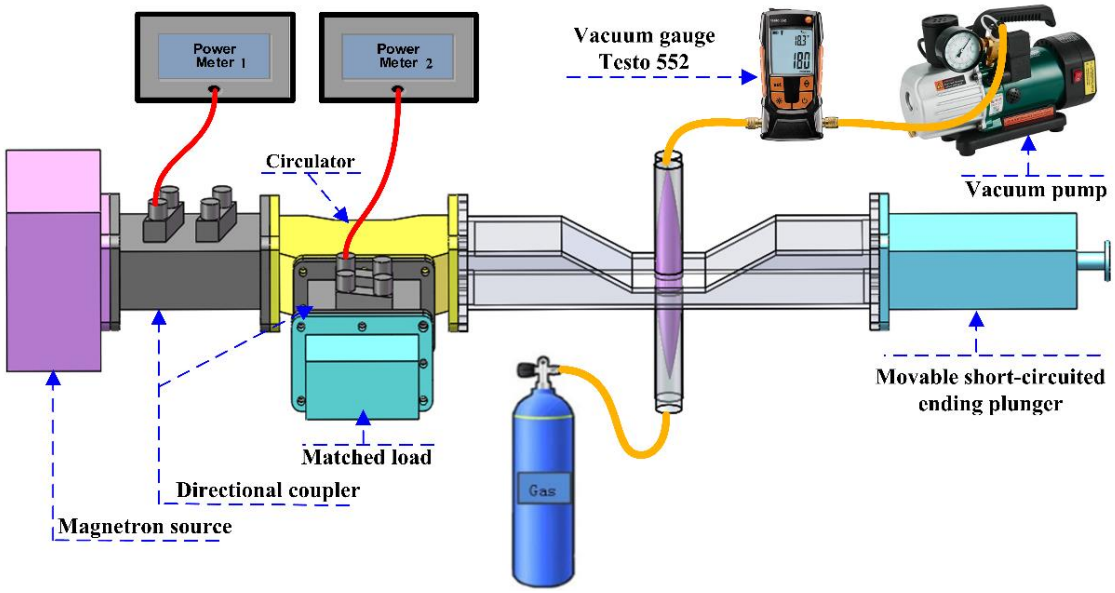


**Figure 3.3** Schematic diagram of the experimental system at low pressures.

### 3.2.2 Experiment procedure

Pure argon (purity > 99.99%) was chosen to be the working gas of the discharges in all the experiments of this chapter because of its low ionization requirement, inexpensive price and availability. The working gas was supplied from a high-pressure tank and the low-pressure environment was created by a vacuum pump (FUJIWARA 2PCV-2MSV). The actual pressure in experiments was measured by a vacuum gauge (TESTO 552) whose measurement range is 0-2666 Pa.

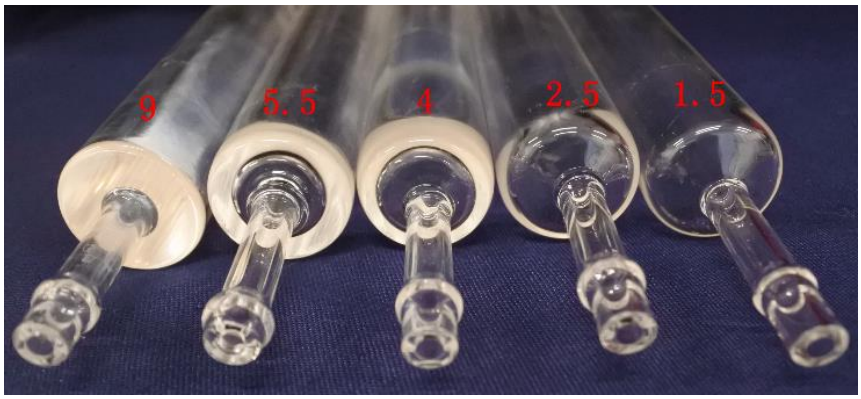


**Figure 3.4** Photo of the glass tubes with different wall thicknesses (1.5, 2.5, 4, 5.5 and 9 mm) applied in experiments at low pressures.

Figure 3.4 presents the glass tubes applied in the experiments at low pressures, which have the same outer diameter (30 mm), the same material (quartz) and the same length (600 mm). The only difference is that the thicknesses of the glass tube walls are 1.5, 2.5, 4, 5.5 and 9 mm respectively. The glass tubes with these wall thicknesses were

chosen because of their availability in our laboratory. The gas inlet and outlet of the glass tubes have a pagoda-like shape for the connection with the gas feeding pipe.

To trigger the discharge successfully, the gas pressure in the glass tube was initially decreased to the minimum value of the vacuum system (approximately 100 Pa) so that microwave breakdown could occur in the glass tube at a low input power (approximately 500 W). After the discharge was triggered successfully, the gas pressure and the input microwave power can be adjusted according to the experimental requirements within the ranges that the experimental system allowed (100 W-1000 W, 150 Pa-2000 Pa). When the discharges reached steady state, the input and the reflected microwave powers of the plasma torch were measured and recorded. In this way, the power coupling efficiencies of the plasma torch were measured with the glass tubes above under different operation conditions (different input microwave powers and pressures). During all the experiments in present study, the short-circuited ending kept to attach to the end of the MPT without moving.

## 3.3 Results and analysis

### 3.3.1 Effects of the glass tube on improving the power coupling efficiency

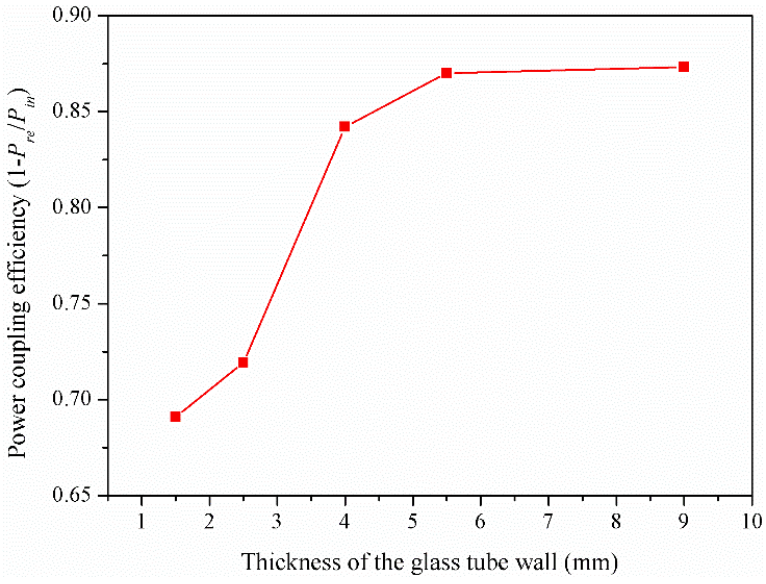


**Figure 3.5** Power coupling efficiency versus the glass tube wall thickness under the pressure of 1000 Pa and the input microwave power of 500 W

Figure 3.5 gives the power coupling efficiencies of the MPT under the gas pressure of 1000 Pa and the input power of 500 W for the five glass tubes as shown in Figure

3.4. It shows that the power coupling efficiency improves with the increase of the glass tube wall thickness. When the thickness of the glass tube wall is 1.5 mm, the power coupling efficiency is lower than 70%. Simply changing the glass tube with wall thicknesses of 5.5 and 9 mm, a power coupling efficiency higher than 87% (improvement of 17%) is obtained. An acceptable power coupling efficiency of the plasma torch around 90% can be achieved naturally by choosing a proper glass tube without using any external tuning measures.

### 3.3.2 Mechanism of the efficiency-improving method

In order to explain the glass tube effects on the power coupling efficiency of the plasma torch shown above, we turned to seek help from the transmission line theory. Figure 3.6 presents the equivalent circuit of the microwave plasma source detailing its impedance matching problem.

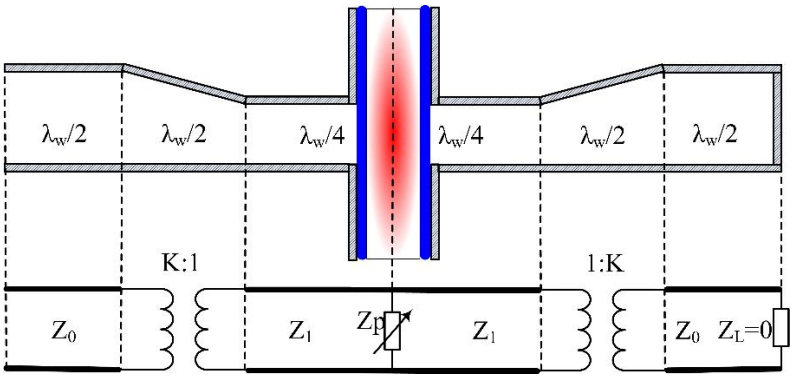


**Figure 3.6** Equivalent circuit of the MPT.

$\lambda_w$ is the working wavelength of the microwave at frequency of 2.45 GHz in the rectangular waveguide WR430. K refers to the impedance transformation ratio of the tapered rectangular waveguide part. $Z_L$ is the impedance of the short-circuited ending, which equals to zero. $Z_0$ and $Z_1$ are the characteristic impedances of the standard rectangular waveguide WR430 and the height-reduced rectangular waveguide respectively. $Z_P$ is the impedance of the discharge tube including the plasma column, the glass tube and the metallic enclosure. The estimated values of $Z_0$, $Z_1$ and K can be found in reference [71].

From the point view of transmission line theory, the impedance matching will be achieved and the power refection will be minimized, when $Z_p = Z_1$. For the discharge tube parts out of the rectangular waveguide, it was found in our previous works [51,

75] that these parts with metallic enclosure can form a two-conductor like coaxial waveguide supporting the input microwave to propagate along the plasma column in coaxial waveguide modes. For a coaxial waveguide, its characteristic impedance can be optimized by changing the dielectric thickness. Therefore, changing the glass tube wall thickness enables $Z_P$ to be close to $Z_1$. Accordingly, the power coupling efficiency of the MPT is improved.

## 3.4 Dependence of the efficiency-improving method on operation conditions

The above results demonstrate that it is possible to achieve an acceptable power coupling efficiency of the MPT around 90% once the glass tube is properly chosen. In order to figure out whether it works in other different operation conditions, experiments under different input powers and pressures were carried out.

### 3.4.1 Different input microwave powers

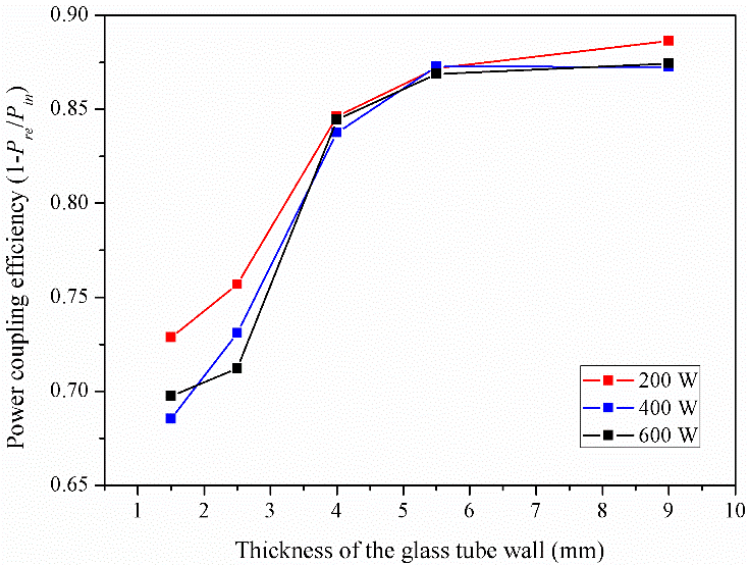


**Figure 3.7** Power coupling efficiency versus the glass tube wall thickness under different powers at the gas pressure of 1000 Pa.

Figure 3.7 shows the changes of the power coupling efficiencies with the increase of the glass tube wall thickness for three input microwave powers (200, 400 and 600 W) at the gas pressure of 1000 Pa. It can be seen that, for all these input powers, the power coupling efficiency becomes higher when the thickness of the glass tube wall increases.

When the glass tube wall thickness is 1.5 mm, the power coupling efficiencies are all around 70% and lower than 75%. However, while the thickness of the glass tube wall is larger (5.5 and 9 mm), the power coupling efficiencies get significant increases, which are all higher than 87%. Furthermore, Figure 3.7 also shows similar improving tendency that the power coupling efficiencies change with the increase of the glass tube wall thickness for three different input microwave powers. It indicates that increasing the glass tube wall thickness improves the power coupling efficiency of the MPT and this effect is relatively independent of the input microwave powers.

Generally, a higher input power means more ionization and more electrons, resulting in a higher microwave-reflection capability of the plasma. However, in Figure 3.7, it can be seen that the power coupling efficiencies for the glass tubes with the wall thicknesses of 4, 5.5 and 9 mm have a little change when the input power is different. People may confuse about why the power reflection does not go up with the increase of the input microwave power.

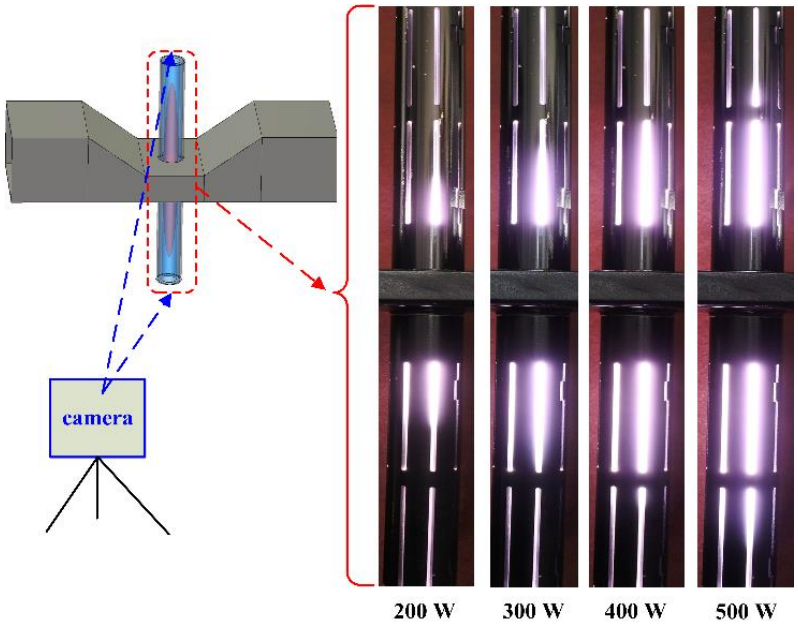


**Figure 3.8** Discharge photos for different input powers with the 9-mm-wall-thickness glass tube at the pressure of 1000 Pa.

The photos in Figure 3.8 record the influence of the input microwave power on the discharge properties and give the whereabouts of the increased input microwave power. It can be observed that the plasma column extends towards both ends of the glass tube with the increase of the input microwave power. Actually, when the plasma column is successfully launched, the discharge tube with metallic enclosure becomes a two-conductor like coaxial waveguide which is no longer cut-off for the input microwave

at the frequency of 2.45 GHz. The input microwave enters the metallic enclosure, propagates along the plasma column and drives the plasma column to become longer as the power increases [51, 37]. Therefore, the increased input power was not reflected but mostly absorbed by the plasma column in the metallic enclosure.

### 3.4.2 Different pressures

Besides the input microwave power, pressure is another important factor which greatly influences the discharge properties and may consequently disable the efficiency-improving method. Figure 3.9 shows the changes of the power coupling efficiencies with the increase of the glass tube wall thickness at the gas pressure of 500 Pa. Compared with the results in Figure 3.7, the power coupling efficiencies do not improve monotonically with the increase of the glass tube wall thickness. However, the power coupling efficiency still can be optimized to be higher than 85% and close to 90% at the pressure of 500 Pa when choosing a glass tube with a much thicker wall (5.5 and 9 mm). Besides, the improvement of the power coupling efficiency seems to be independent of the input microwave powers at the pressure of 500 Pa as well.

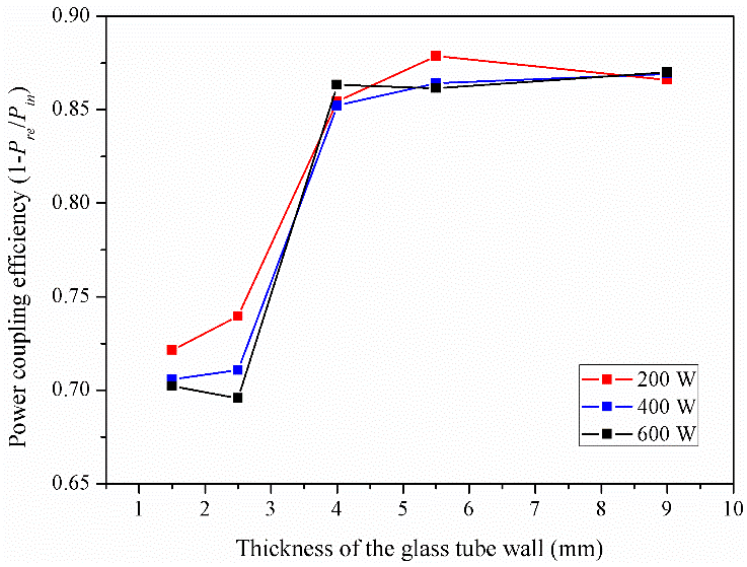


**Figure 3.9** Power coupling efficiency versus the glass tube wall thickness under different powers at the gas pressure of 500 Pa.

Besides the low-pressure cases, the MPTs working under atmospheric pressure are very attractive and have a lot of applications as well. In order to test whether the power coupling efficiency of the MPT can be improved under atmospheric pressure by simply increasing the glass tube wall thickness, similar experiments were carried out with a

little change to the experimental system shown in Figure 3.2 and Figure 3.3. By adding a gas flow meter to the gas bottle outlet and removing the vacuum pump and gauge, the experimental system for low pressures turns to be applicable for the experiments under atmospheric pressure. Figure 3.10 shows the glass tubes with the wall thicknesses of 2.5, 4 and 9 mm applied in the atmospheric experiments.

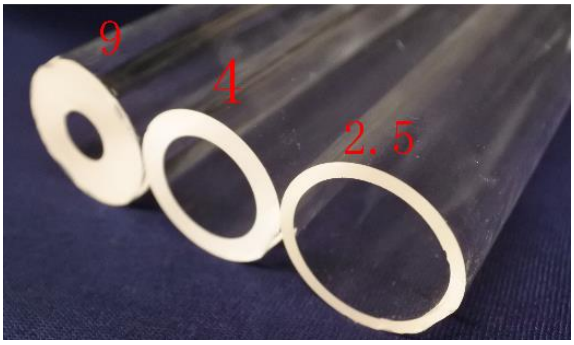


**Figure 3.10** Photo of the glass tubes with different wall thicknesses (2.5, 4 and 9 mm) for the atmospheric experiments.

Figure 3.11 shows the power coupling efficiencies for the three glass tubes at the gas inflow rate of 1 L•min$^{-1}$ under atmospheric pressure and different microwave input powers. The power coupling efficiency for the glass tube with a larger wall thickness is always higher than that for the thinner-wall glass tubes, no matter what the input power is. Furthermore, the power coupling efficiencies for the glass tubes with the wall thicknesses of 4 and 9 mm are even higher than 90%, when the input power is 200 W. It demonstrates that increasing the glass tube wall thickness is able to improve the power coupling efficiency of the MPT under atmospheric pressures as well.

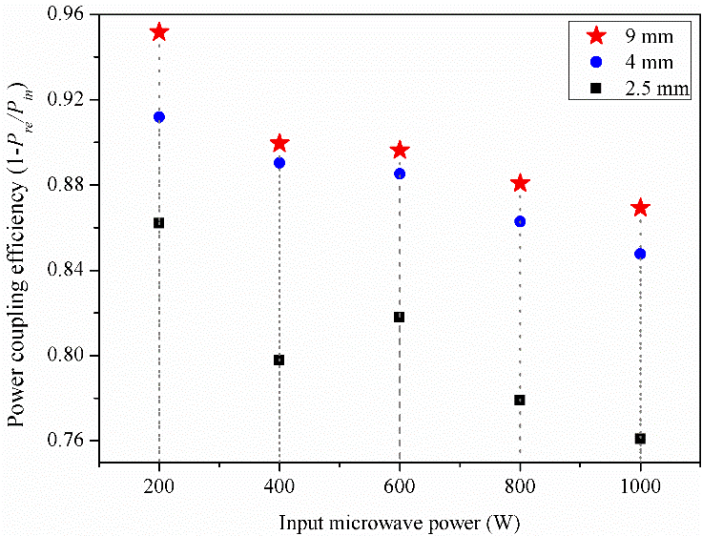


**Figure 3.11** Power coupling efficiencies for three different glass tube wall thicknesses (2.5, 4 and 9 mm) at the gas inflow rate of 1 L•min$^{-1}$ under atmospheric pressure and different input powers

Under atmospheric pressure, the gas inflow rate is very influential to the discharge properties [69, 7]. Therefore, experiments under higher gas inflow rates were also performed. It is worth noting the steam-like filamentary discharges [76, 77, 78] were observed in the experiments under the atmospheric pressure. Figure 3.12 gives the photos of the argon discharge filaments from the top view of the MPT (view from the gas outlet). When the gas inflow rate was lower than 6 L•min$^{-1}$, the filamentary discharges were relatively stable, allowing the measurement of power coupling efficiency. However, when the gas inflow rate was higher than 6 L•min$^{-1}$ under atmospheric pressure, the filamentary discharges became very unstable, resulted in a drastically time-varying power reflection. Consequently, measurements of the power coupling efficiency in these cases became meaningless.

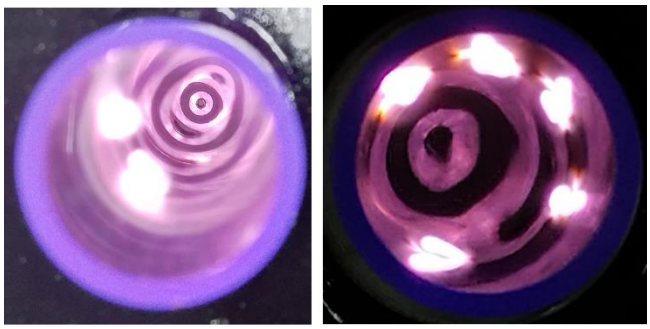

(a) (b)

**Figure 3.12** Photos of the argon discharge filaments (top view from the gas outlet) under atmospheric pressure at the inflow rate of 1 L•min$^{-1}$ for different input powers. (1) less than 200 W (2) 500 W.

## 3.5 Conclusion

In this chapter, experiments were conducted to investigate the glass tube effects on the power coupling efficiency of a MPT with metallic enclosure under different operation conditions. Corresponding theoretical analysis regarding the impedance matching problem in the MPT was given to explain the reasons why the glass tube is able to significantly influence the power coupling efficiency. Our main conclusions are summarized as follows:

(1) Increasing the thickness of the glass tube wall is able to improve the power coupling efficiency under both low pressures and atmospheric pressure. Furthermore, when the input microwave power becomes different, this efficiency-improving method is still valid.

(2) A power coupling efficiency around 90% can be achieved by simply choosing a proper glass tube with its wall thickness in particular range rather than using external tuning devices like the movable short-circuit ending plunger or the three-stub tuner. For the MPT in present study, the wall thickness should be 5.5-9 mm.

However, the steam-like filamentary discharges were also observed in the experiments under atmospheric pressure. For high gas inflow rates (>6 $L \bullet min^{-1}$), the filamentary argon discharges became very unstable resulted in a time-varying power reflection. Experiments with different gases or gas mixtures but without the filamentary discharges are required to further investigate the glass tube effects on the power coupling efficiency, which will be our future work.

# Chapter 4 Two-dimensional axisymmetric fluid model of the argon plasma in MPTs under atmospheric pressure

## 4.1 A brief Introduction of the plasma modelling methods

In chapter 2, we theoretically analysed and numerically modelled the microwave propagation in two waveguide-based MPTs. However, the plasma parameters were predefined as constants and manually input to the model, thereby, meaning the plasma was assumed not produced by the microwave. The simulations can be only used to analyse the field distribution characteristics of the microwave with an assumed plasma column. In order to figure out exactly how the plasma interacts with microwave in MPTs, it is necessary to adding the plasma physics into modelling process.

Generally, there are two main types of plasma modelling methods that are commonly used: the fluid model and the kinetic model. The fluid model treats plasma as a continuous fluid and solves a set of equations to obtain corresponding microscopic plasma parameters such as density, temperature, averaged velocity, pressure and so on. It needs to assume a velocity distribution function to determine the transport coefficients for fluid simulations, where the Maxwell-Boltzmann distribution is often assumed.

The fluid model is usually accurate, when the plasma is high-density and collisional [ 79 ]. Kinetic models of plasma do not need to assume a Maxwell-Boltzmann distribution for plasma velocity but to determine the particle velocity at each point and spatial distributions of the charged particles in plasma. It is often used to describe the collisionless plasmas in extremely low pressures [1]. Sometimes, the fluid modelling is combined with the kinetic method and became the so-called hybrid method.

In modelling large-size plasmas, fluid model is generally a much better choice than kinetic method that is more computationally intensive than fluid approach, for example,

modelling the discharges in the MPTs in present thesis. Furthermore, even with the fluid method, modelling the MPTs especially in multiple dimensions is also very computationally demanding [80, 81].

In fact, to the author's knowledge, only a few numerical plasma simulations have been conducted to investigate the MPTs especially in two or three dimensions. In 2007, a two-dimensional model was proposed regarding the discharge properties within a lathy glass tube in a MPT operating at the microwave frequency of 915 MHz [65]. In 2013, a MPT was modelled with emphasis on the distributions of plasma parameters under a high gas inflow rate in two dimensions [66]. In 2016, V. Georgieva compared the classic drift-diffusion approximation and the simplified ambipolar diffusion approximation in modelling the discharges in a waveguide-based MPT with fluid model at intermediate pressure [67]. Recently, M. Baeva [82] established a three-dimensional model based on fluid method to simulate the argon plasmas under atmospheric pressure in a waveguide-based MPT and compared the results from a two-dimensional simulations.

In our team, we proposed a two-dimensional axisymmetric fluid mode to numerically study the surface wave formation and the plasma column sustentation in a MPT operating at 2.45 GHz [51]. Besides, we improved the two-dimensional mode, having investigated the gas flow effects on the discharge properties and the travelling wave propagation in waveguide-based MPT [69].

## 4.2 Simplification of the calculation domain

### 4.2.1 Geometrical model and calculation domain

The discharges in the MPTs involves microwave propagation and attenuation, complex plasma chemistry, transport of different species, energy and momentum conservations. When describing it with even the much simpler fluid method, the mathematical model is still a large and strongly nonlinear equation system. It requires a dense mesh structure and a considerably long time to achieve a solution with a proper convergence, especially in three dimensions. Therefore, we start from a much simpler two-dimensional mode, in which only the cylindrical discharge tube is considered in the calculation.

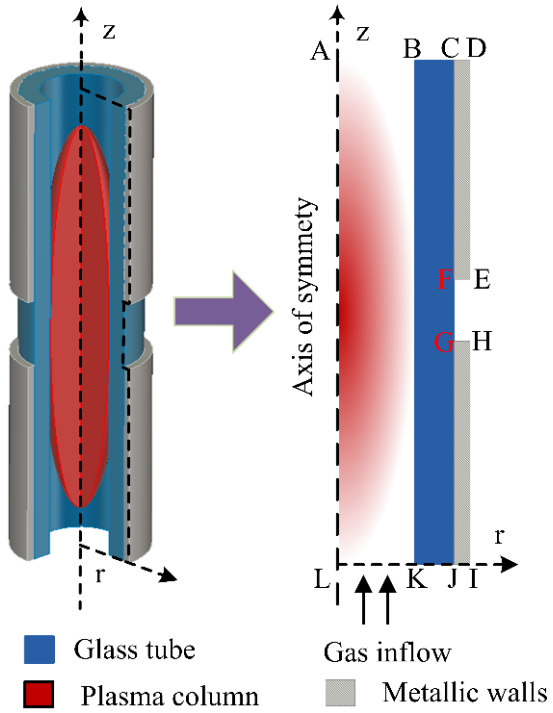


Figure 4.1 Axisymmetric simplification of the calculation domain in two dimensions.

In chapter 2, we have given two waveguide-based MPTs, which actually share the same structure of the discharge tubes (glass tube plus the metallic enclosure). Figure 4.1 shows the schematic structure of the discharge tube and the axisymmetric simplification applied to the calculation domain. Detailed discussion about the validity and the limitations of this simplifications is given in the following section.

Table 4.1 gives the geometrical size of the computational domain as an example for the calculations in next chapter.

Table 4.1 Geometrical size of the computational domain.

| Object | Length | Object | Length |
|---|---|---|---|
| AB/LK | 12mm | AL/BK/CJ/DI | 150mm |
| BC/KL | 3mm | FG | 20mm |
| CD/FE/GH/JI | 2mm | CF/DE/GJ/HI | 65mm |

### 4.2.2 Validity and limitation of the two-dimensional axisymmetric simplification

In fact, the axisymmetric simplification of the computational domain is based on the assumption that the electromagnetic wave electric field in the discharge tube is

azimuthally symmetric. The same simplification method can be also found in references [65, 66, 67].

For the MPTs with metallic enclosure in present thesis, the axisymmetric simplification is only valid when the travelling wave in the discharge tube propagates in pure TEM mode (azimuthally symmetric mode), according to our analysis in Chapter 2. It means that the plasma column is required to be able to form the two-conductor-like waveguide with the metallic enclosure. The argon plasma in MPTs under atmospheric pressures can meet such a requirement, because it generally has an electron number density larger than $10^{19}m^{-3}$ and the collision frequency higher than $10^{10}$ Hz [83, 84].

Besides, the axisymmetric simplification is valid in the following two cases:

(1) For the one-port and two-port MPTs in Figure 2.1, the thickness and the relative permittivity of the glass tube allow only the pure TEM mode to exist, as shown in Figure 2.5 in Chapter 2.

(2) For the two-port MPT particularly, when the microwaves come from both ports with the same frequency, phase and power, the travelling wave in the discharge tube still propagates mainly in TEM mode, although the discharge tube allows higher-order non-axisymmetric $TE_{11}$ mode to exist.

Except the above two circumstances, the axisymmetric simplification can not be used to simplify the calculation domain of the discharge tubes of the MPTs shown in Figure 2.1, because the travelling wave electric field in the discharge tube is not axisymmetric anymore.

For a two-dimensional model with the axisymmetric simplification in figure 4.1, if the material of the glass tube is quartz (relative permittivity is generally about 3.5-4), two-dimensional model can simulate the discharges in both case (1) and case (2), if the thickness of the glass tube wall is larger than 10 mm.

However, when the thickness of the glass tube wall is smaller than 10 mm, for example, the size in Table 4.1, higher-order $TE_{11}$ is able to be excited and the two-dimensional mode can be only used to case (2).

Besides this validity limitation, the axisymmetric simplification has introduced the following limitations as well, because it neglected the rectangular waveguide parts in calculation.

(a) The microwave electric field around the plasma column in the rectangular waveguide is assumed to be axisymmetric. In fact, it is not perfectly axisymmetric.

(b) Simplification in two dimensions disables direct evaluation of the important power coupling efficiency from $S_{11}$ parameter.

## 4.3 Two-fluid model of the microwave argon plasma under atmospheric pressure with ambipolar diffusion approximation

The discharges in MPTs are weakly ionized gases. Therefore, they are classified as the non-equilibrium plasmas, in which the electron temperature is much higher than the temperature of heavy species mixture (ions, excited and neutral atoms). The two-fluid model is one of the popular fluid methods, where the heavy species and electrons are described separately.

### 4.3.1 Chemical reactions of the atmospheric argon plasma

Table 4.2 shows 15 reduced reactions considered in our thesis, which keep the main feature of argon gas plasma chemistry [85, 86, 87].

Excited neutrals at different energy levels are lumped into two blocks: 4s block and 4p block at energy levels of 11.56eV and 13.17eV respectively.

Atomic ions Ar+ (15.76eV) and molecular ions $Ar_2$+ (15.01eV) are taken into consideration. It is worth noting that the molecular ions $Ar_2$+ are necessary in modelling argon plasmas under atmospheric pressure, because the dissociative recombination (reaction 11) can be the predominant electron loss process in high pressures [88].

Table 4.2 Reactions considered in this model

| No. | Reaction | Reaction Rate | $\Delta\varepsilon(\mathrm{eV})$ |
|---|---|---|---|
| 1 | e+Ar=>e+Ar(4s) | $5\times10^{-15}\left(\mathrm{T_e}\left[\mathrm{eV}\right]\right)^{0.74}\exp\left(\frac{-11.56}{\mathrm{T_e}\left[\mathrm{eV}\right]}\right)$ | 11.56 |
| 2 | e+Ar=>e+Ar(4p) | $1.4\times10^{-14}T_e^{0.71}\left[\mathrm{eV}\right]\exp\left(\frac{-13.17}{T_e\left[\mathrm{eV}\right]}\right)$ | 13.17 |
| 3 | e+Ar(4s)=>e+Ar(4p) | $8.9\times10^{-13}T_e^{0.51}\left[\mathrm{eV}\right]\exp\left(\frac{11.56-13.17}{T_e\left[\mathrm{eV}\right]}\right)$ | 1.61 |
| 4 | e+Ar(4s) =>e+Ar | $4.3\times10^{-16}T_e^{0.74}\left[\mathrm{eV}\right]$ | -11.56 |
| 5 | e+Ar(4p) => e+Ar | $3.9\times10^{-16}T_e^{0.71}\left[\mathrm{eV}\right]$ | -13.17 |
| 6 | e+Ar(4p) =>e+Ar(4s) | $3\times10^{-13}T_e^{0.51}\left[\mathrm{eV}\right]$ | -1.61 |
| 7 | e+Ar=>2e+$Ar^+$ | $2.3\times10^{-14}\left(\mathrm{T_e}\left[\mathrm{eV}\right]\right)^{0.68}\exp\left(\frac{-15.76}{T_e\left[\mathrm{eV}\right]}\right)$ | 15.76 |
| 8 | e+Ar(4s)=>2e+$Ar^+$ | $6.8\times10^{-15}\left(\mathrm{T_e}\left[\mathrm{eV}\right]\right)^{0.67}\exp\left(\frac{11.56-15.76}{T_e\left[\mathrm{eV}\right]}\right)$ | 4.2 |
| 9 | e+Ar(4p)=>2e+$Ar^+$ | $1.8\times10^{-13}\left(\mathrm{T_e}\left[\mathrm{eV}\right]\right)^{0.61}\exp\left(\frac{13.17-15.76}{T_e\left[\mathrm{eV}\right]}\right)$ | 2.59 |
| 10 | 2e+$Ar^+$ =>e+Ar | $8.75\times10^{-39}\left(\mathrm{T_e}\left[\mathrm{eV}\right]\right)^{-4.5}$ | -15.76 |
| 11 | e+$Ar_2^+$=>Ar+Ar(4s) | $1.04\times10^{-12}\left(\frac{\mathrm{T_e}\left[\mathrm{K}\right]}{300}\right)^{-0.67}\times\frac{1-\exp\left(-418/\mathrm{T}\left[\mathrm{K}\right]\right)}{1-0.31\exp\left(-418/\mathrm{T}\left[\mathrm{K}\right]\right)}$ | -3.45 |
| 12 | e+$Ar_2^+$=>e+Ar+$Ar^+$ | $1.11\times10^{-12}\times\exp\left(-\frac{2.94-3\times\left(\mathrm{T_e}\left[\mathrm{eV}\right]-0.026\right)}{\mathrm{T_e}\left[\mathrm{eV}\right]}\right)$ | 0.75 |
| 13 | 2Ar+$Ar^+$=> Ar+$Ar_2^+$ | $2.25\times10^{-43}\left(\frac{\mathrm{T}\left[\mathrm{K}\right]}{300}\right)^{-0.4}$ | |
| 14 | Ar+$Ar_2^+$=> 2Ar+$Ar^+$ | $5.22\times10^{-16}\exp\left(\frac{-1.304}{\mathrm{T}\left[\mathrm{eV}\right]}\right)\mathrm{T}^{-1}\left[\mathrm{eV}\right]$ | |
| 15 | e+M=>e+M (M=Ar, Ar(4s), Ar(4p)) | $\nu_m=\left\{\frac{5\times10^{-20}}{\left(1+1.7\times10^{-3}T_e\right)^2}-3\times10^{-21}+2.8\times10^{-24}T_e-4.1\times10^{-34}T_e^{\,3}\right\}\bullet\left(N_n+n_s+n_p\right)\bullet\left(\sqrt{\frac{8K_BT_e}{\pi m_e}}\right)$ | |

The reaction rates for processes 10 and 13 have units of $m^6/s$. The other reaction rates have units of $m^3/s$.

### 4.3.2 Microwave field - Helmholtz equation

In the MPTs, both the microwave in the rectangular waveguide and the travelling wave in the discharge tube are governed by the Helmholtz equation in frequency domain as follows:

$$\nabla \times \left( \mu_r^{-1} \nabla \times \vec{E} \right) - k_0^2 \left( \varepsilon_r - \frac{j\sigma}{\omega \varepsilon_0} \right) \vec{E} = 0 \tag{4.1}$$

where $\omega$ is the microwave angular frequency, $k_0$ is the free-space wavenumber, $\sigma$ is the conductivity, and $\varepsilon_r$ is the relative permittivity. In the rectangular waveguide, $\sigma$ and $\varepsilon_r$ are respectively 0 and 1, corresponding to the electromagnetic properties of air. For the glass tube wall, $\sigma$ and $\varepsilon_r$ are respectively 0 and 3.5. In plasma, $\sigma$ is $\sigma_p$ in equation (2.1), when $\varepsilon_r = 1$. Equivalently, $\varepsilon_r$ can be $\varepsilon_{rp}$ in equation (2.2), when $\sigma = 0$.

With a two-dimensional axisymmetric modelling, the rectangular waveguide parts are neglected in calculation. Therefore, it can not model the power absorption and reflection from the incoming microwave in the rectangular waveguide. The total plasma-absorbed microwave power is a given parameter. The wave excitation in Figure 4.1 is modelled by the antenna boundary ($E_z = 1$ V/m on boundary FG), as described by M. Moisan [65]. Under this antenna boundary, the microwave power density can be obtained by:

$$Q_{anten} = \frac{1}{2} \mathrm{Re}(\sigma_P \vec{E} \bullet \vec{E}^*) \tag{4.2}$$

Here, *Re* denotes the real part of the expression and $*$ denotes the complex conjugate. If we do an integration to $Q_{anten}$ in the plasma volume, the plasma-absorbed power density can be obtained under a given total power $P_{total}$.

$$Q_{EM} = \frac{P_{total}}{\iiint_v Q_{anten} d_v} Q_{anten} \tag{4.3}$$

### 4.3.3 Number densities of different species - Continuity equations based on the mass conservation law

The transport of each species in the plasma is described by a set of continuity equations based on mass conservation law.

$$\nabla\bullet\left(-D_k\nabla n_k\right)+\left(\vec{u}\bullet\nabla\right)n_k=R_k \tag{4.4}$$

where $n_k$ is the species number density of species $k$, $D_k$ is the corresponding diffusion coefficient, and $R_k$ is the species source term dominated by the plasma chemistry. The index $k$ indicates the atomic ions Ar+ ($k$=$i$1), the molecular ions $Ar_2$+ ($k$=$i$2), the excited species Ar(4s) ($k$=s) and Ar(4p) ($k$=p). $\bar{u}$ is the plasma bulk flow velocity, it donates to the forced species convection and it also contributes to the species loss.

According to the plasma chemistry in Table 4.2, the species source term of each component in equation (4.4) can be determined by the following equation:

$$R_k=\sum_N^M k_N n_i n_j \tag{4.5}$$

Here, $N$ and $M$ are the serial number and the total amount of reactions that involve species $k$, respectively. $k_N$ is the reaction rate of reaction $N$, $n_i$ and $n_j$ are the number densities of the corresponding reactants. It is worth to note that the process 10 and 13 are three-component reactions that contribute to the species source with the form $k_{10}n_e n_e n_{i1}$ and $k_{13}N_n N_n n_{i1}$. $N_n$ is the number density of the ground-state argon atom, which can be estimated from the ideal gas law in equation (4.11).

### 4.3.4 Temperatures of electrons and heavy species mixture - Heat transfer equation based on the energy conservation law

All the heavy species, including ions, excited atoms and ground-state neutral atoms, are assumed to share a common temperature $T$, which is different from the electron temperature $T_e$. They are described by two energy balance equations respectively as follows:

$$\nabla\bullet\left(\frac{5}{2}K_B T_e\vec{\Gamma}_e-\frac{5}{2}K_B n_e D_e\nabla T_e\right)+\left(\vec{u}\bullet\nabla\right)\left(\frac{3}{2}T_e K_B n_e\right)=Q_{EM}-Q_{el}-Q_{inel} \tag{4.6}$$

$$\nabla\bullet\left(-k_h\nabla T\right)+\rho_h C_p\vec{u}\bullet\nabla T=Q_{el}+Q_{inel} \tag{4.7}$$

Here, $K_B$ is the Boltzmann constant, $T_e$ is the electron temperature in Kelvin, $T$ is the heavy species mixture temperature in Kelvin as well, $n_e$ is the electron number density, $\overrightarrow{\Gamma_e}$ is the electron number density flux, $D_e$ is the electron free diffusivity, which can be obtained from the Einstein relations [51], with the electron elastic collision frequency.

$Q_{EM}$ is the plasma-absorbed power density from the travelling wave in the discharge tube, which is the only external energy source for the plasma and can be determined from equation (4.3). $Q_{el}$ and $Q_{inel}$ are the power density change due to electron elastic collisions (reaction No.15 in Table 4.2) and inelastic collisions (reactions No.1-12 in Table 4.2) respectively, as given in equations (4.8) and (4.9) accordingly.

$$Q_{el} = \frac{3}{2} n_e K_B \frac{2m_e}{m_{Ar}} \nu_m \left(T_e - T\right) \tag{4.8}$$

$$Q_{inel} = q \sum_{N}^{12} k_N n_e n_j \Delta\varepsilon_N \tag{4.9}$$

$m_{Ar}$ is the argon atomic mass weight. 12 is total amount of the electron collision reactions, and $\triangle\, \varepsilon(eV)$ is the energy loss per electron in the reaction $N$. In weakly-ionized plasmas, electrons initially absorb the energy from the sustaining travelling wave, and then transfer their energy to the heavy species via electron elastic and inelastic collisions. Therefore, $Q_{el}$ and $Q_{inel}$ are negative sources for the electron temperature and positive sources for the heavy species temperature.

$k_h$ is the thermal conductivity of the heavy species mixture, which is a temperature-dependent parameter and approximately equals to $3.5 \times 10^{-4} T[K]^{0.68}$. Because the argon gas in this study is weakly ionized, the thermal capacity $C_p$ of the heavy species mixture is set to $520\, J/\left(K_g \cdot K\right)$, which is same as that of argon gas under atmospheric pressure. $\rho_h$ is the mass density of the heavy species mixture without electrons, which is the total mass density of ions, excited and ground-state atoms. Due to the huge mass weight difference between the electron and the argon atom, it is reasonable to assume that $m_{Ar} = m_{Ar(4s)} = m_{Ar(4p)} = m_{Ar+} = 0.5 m_{Ar_2+}$. Therefore, $\rho_h$ can be obtained with the following equation:

$$\rho_h = N_n m_{Ar} + n_s m_{Ar} + n_p m_{Ar} + n_{i1} m_{Ar} + n_{i2} 2m_{Ar} + n_e m_e \tag{4.10}$$

$N_n$ can be determined by the ideal gas law as follows:

$$P = N_n K_B T + n_e K_B T_e + n_s K_B T + n_p K_B T + n_{i1} K_B T + n_{i2} K_B T \tag{4.11}$$

$P$ is the spatially-distributed pressure obtained from the Navier-Stokes equation.

### 4.3.5 Gas flow - Navier-Stockes equations based on mass and momentum conservation laws

Based on estimation of the Reynolds number in equation (4.12), it is able to identify whether the gas flow is a laminar flow or a turbulent flow. For the argon gas flow in the MPT having a glass tube with the inner diameter of 24 mm (Table 4.1), a laminar flow can be ensured, when the gas inflow rate is smaller than 20 L•min$^{-1}$. (The transition to a turbulent flow in pipes occurs generally when $R_e \approx 2300$)

$$\mathrm{Re} = \frac{\rho u d}{\mu} \tag{4.12}$$

A laminar gas flow can be described by the Navier-Stokes equation (4.13) with a mass conservation constrain (4.14) as follows:

$$\rho\left(\vec{u}\bullet\nabla\right)\vec{u} = -\nabla P + \nabla\bullet\left[\mu(\nabla\vec{u} + (\nabla\vec{u})^T) - \frac{2}{3}\mu(\nabla\bullet\vec{u})\vec{I}\right] \tag{4.13}$$

$$\nabla\bullet\left(\rho\vec{u}\right) = 0 \tag{4.14}$$

where $\mu$ is the dynamic viscosity, $\vec{I}$ is the unit tensor, $P$ is the pressure and $\rho$ is the plasma mass density including electrons. Since the electron mass density is negligibly small, the mass density of the heavy species mixture $\rho_h$ is approximately equal to plasma mixture mass density $\rho$ with electrons.

### 4.3.6 Ambipolar diffusion approximation based on the electric neutrality.

One may have noticed that there are no equations above to describe the electron number density $n_e$ and the electron number density flux $\overrightarrow{\Gamma_e}$. In fact, in this thesis, we did not follow the classic fluid model with drift-diffusion approximation. Instead, we made use of the ambipolar diffusion approximation, which is can be deduced from the classic drift-diffusion flux with two additional assumptions [ 89 ]. The first one is the assumption of electric neutrality of the plasma. With this assumption, the electron number density can be estimated as follows:

$$n_e = n_{i1} + n_{i2} \tag{4.15}$$

We do not need to solve another continuity equation to obtained the electron number density.

Besides, another assumption is that the plasma is highly collisional ($n_e$>$10^{14}$ $m^{-3}$) [89]. In this case, the highly dense charged particles will naturally form a strong space-charge electric field making the positive charge flux approximately equal to the negative one. Therefore, we have:

$$\overrightarrow{\Gamma_e} = \overrightarrow{\Gamma_{i1}} + \overrightarrow{\Gamma_{i2}} = -D_{i1}\nabla n_{i1} - D_{i2}\nabla n_{i2} \tag{4.16}$$

$D_{i1}$ and $D_{i2}$ are the ambipolar diffusion coefficients [89] for the atomic ions and molecular ions respectively, and are determined by:

$$D_k \approx D_{f,k}\left(1+\frac{T_e}{T}\right) \tag{4.17}$$

$D_{f,k}$ is the free diffusivity of ions. Detailed description about the ambipolar diffusion approximation can refer to references [67, 89].

Because of the two assumptions made in equations (4.15) and (4.16) above, the fluid mode with ambipolar diffusion approximation has the following limitations:

a) Due to the electric neutrality assumption in equation (4.15), the non-neutral plasma sheath is neglected in the calculation. Consequently, the microwave-plasma energy coupling is incomplete in our model. Specifically, the plasma-absorbed microwave power is underestimated because the microwave energy deposited in the sheath is neglected. The power density change due to the space-charge electric field is ignored. Consequently, electron temperature and density are overestimated, and the temperature of heavy species mixture is underestimated.
b) It is not valid at extremely low pressures, because plasmas in these cases generally have a thick sheath that can not be ignored.
c) To derive the equation of ambipolar diffusion coefficients (4.17), it is assumed that the number density distributions of ions has similar shapes. It may introduce difference between the fluid models with the ambipolar diffusion approximation and the classic drift-diffusion approximation, for the plasmas with multiple kinds of ions [90].

However, despite the limitations above, the fluid mode with ambipolar diffusion approximation is still very popular in modelling the discharges both in the waveguide-

based MPTs and the coaxial surfatron MPT. Relevant numerical fluid modelling can be found in references [65, 66, 67, 91]. It is popular because of the following advantages over the classic drift-diffusion approximation:

(1) The mathematical model has been greatly simplified. Calculation of the static electric field due to space charge from Poisson equation is reduced. It contributes greatly to the convergence of the fluid model, when solving it numerically.

(2) The continuity equation to calculate electron number density is reduced, thereby, contributing to reduce the couplings between each equation.

(3) The continuity equations to describe the transport of each species has been simplified to the diffusion-convection equation form, which enables to solve the equation system in stationary state.

Although the ambipolar diffusion approximation has inevitably introduce errors in modelling the discharges in the MPTs, we believe the errors are acceptable because of the following reasons:

(a) In the cases similar to ours (atmospheric plasma under the microwave radiation at the frequency of 2.45 GHz) [7, 83, 84], typical values for the electron number density and the electron temperature are generally on the order of $10^{19}$-$10^{21}$ $m^{-3}$ and 1-2 eV, respectively. Hence, the Debye length of the plasma $\lambda_D = \sqrt{\varepsilon_0 T_e / e n_e}$ is estimated as $7.43\times10^{-5}$ mm to $3.32\times10^{-4}$ mm, which is approximately equal to the thickness of the non-neutral plasma sheath. Compared with the inner radius of the glass tube (12 mm), it is reasonable to neglect the extremely thin non-neutral plasma sheath and assume quasi-neutrality in the discharge tube. Furthermore, under such a high number density of the charged species ($10^{19}$-$10^{21}$ $m^{-3}$), a slight difference between the distributions of electrons and ions will result in a strong space-charge electric field, which in turn forces the electrically negative electron flux approximately equal to the positive ion flux. Therefore, it is reasonable to apply the ambipolar diffusion approximation in this study.

(b) In 2017, a joint research group from Belgium and Netherland [67] compared the ambipolar diffusion approximation with the classic drift-diffusion approximation in modelling the surface-wave-sustained plasma in a waveguide-based MPT (Pressure: 1000 Pa, Power: 50-200 W). Part of the results were even validated by

experiments. The results from both approximations agree with each other in general, although there indeed exists some difference. Under atmospheric pressure and larger microwave deposition powers, the non-neutral plasma sheath will become much thinner and the ambipolar diffusion approximation will be naturally more valid.

### 4.3.7 Transport properties of each species

Seeking the valid transport coefficients for the heavy species under different conditions is always a problem in the plasma fluid modeling [92]. In present thesis, the transport coefficients of the heavy species ($D_s$, $D_p$, $D_{f,k}$) are calculated from a more general Wilke's formula are calculated [93] with the binary diffusion theory [94, 95], which gives the model more flexibility under different conditions compared with the limited E/N data from experiments.

### 4.3.8 Boundary conditions

For the microwave field, only the plasma column part and the glass are considered in the calculation domain. The metallic shielding walls are treated as the perfect electric conductors (PEC). An antenna excitation boundary is imposed on FG as in equation (4.18), which simulates the normalized input microwave electric field at the glass tube walls in the waveguide.

$$E_z = 1 \text{ V/m} \tag{4.18}$$

where $E_z$ indicates the z component of the microwave electric field. Because of the exposure to the air, the inlet and outlet of the discharge tube (AB, BC, LK and KJ) are modeled by the scattering boundary conditions as follows:

$$\vec{n} \bullet \nabla E_z + \mathrm{i} k_0 E_z = 0 \tag{4.19}$$

$\vec{n}$ is the outward normal vector of the corresponding boundary. For the plasma species continuity equations, only the plasma column part is considered in the calculation domain. When the electrons, ions and excited atoms reach the glass tube wall, these particles are assumed to be absorbed by the wall [96]. To describe this kind of particle loss, a set of Neumann boundary conditions are applied on the inner glass tube wall (BK) as follows:

$$\vec{n}\bullet\left(-D_k\nabla n_k\right)=\frac{1}{4}n_k\sqrt{\frac{8K_BT}{\pi m_k}} \tag{4.20}$$

Correspondingly, the electron energy conservation equation has the same calculation domain, and the electron kinetic energy loss due to the electron surface quenching reactions can be given by:

$$\vec{n}\bullet(\frac{5}{2}K_BT_e\overrightarrow{\Gamma_e}-k_e\nabla T_e)=\frac{5}{2}K_BT_e\left(\frac{1}{4}n_e\sqrt{\frac{8K_BT_e}{\pi m_e}}\right) \tag{4.21}$$

The entire discharge tube, including the plasma column part, the glass and the metallic shielding conductors, is considered in the calculation domain of the energy conservation equation for the heavy species. A set of surface-ambient radiation boundaries [97] are imposed on the outer walls of the metal and the glass tube (BC, CD, DE, EF, FG, GH, HI, IJ, JK), and are given by:

$$\vec{n}\bullet\left(-k_h\nabla T\right)=\beta K_{SB}\left(T^4-{T_{amb}}^4\right) \tag{4.22}$$

$\beta$ is the emissivity of copper or quartz glass depending on the material. In our study, they are set to 0.5 and 0.9 for the copper and the quartz glass respectively. $K_{SB}$ is the Stefan-Boltzmann constant. $T_{amb}$ is the temperature of the surrounding environment, which is assumed to be 293.15 Kelvin. From physical point of view, the more realistic boundary should include both the unforced natural air convection cooling and the thermal radiation. However, for a small-diameter vertical cylinder (discharge tube) in our case, the contribution of the natural convection cooling is much smaller compared with the thermal radiation [97, 98]. (The thermal radiation is approximately five times larger than the air convection cooling when T=1000 ℃). Besides, taking account of the natural convection cooling greatly decreases the calculation convergence. Therefore, the natural convection air cooling is neglected and only the thermal radiation is considered in the thermal boundary condition (4.22).

However, this boundary is still a compromise option in our study and its validity is limited when the temperature on the outer walls of the metal is low (low plasma-absorbed microwave power) or the radius of the discharge tube is large. Although this boundary condition is not perfectly realistic, it is much improved compared with the simpler Dirichlet boundary condition imposing a constant temperature on the inner glass tube walls in other studies [65, 66, 67, 69].

For the gas flow equation, the gas inflow velocity at the gas inlet (LK) is given by:

$$u_{in} = \frac{2\phi}{\pi R^2}\left[1-\left(\frac{r}{R}\right)^2\right] \tag{4.23}$$

where $\phi$ is the gas inflow rate, $R$ is the inner radius of the glass tube, and $r$ is the radial coordinate of the gas inlet. The pressure at the gas outlet (AB) is set to an atmospheric pressure $P_0$, and its boundary condition is described as:

$$\vec{n}\bullet\left[-P\vec{I}+\mu(\nabla\vec{u}+(\nabla\vec{u})^T)-\frac{2}{3}\mu(\nabla\bullet\vec{u})\vec{I}\right]=-P_0 \tag{4.24}$$

## 4.4 Numerical implementation and calculation procedure

### 4.4.1 Numerical implementation

The mathematical model can be implemented and solved in a commercial software package named COMSOL Multiphysics with its user-defined PDE interface. The total number of the mesh elements is 34732. A frequency-stationary solver is chosen to solve the equations. The segregated convergence criterion is 0.001 and the relative tolerance is 0.01. The model is calculated on a computer with an i7-5500U CPU and 16GB of RAM. It takes approximately 2 hours to complete one calculation of the model.

### 4.4.2 Calculation procedure

Figure 4.2 shows procedure of the numerical calculation in COMSOL Multiphysics. The calculations start with assumed initial values for different species continuity equations along with a given gas inflow rate and a microwave deposited power. Within a loop, each segregated PDE has its own convergence criterion to control the number of iteration steps. The iteration will stop and go to the next PDE when it meets the convergence criterion ((Current results-Results in last iteration)/ Results in last iteration< Convergence criterion). Out of the loop, there is also a relative tolerance to control the number of loops. The convergence criterion is similar ((Current results-Results in last loop)/ Results in last loop< Relative tolerance).

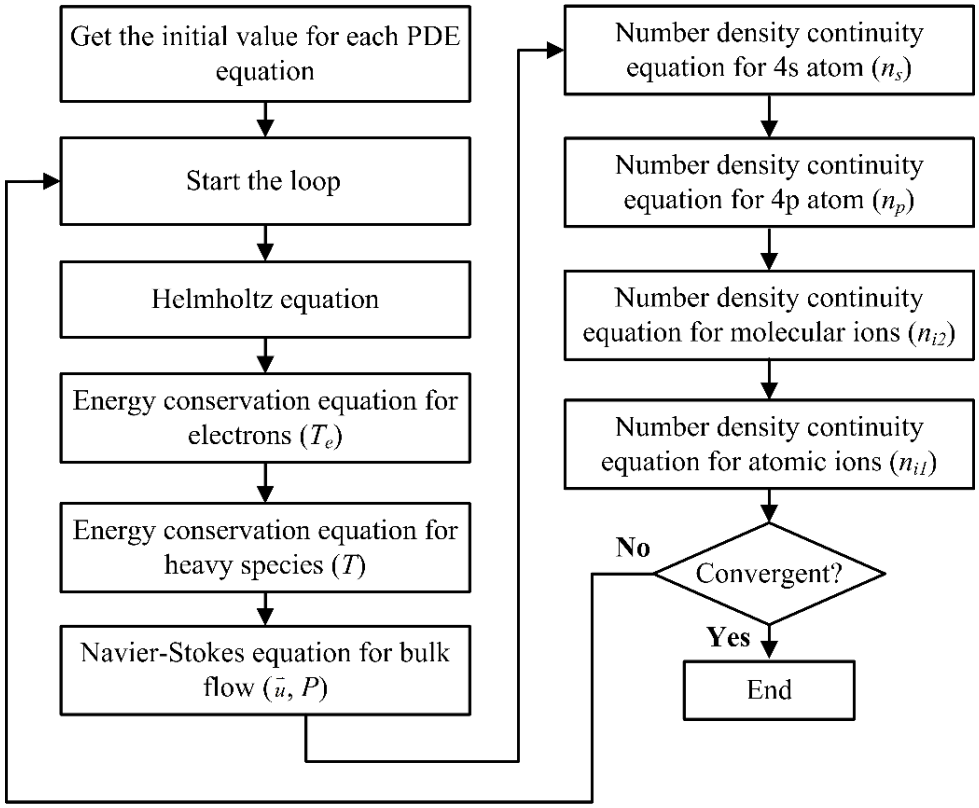


**Figure 4.2** Calculation procedure

## 4.5 Conclusion

In this chapter, we have proposed a two-dimensional axisymmetric fluid model based on the ambipolar diffusion approximation to characterize the argon discharges in MPTs under atmospheric pressure. The major approximations applied in the model are the axisymmetric simplification to the calculation domain in Figure 4.1 and the ambipolar diffusion approximation. Their validity and limitations have been discussed in details and given in section 4.22 and 4.3.6 respectively. The validity and limitations of this model should be carefully treated, when extending it to other cases. Actually, a fluid model in three dimensions without these limitations is our final goal.

# Chapter 5 Wave propagation and discharge maintenance in a MPT under different operation conditions

## 5.1 Background

As we previously showed in chapter 1, there are some phenomena and problems in the applications of MPTs remain unclear or unsolved. In many experiments [11, 99,7] including ours (Figure 3.8), it was observed that the plasma column length increases when the microwave input power goes up. A lot of people still tend to believe that the discharge occurs only in resonant cavity and the plasma column extension is the results of gas flow or particle density gradient. Regarding this problem, M. Moisan and his co-operators contributed a lot to explain it [100, 101, 102, 37]. However, as we analysed in chapter 2, the MPTs with metallic enclosure are a little different with the MPTs having discharge tubes exposed in air. Therefore, in this chapter, we will try to give some numerical insights for the wave propagation characteristics and the discharge maintenance mechanism in the MPT with metallic enclosure, with the two-dimensional fluid model in chapter 4.

Besides, in most industrial applications, the MPTs are required to have a high material disposal rate. The easiest way to achieve that is generally increasing the microwave power and the gas inflow rate. Meanwhile, a high gas flow velocity is expected to be helpful to cool down the glass tube and to prevent it from being overheated. However, it is found that the glass tube is melted even at a high enough axial gas inflow rate when the MPT is operated with an input microwave power at the level of several hundred watts [11, 103]. This glass overheating problem finally results in the power limitation of the MPT, and thereby limits its industrial applications. In our experiments, it was found that the gas flow greatly influences the plasma column in its length and shape, which has been also reported by other researchers [104, 105, 106, 107]. Moreover, it is observed that the discharge in the MPT becomes unstable with an increase in the gas inflow rate, and even becomes extinct when the gas inflow rate is

sufficiently high. Similar discharge instability and extinction have been observed in the experiments conducted by Sturm et al. [23] as well. All these problems require further investigations about the mechanism of the gas flow effects on the discharge.

Therefore, in this chapter, we will use the two-dimensional model based on fluid method in chapter 4 to

(1) Investigate the mechanism of discharge maintenance and plasma column extension with the increase of microwave power.

(2) Numerically investigate the wave propagation in discharge tube.

(3) Figure out reasons why the plasma column becomes short with the increase of the gas inflow rate.

(4) Figure out the reasons why it does not work to cool down the glass tube by increasing the gas inflow rate.

It is worth noting that only the cylindrical discharge tube was considered in the two-dimensional model in chapter 4and an axisymmetric simplification was applied to further simplify the calculation domain. The model with the geometrical sizes in Table 4.1 only corresponds to a two-port MPT, where the microwaves come from both ports with the same frequency, phase and power, as shown in Figure 5.1.

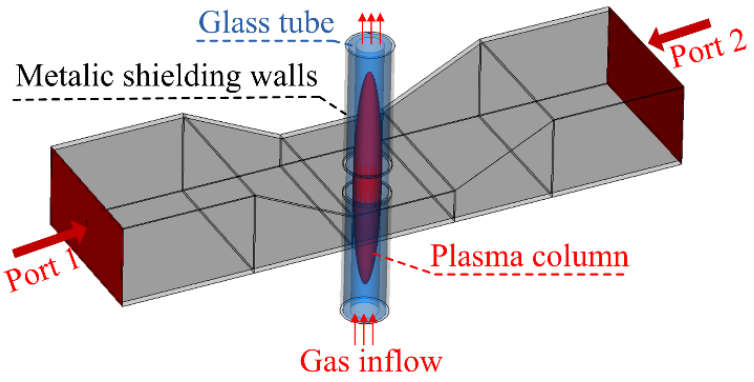


**Figure 5.1** Schematic diagram of the two-port MPT with microwave

## 5.2 Mechanism of plasma column extension and discharge maintenance

The results in section 5.2 are obtained with the two-dimensional model under different microwave powers (200-600 W) and a constant gas inflow rate of 1 L•min$^{-1}$.

### 5.2.1 Numerical modelling of the plasma column extension with the increase of microwave power

As one of the most noticeable plasma features, the variation of the plasma column length is often visually observed to record the discharge change in the MPTs. However, the plasma column we saw in experiments is a complicated plasma mixture. Its length variation involves complicated plasma collisional reactions and migrations of different species.

Electron, which has a much smaller mass weight and a higher mobility compared with ions and excited atoms, is the most active species in the plasma mixture and plays an important role in the discharge maintenance. Therefore, the change of the electron number density can provide a significant indication of the plasma column length variation.

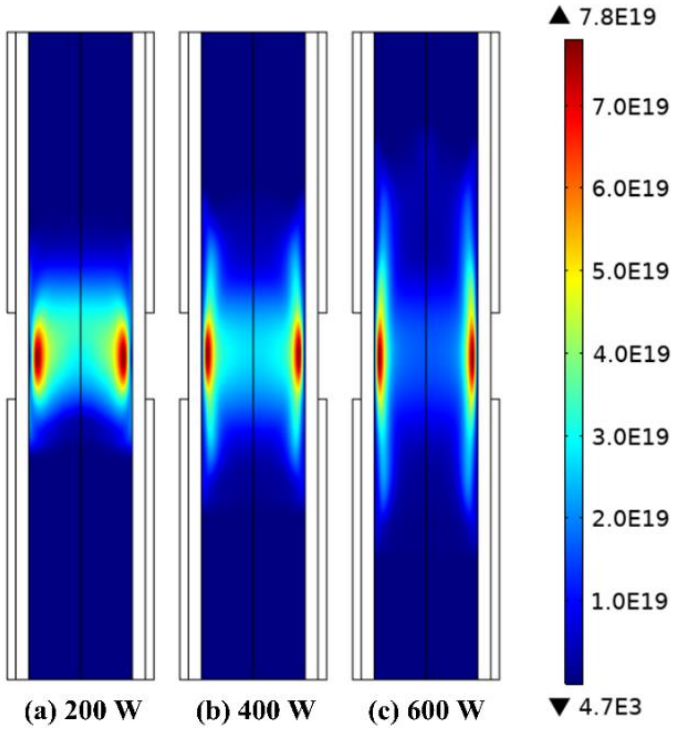


**Figure 5.2** Electron number density (units:1/m$^3$) for different plasma-absorbed microwave powers ($\emptyset = 1$ L • min$^{-1}$). (a) 200 W, (b) 400 W, (c) 800 W

Figure 5.2 shows the electron number density distributions for different plasma-absorbed microwave powers ($P_{total}$). In order to illustrate the results more lively, a mirror skill is used to present the data on a vertical slice of the cylindrical discharge tube. This skill is applied in the following figures as well.

With the increase of the plasma-absorbed microwave power, it can be observed in Figure 5.2 that the electron number density changes in the following three aspects:

1) The value of electron number density increases significantly.

2) The region with higher electron number density in the plasma column gradually moves close to the glass tube walls.

3) The region with higher electron density in the plasma column becomes increasingly longer in the axial direction.

To some extent, the change of the electron number density profile indicates the variation of the plasma column shape. The electron number density distribution implies that the plasma column is confined mainly within the interaction area between the cylindrical glass tube and the rectangular waveguide, when the total plasma-absorbed microwave power is low (200 W).

However, as the total plasma-absorbed microwave power increases, the plasma column becomes stretched and extends out from the rectangular waveguide area towards both ends of the glass tube. This numerical result regarding the plasma column extension agrees well with the experimental observations from both our works (Figure 3.8) and other studies [11, 99, 7]. Besides, the magnitudes of the electron number densities are also in the same orders as other numerical calculations with a similar MPT [66, 67, 82]. It can prove the validity of our numerical calculations.

### 5.2.2 Formation of the two-conductor-like waveguide structure

It is easy to get that a higher input microwave power brings more energy, resulted more ionizations and a higher electron number density. However, why the plasma column has such an electron number density distribution as shown in Figure 5.2 and why the plasma column extends towards both ends of the glass tube? It is actually associated with the propagation and attenuation of the travelling wave in the discharge tube. Detailed explanations will be given in the following paragraphs.

Figure 5.3 shows the distributions of the real part of relative plasma permittivity under different plasma-absorbed microwave powers.

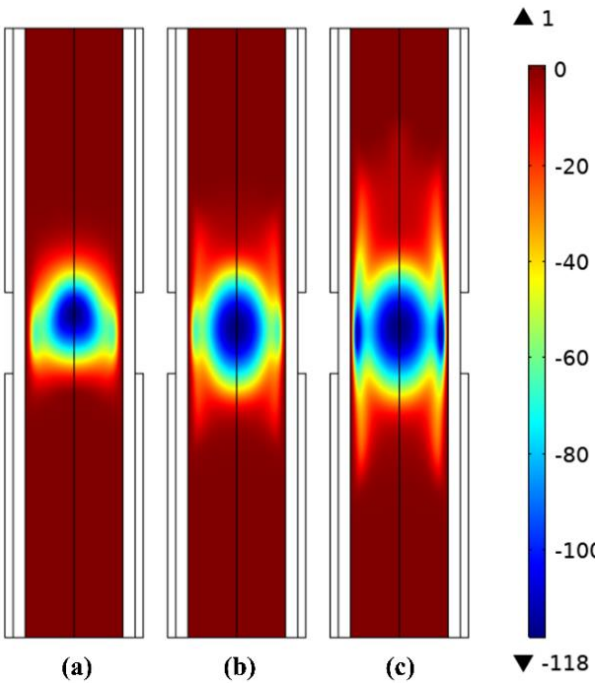


**Figure 5.3** Real part of the plasma relative permittivity for different plasma-absorbed microwave powers ($\emptyset = 1$ L • $\mathrm{min}^{-1}$). ). (a) 200 W, (b) 400 W, (c) 600 W

It can be seen that negative values can be found in the real part of relative plasma permittivity for the three plasma-absorbed microwave powers. However, there still exists some differences.

When $P_{total} = 200\ W$, the negative values focus mainly in the center of the plasma column and in the rectangular waveguide part. For the discharge tube parts out of the rectangular waveguide, the plasma still have positive real part of relative plasma permittivity. It indicates that the two-conductor-like waveguide structure has not be well formed for a small power of 200 W. It can be inferred that the input microwave is not able to propagate in the discharge tube for a long distance.

However, when the plasma-absorbed microwave power $P_{total}$ increases, the negative-value part of the relative plasma permittivity moves close to the inner glass tube wall and extends out of the rectangular waveguide as well. In this case, plasma column together with the outer metallic enclosure turns to be a two-conductor-like waveguide eliminating the cut-off limitation and allowing the input microwave to propagate in it.

Figure 5.4 shows correspondingly the real part of the plasma conductivity for different plasma-absorbed microwave powers.

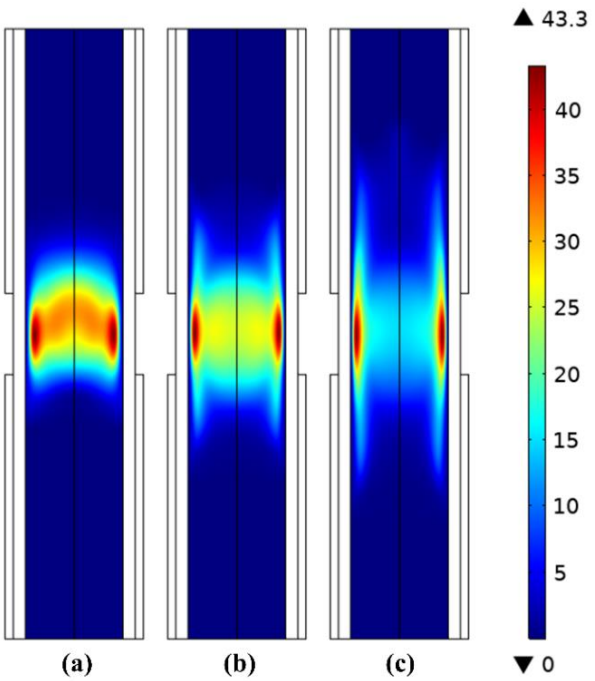


**Figure 5.4** Real part of the plasma conductivity (Units: S/m) for different plasma-absorbed microwave powers ($\emptyset = 1\ \mathrm{L} \bullet \mathrm{min}^{-1}$). (a) 200 W, (b) 400 W, (c) 600 W

Figure 5.3 and 5.4 demonstrate that the plasma column gets an increasing electrical conductivity, as the microwave power deposited into the plasma column continues to increase. Thus, when the plasma-absorbed microwave power increases, the plasma column obtains an increasing capability of shielding the microwave from penetrating into it. For a plasma-absorbed microwave power ($\mathrm{P}_{total} > 200\ W$), the two-conductor-like waveguide structure has formed for the discharge tube.

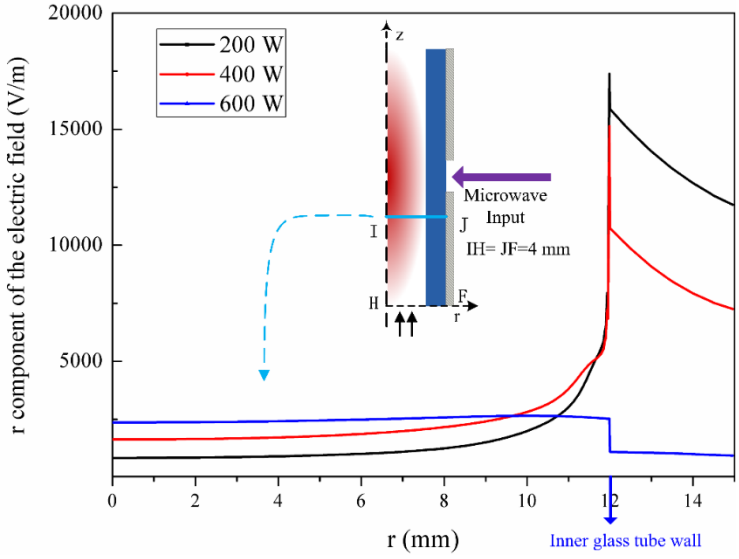


**Figure 5.5** Intensity of the microwave electric field r component (abs($E_r$)) for different plasma-absorbed microwave powers ($\emptyset = 1\ \mathrm{L} \bullet \mathrm{min}^{-1}$)

Figure. 5.4 presents the radial distribution of the microwave electric field intensity, which can illustrate the dependence of the microwave shielding ability of the plasma column on the plasma-absorbed microwave power.

It shows that the intensity of the electric field reaches a considerably high value at the interaction boundary of the plasma column (conductor) and the glass. Subsequently, it attenuates quickly within a small depth in the plasma column. The larger microwave power the plasma absorbs, the more conductive the plasma column is, the more difficultly the microwave can penetrate into the plasma column, the stronger capacity the plasma column obtains to shield the microwave.

Due to the microwave shielding, the electrons in the skin depth area obtained much more microwave energy compared with the electrons in the other regions of the plasma column, which resulted in a larger ionization rate and a higher electron number density in the skin depth area. Thus, a decrease in the microwave penetration depth will lead the higher electron density region in the plasma column to move gradually close to the inner glass tube wall, as shown in Figure 5.2.

All the analysis above demonstrate that the plasma column becomes increasingly conductive or reflective with the increase of the plasma-absorbed microwave power. However, being more conductive doesn't absolutely imply a greater reflection of the input microwave power.

Either before the discharge or when the plasma-absorbed microwave power is low enough, the electron number density can be lower than the critical electron number density. Thereby, the plasma column is not sufficiently conductive to be considered as a conductor, and the relative permittivity of the material in the discharge glass tube can be in the range between 0 and 1. In this case, the cylindrical discharge tube is a cut-off circular waveguide for the input microwave at the frequency of 2.45 GHz. Below is the calculation expression of the cut-off frequency for the lowest electromagnetic mode $TE_{11}$ of a circular waveguide.

$$f_{circular} = \frac{1.8412c}{2\pi R} \tag{5.1}$$

*R* is the inner radius of the discharge tube, and *c* is the speed of light in vacuum. The cut-off frequency of the cylindrical discharge tube under the current size is estimated as 5.8607 GHz without considering the influence the glass. 2.45 GHz, as the working

frequency of the MPT, is lower than this cut-off frequency. Thus, the discharge tube is cut-off for the input microwave and no propagating electromagnetic mode exists in it. However, when the plasma-absorbed microwave power is sufficiently high, the plasma column can be treated as a good conductor and the discharge tube becomes a two-conductor-like coaxial waveguide, allowing the input microwave to propagate in the discharge tube and sustain the discharge.

### 5.2.3 Wave dissipation and discharge maintenance

In the MPT, the input microwave is the only external source to sustain the discharge. Thus, propagation and dissipation of the travelling wave in the discharge tube become extremely vital for the discharge maintenance.

Although we have strongly emphasized the microwave shielding ability of the plasma column in the travelling wave formation section above, a part of the travelling wave still can enter the plasma column and be absorbed by the plasma column. Differed from the real good metal conductors such as copper (electric conductivity on the order of $10^7$ S/m typically), the plasma column has a relatively lower electric conductivity as shown in Figure 5.4. Thus, the microwave penetration depth into the plasma column is much larger than that into copper.

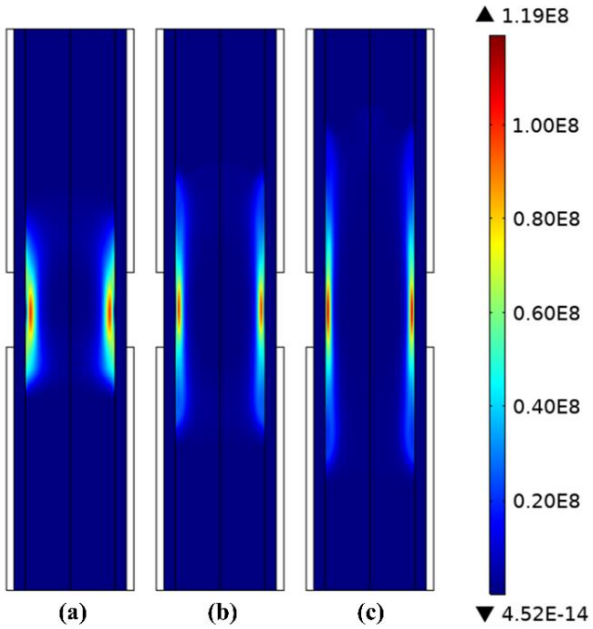


**Figure 5.6** Distributions of the plasma-absorbed microwave power density (Units: W/m$^3$) ($\emptyset = 1$ L • min$^{-1}$). (a) 200 W, (b) 400 W, (c) 600 W

Figure 5.6 presents the distributions of the plasma-absorbed microwave power density in the plasma column. It demonstrates that the travelling wave indeed has penetrated into the plasma column and deposited in it. Although the skin depths are limited, they are not as small as the skin depth of the good metal conductors such as copper. Typically, copper has a microwave skin depth on the order of 1 μm. It indicates that the plasma column has a much stronger potential to absorb the microwave, compared to the good metal conductors.

Figure 5.7 presents the imaginary part of the relative permittivity of the plasma column for different plasma-absorbed microwave powers. The highlight is the large absolute value of the imaginary part of the relative permittivity. It indicates that the plasma column has a strong capability to absorb the microwave power especially in the skin depth area. Once the input microwave penetrates into the plasma column, it will be absorbed by the plasma column quickly. Thus, the "coaxial waveguide" is a highly lossy waveguide for the travelling wave. As the travelling wave propagates along the plasma column, it dissipates within the microwave penetration depth as well.

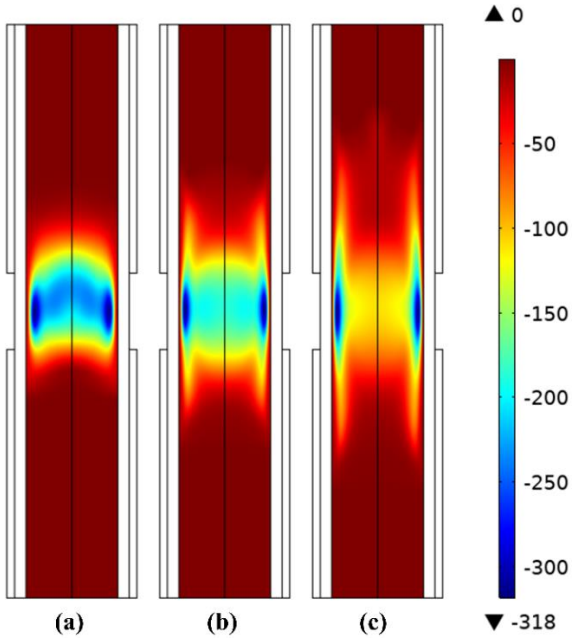


**Figure 5.7** Imaginary part of the plasma relative permittivity for different plasma-absorbed microwave powers ($\emptyset = 1\ \mathrm{L} \bullet \mathrm{min}^{-1}$). (a) 200 W, (b) 400 W, (c) 600 W

For the propagation of the travelling wave, smaller skin depth of the plasma column helps the travelling wave propagate in longer distance towards both the gas inlet and the outlet. More specifically, the larger microwave power that the plasma column has

absorbed, the higher electron number density it has, the smaller skin depth that the plasma column gets, and the longer distance that the travelling wave can propagate in.

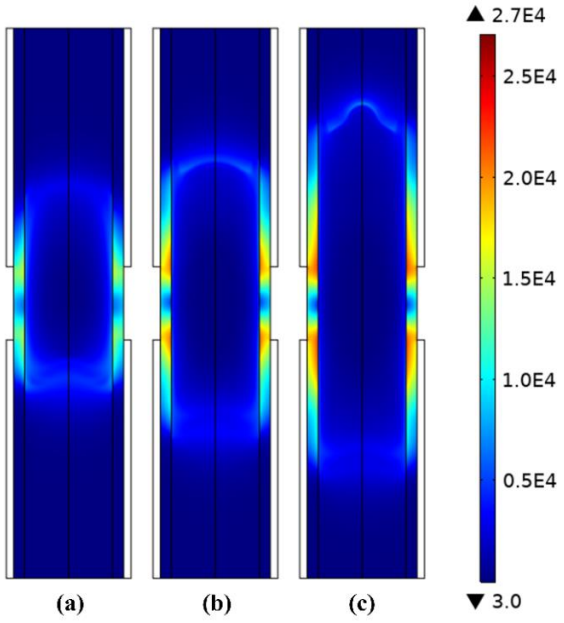


**Figure 5.8** Intensity of the microwave electric field in the discharge tube (Units: V/m) for different plasma-absorbed microwave powers ($\emptyset = 1\ \mathrm{L} \bullet \mathrm{min}^{-1}$). (a) 200 W, (b) 400 W, (c) 600 W

Figure 5.8 shows the microwave electric field intensity distributions in the discharge tube for three different plasma-absorbed microwave powers. When the total plasma-absorbed microwave power is low, the electromagnetic wave is restricted to exist primarily within the rectangular waveguide. The plasma column is not a good enough conductor to sustain the extension of the travelling wave out from the rectangular waveguide. As the plasma-absorbed microwave power grows, the electromagnetic wave starts to extend out from the rectangular waveguide and propagates along the plasma column towards both the gas inlet and the outlet, as shown in Figure 5.7 (b) and (c). Furthermore, it is notable that there is a high consistency between the microwave propagation distance in Figure 5.8 and the axial extension length of the plasma column in Figure 5.2. This consistency implies that the plasma column length is actually determined by the propagation distance of the travelling wave, because travelling wave is the only external source to sustain the plasma column.

In conclusion, the plasma column extension is actually driven by the travelling wave. The propagation of the travelling wave towards both the gas inlet and the gas outlet enables the plasma column to be extended in both directions. As the travelling wave propagates along the plasma column, the microwave power is deposited into the plasma

column to sustain the discharge within the microwave penetration depth. Besides, the propagation distance of the travelling wave actually determines the plasma column length under a low gas inflow rate.

## 5.3 Mechanism of plasma column shortening and glass overheating

The following results in section 5.3 are obtained with the two-dimensional model in chapter 4 under different gas inflow rates (1-20 $\mathrm{L} \bullet \mathrm{min}^{-1}$) and a constant plasma-absorbed microwave power ($\mathrm{P}_{total} = 500\ W$).

### 5.3.1 Numerical modelling of the plasma column shortening with the increase of gas inflow rate

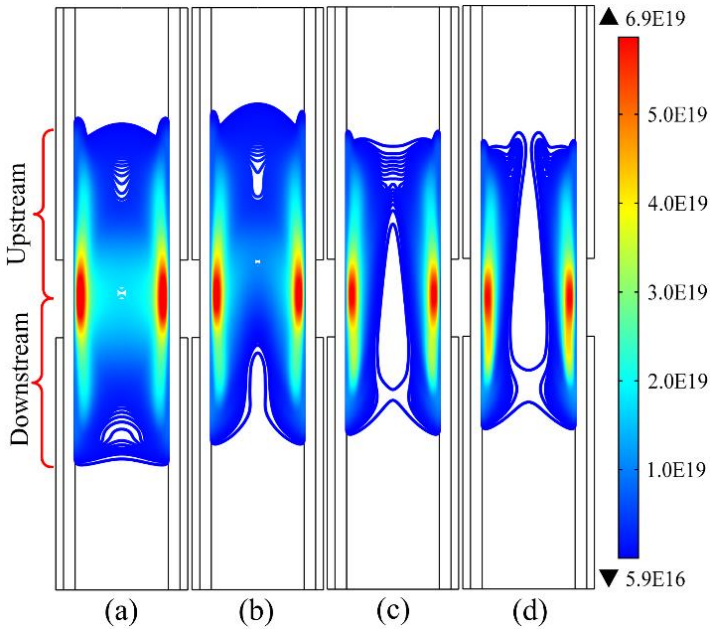


**Figure 5.9** Contour plot with 500 levels of the electron number density (units: $1/m^3$) for different gas inflow rates ($P_{total} = 500W$). (a) 1 L•min$^{-1}$, (b) 4 L•min$^{-1}$, (c) 10 L•min$^{-1}$, (d) 16 L•min$^{-1}$.

Figure 5.9 shows the electron number density distributions for four gas inflow rates. Due to the high electron number density gradients, 500 contour levels are chosen to illustrate the distributions of the electron number density. The blank parts only indicate the electron number density in these areas are lower than $5.9 \times 10^{16}\ (m^{-3})$, and do not mean that they are empty. In addition, Figure 5.9 presents the changes of the electron number density profile, which indicate the variation of the plasma column length.

It can be seen that the upstream plasma column length initially experiences a slight increase around the gas inflow rate of 4 L•min$^{-1}$. Subsequently, the upstream plasma column length decreases slightly with the increase of the gas inflow rate. In contrast, the downstream plasma column is shortened significantly throughout the increase of the gas inflow rate. These changes agree well with the phenomena observed in other experimental researches [104-107]. Furthermore, when the gas inflow rate increases, more electrons are carried out of the discharge tube by the increasingly strong convection. Consequently, the electron loss to the glass (surface reaction in the boundary condition section) becomes less important. As a result, the electron number density inside the plasma column falls down, and a "hollow hole" seems to occur in the center of the plasma column, when the gas inflow rate is higher (>10 L•min$^{-1}$). It indicates that the discharge does not entirely fill the radial cross-section of the glass tube, and this radial contraction [108] becomes increasingly strong as the gas inflow increases.

### 5.3.2 Wave propagation with the increase of gas inflow rate

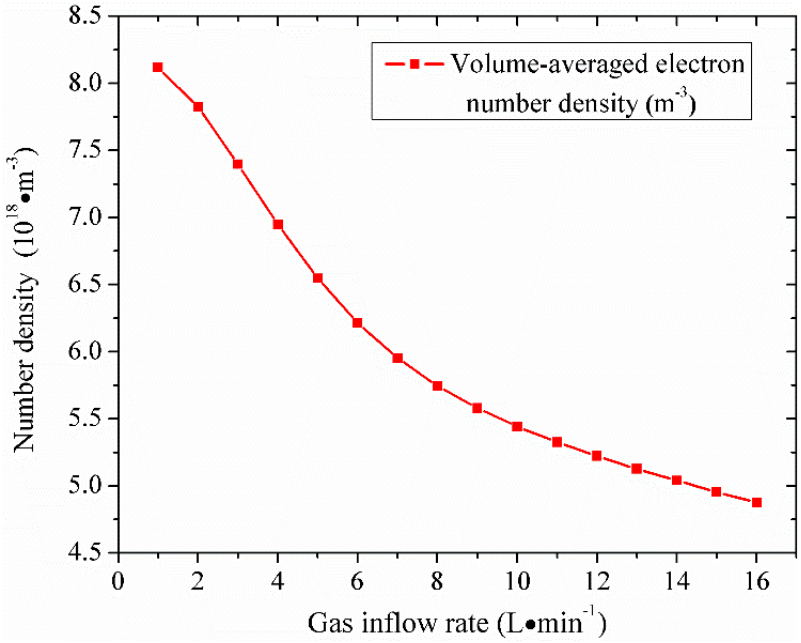


**Figure 5.10** Volume-averaged electron density change as a function of the gas inflow rate ($P_{total} = 500W$)

Figure 5.10 shows the decrease of the volume-averaged electron number density with the increase of the gas inflow rate. The volume average calculation in Figure 5.10 follows the expression $\overline{n_e} = \iiint n_e dv/V$, in which V indicates the volume of

cylindrical plasma domain. It can be observed in Figure 5.10 that the electron number density decreases significantly with the increase of the gas inflow rate. The reason is simple. When the gas inflow rate increases, the corresponding forced convection leads more plasma species out of the discharge tube resulting in a larger electron loss.

Despite the simple particle loss introduced by the increasingly strong convection due to the increase of the gas inflow rate, it is found that the change of the travelling wave propagation in the discharge tube also contributes a lot to the plasma column shortening.

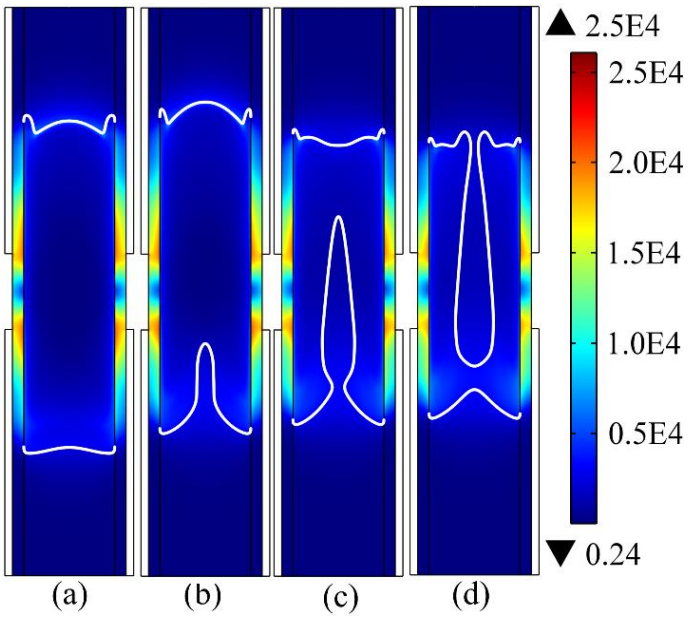


**Figure 5.11** Distributions of the microwave electric field intensity (units: V/m) for different gas inflow rates ($P_{total} = 500W$). (a) 1 L•min$^{-1}$, (b) 4 L•min$^{-1}$, (c) 10 L•min$^{-1}$, (d) 16 L•min$^{-1}$. The white curve indicates an electron number density contour at the level of $7.6 \times 10^{16}$ $(1/m^3)$.

Figure 5.11 shows the microwave electric field intensity for different gas inflow rates. A contour of the electron number density at the level of $7.6 \times 10^{16}$ $(m^{-3})$ is applied to highlight the change of plasma column length. $7.6 \times 10^{16}$ $(m^{-3})$ is an approximated critical electron number density [2] for the plasma under the microwave radiation at the frequency of 2.45 GHz. When the electron number density is high enough to exceed this critical value, the real part of the plasma permittivity becomes negative, and the plasma starts to behave like a conductor.

In the regions where $n_e > 7.6 \times 10^{16}$ $(m^{-3})$, the two-conductor-like "coaxial waveguide" forms, which allows the travelling wave to propagate in these regions. In the regions where $n_e < 7.6 \times 10^{16}$ $(m^{-3})$, these plasma column parts are not

conductive enough to be treated as conductors. Without the inner conductors, the "coaxial waveguide" in these regions turns back to be cylindrical waveguides that are cutoff for the microwave at frequency of 2.45 GHz. The travelling wave in these regions stops propagating and soon evanesces in a short distance, as can be seen in the regions near the gas inlet and outlet in Figure 5.11.

When the electron number density drops off with the increase of the gas inflow rate, the electric conductivity and the length of the inner conductor (plasma column) decrease as well, resulting in the change of the travelling wave propagation distance. Because the travelling wave is the only external energy source to sustain the discharge in the glass tube, the change of the travelling wave propagation distance introduced by the gas flow will in turn influence the plasma column length.

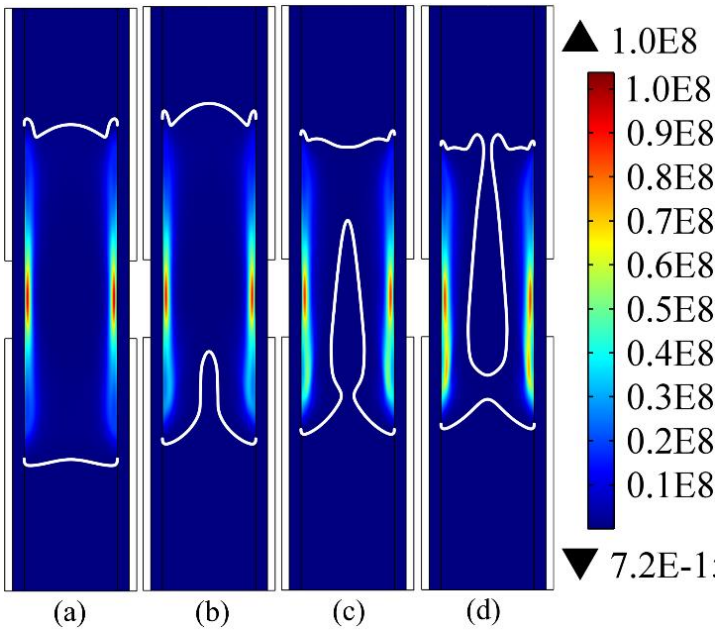


**Figure 5.12** Distributions of the plasma-absorbed microwave power density (units: W/m$^3$) for different gas inflow rates ($P_{total} = 500W$). (a) 1 L•min$^{-1}$, (b) 4 L•min$^{-1}$, (c) 10 L•min$^{-1}$, (d) 16 L•min$^{-1}$. The white curve indicates an electron number density contour at the level of $7.6 \times 10^{16}$ $(1/m^3)$.

Once the propagation distance of the travelling wave changes, the distribution of the microwave power density deposited into the plasma column varies accordingly. Figure 5.12 illustrates the changes of plasma-absorbed microwave power density for different gas inflow rates. It shows that the plasma has absorbed a negligibly small amount of microwave power density in the regions where $n_e < 7.6 \times 10^{16}$ $(m^{-3})$. Without the only external microwave energy supply, the discharges in these regions will soon fade out and become extinct, resulting in the decrease of the plasma column length.

Furthermore, based on Figure 5.10 and 5.11, we can reasonably infer that the propagation distance of the travelling wave will continue to decrease, when the gas inflow rate becomes increasingly large (> 20 L•min$^{-1}$). Finally, the travelling wave will disappear in the cylindrical discharge tube and microwave will only exist in the rectangular waveguide. Consequently, the discharge in the discharge tube of the MPT will become unstable and even extinct without the only external energy source (the travelling wave in the discharge tube).

In conclusion, the gas flow is able to influence the travelling wave propagation in the surface-wave-sustained plasma torch. The plasma column length contraction is not only because of the particle loss introduced by the increasingly strong gas flow convection but also because of the consequent reduction of the travelling wave propagation distance. Moreover, the absence of the travelling wave at a high gas inflow rate contributes greatly to the plasma column extinction and the discharge instability.

### 5.3.3 Glass overheating problem

Generally, industrial applications expect the MPTs to work under a high microwave power for a long enough time. However, as we illustrated in section 5.1, the glass tube is often overheated even at a low microwave power (<500 W) and a high gas inflow rate (>16 L•min$^{-1}$), which seriously limits the power capacity of the MPTs and slows their large-scale industrial applications. Therefore, it is significant to figure out how the gas flow influences the heavy species temperature and why the glass tube is overheated even at a high gas inflow rate.

Figure 5.13 shows the velocity distributions of the argon gas under four different gas inflow rates. When the gas inflow rate increases, the velocity field increases accordingly. However, it can be observed in Figure 5.13 that the velocity near the gas outlet (upstream part of the discharge tube) and glass inner wall has much higher values. This non-uniformity of gas flow velocity is because the gas flow even can get a response from the temperature change of the heavy species mixture.

Figure 5.14 presents the heavy species temperature distributions for four gas inflow rates. According to the ideal gas law, the mass density of the plasma mixture decreases, as the heavy species temperature goes up. In order to satisfy the mass conservation law,

the velocity in the higher-temperature areas will rise accordingly, which can be validated by comparing Figure 5.13 and Figure 5.14.

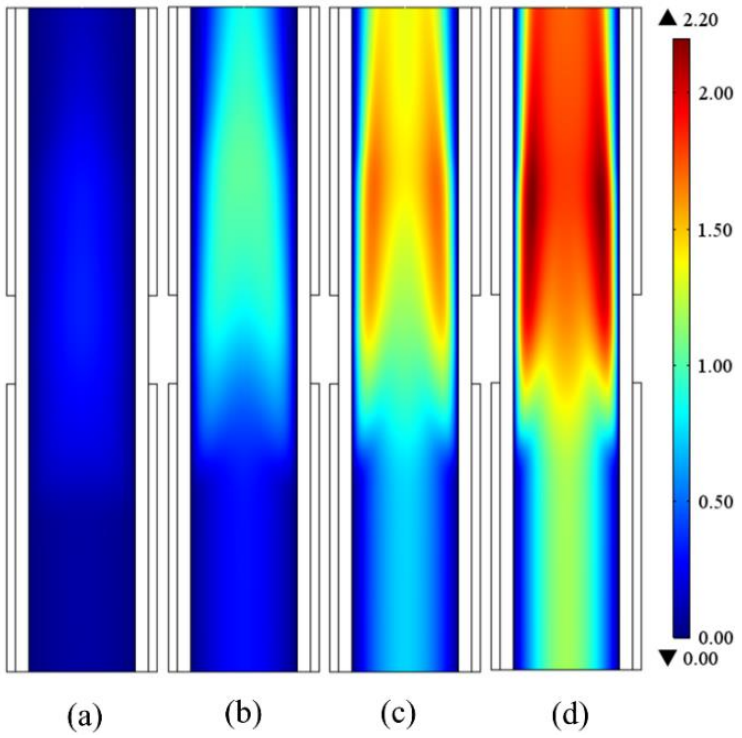


**Figure 5.13** Distributions of the gas flow velocity magnitude (units: m•s$^{-1}$) for different gas inflow rates. (a) 1 L•min$^{-1}$, (b) 4 L•min$^{-1}$, (c) 10 L•min$^{-1}$, (d) 16 L•min$^{-1}$.

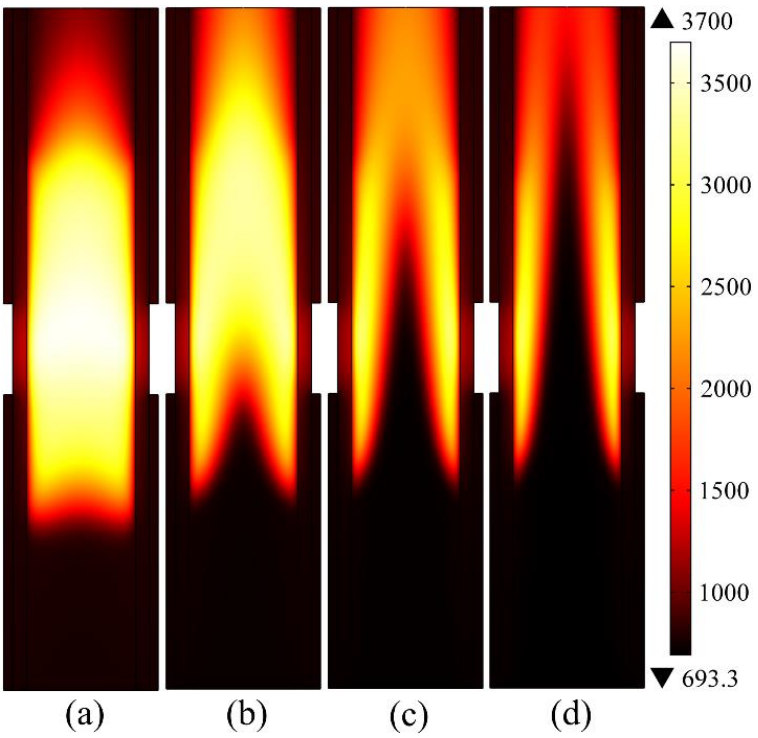


**Figure 5.14** Temperature distributions of the heavy species mixture (units: Kelvin) for different gas inflow rates. (a) 1 L•min$^{-1}$, (b) 4 L•min$^{-1}$, (c) 10 L•min$^{-1}$, (d) 16 L•min$^{-1}$.

Figure 5.14 shows a similar profile variation trend as the electron number density with the increase of the gas inflow rate in Figure 5.9. When the gas inflow rate is low, conduction is the predominant heat transfer mechanism, and the temperature of the heavy species is stabilized mostly by the energy loss to the glass. As the gas inflow increases, more energy is carried out of the discharge tube by the gas flow, and the convection impact becomes stronger than conduction impact in determining the heavy species temperature distribution. Furthermore, although the heavy species temperature indeed drops with an increase in the gas inflow rate, the temperature in the regions close to the glass tube walls remains considerably high.

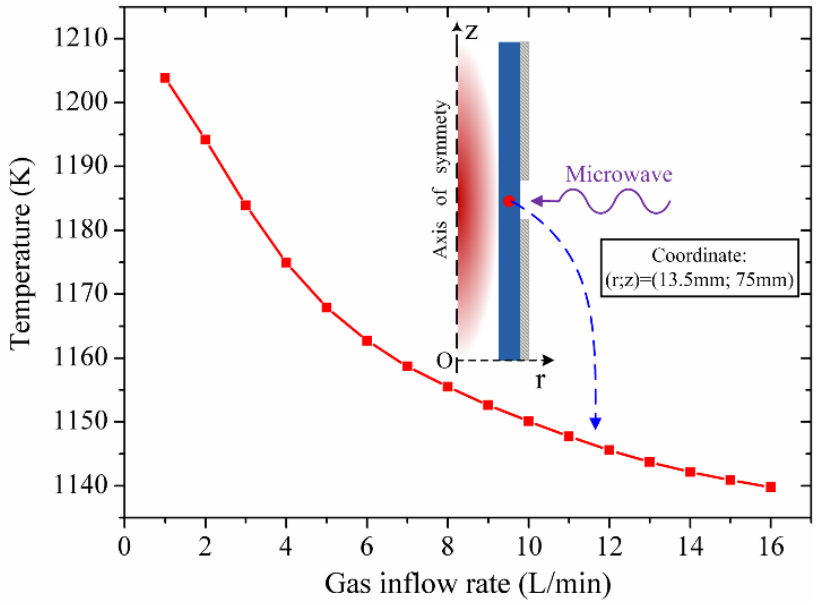


**Figure 5.15** Temperature of the glass on the temperature-maximum point (units: Kelvin) versus gas inflow rate ($P_{total} = 500W$).

Figure 5.15 shows only about 64 ℃ temperature drop occurs on the maximum-temperature point of the glass when the gas inflow rate increases from 1 L•min$^{-1}$ to 16 L•min$^{-1}$. It demonstrates that increasing the gas inflow rate can not solve the glass overheating problem for the MPT operated with only axial gas flow. It requires to seek other measures to prevent the glass from being overheated, such as injecting swirl gas flow [8, 28, 29, 12] or utilizing the forced liquid cooling on the outer glass tube walls.

Combined the results in Figure 5.12, we can carefully draw the conclusion that the glass overheating problem is mainly because of the microwave shielding capability of plasma. Such a capability leads to the microwave heating mainly within the skin depth of the plasma column and close to the inner glass tube wall, as shown in Figure 5.12. Therefore, increasing the gas inflow rate contributes considerably small to the cooling

of the glass tube wall and does not help to solve the glass overheating problem, because the heat source still remains close to the glass.

## 5.4 Conclusion

In this chapter, we have numerically investigated the wave propagation and discharge properties in the discharge tube under different plasma-absorbed powers and gas inflow rates.

The results regarding the plasma column length changes either with the increase of the microwave power or the gas inflow rate have demonstrated good consistency with experimental observations [11, 7, 99, 100, 101, 102, 37]. Besides, the magnitudes and the variation trends of the computed parameters also agree well with other numerical calculations [66, 67, 82] with similar MPTs and under different operation conditions.

Regarding the plasma column extension and the discharge maintenance, we have the following conclusions:

a) When the plasma-absorbed microwave power is low (< 200 W), the plasma is mainly confined in the rectangular waveguide and the input microwave is not able to enter the cylindrical discharge tube.
b) When the plasma-absorbed microwave power continues to increase, the argon plasma column extends out of the rectangular waveguide part, changing the cylindrical discharge tube to a two-conductor-like coaxial waveguide. It removes the limitation of cutoff frequency and allows the input microwave to propagate in the discharge tube towards both gas inlet and outlet. In this way, the input microwave supplies energy to the discharge, being able to sustain a long plasma column.
c) The extension of the plasma column under a low gas inflow rate is found to be motivated by the travelling surface wave. The length of the plasma column is determined by the propagation distance of the surface wave under a low gas inflow rate.

According the results about the gas flow effects on the discharge properties and wave propagation in the discharge tube, we can conclude that:

1) Increasing the gas inflow rate is able to decrease the propagation distance of the travelling wave in the discharge tube, especially in the gas inlet direction.

2) Apart from the particle loss introduced by the increasingly strong gas flow convection, the shortening of plasma column length with an increase in the gas inflow rate is reinforced by the consequent decrease of the surface wave propagation distance. At a high enough gas inflow rate, the discharge instability and extinction are caused by the disappearance of the travelling wave in the cylindrical discharge tube.

3) For a MPT operated with only axial gas flow, increasing the gas inflow rate can not solve the glass overheating problem. It is mainly due to the microwave shielding capability of the plasma column, which restricts the heat source within a small depth of the plasma column from surface and close to the inner glass tube wall.

The conclusions above are valid even when the gas is not the atomic argon gas and turns to be air, helium, neon, carbon dioxide and so on. The calculations in this chapter can provide some numerical insights to better understand the interactions between microwave, discharge and gas flow in the MPT. Besides, the conclusions can be helpful to optimize or better control the MPTs.

# Chapter 6 Three-dimensional fluid modelling based on plane-symmetric simplification

## 6.1 Mathematical model

Although the two-dimensional model in chapter 4 can provide some information about the discharge properties and the wave propagation in the MPTs. However, it can only be used to investigate the MPTs with particular geometrical size, whose discharges are sustained by the travelling wave propagating in azimuthally symmetric TEM mode. Besides, it does not allow to calculate the power coupling efficiency directly, because the plasma-absorbed microwave power is assumed and predefined. In this chapter, we propose a three-dimensional model based on the two-fluid mathematical model in chapter 4, by making use of a plane-symmetric simplification to the calculation domain.

### 6.1.1 Geometrical model and computation domain

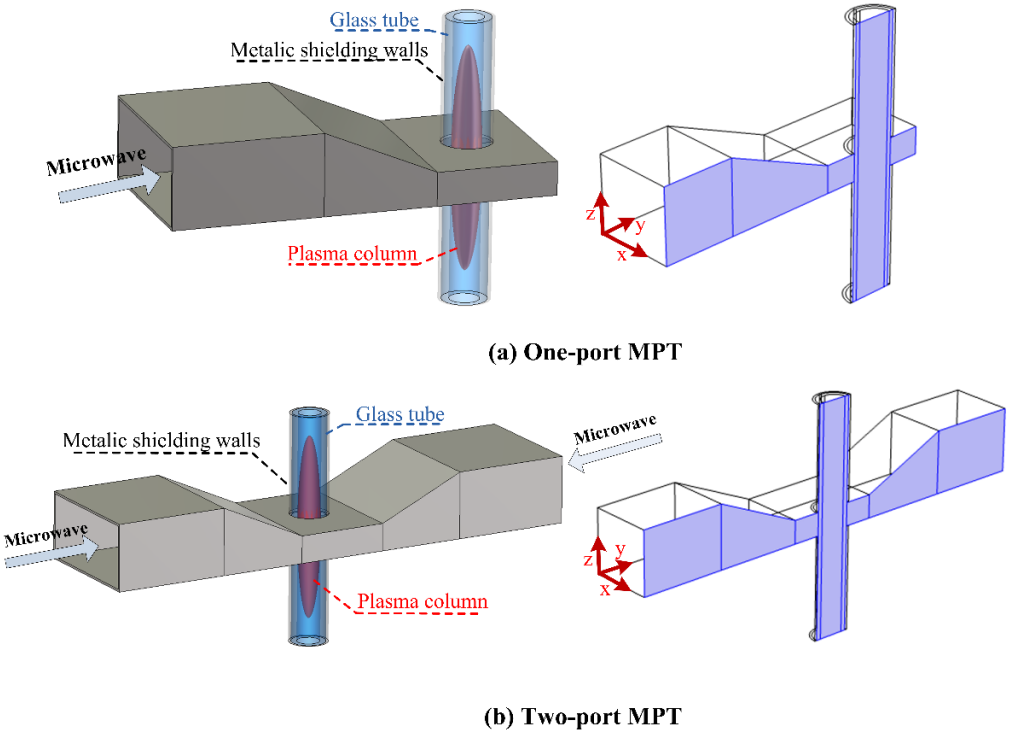


**Figure 6.1** Schematic structures of two types of MPTs and their calculation domains in the modelling.

Figure 6.1 shows the schematic structures of two types of MPTs that will be modelled in three dimensions in this chapter. Besides, it presents the calculation domains for these two types of MPTs with the plane-symmetric simplification. With this simplification, only a half of the MPT structure is taken into calculation.

This simplification is based on the plane-symmetry of microwave field, plasma fluid field and gas flow field in the MPTs show in Figure 6.1. According to our analysis in chapter 2, the microwave in the MPTs propagates in $TE_{10}$ mode in the rectangular waveguide parts and propagates in TEM or in hybrid $TE_{11}$ and TEM modes in the cylindrical discharge tube. In the plane across tube length and in the middle of the long side of rectangular waveguide (the plane with blue colour as shown in the calculation domain in Figure 6.1), the tangential components of magnetic field and the normal components of electric field are zero. It means that electric fields are parallel to the plane while magnetic fluxes are normal to plane [109].

In this case, a perfect magnetic condition (PMC) can be imposed on the plane, although this boundary does not actually exist in the MPT device. It can be used to simplify the calculation domain and reduce calculation demanding. Actually, imposing a PMC boundary inside a microwave component is a common skill in microwave engineering when doing the numerical calculations. It can be easily found in a lot of publications [110]. The distributions of the plasma properties and gas flow field are strongly dependent on the microwave field distribution. If the microwave field is plane-symmetric, these fields will be accordingly plane-symmetric too.

In conclusion, the plane-symmetric simplification is valid on the condition that the microwave in the MPT propagates in in plane-symmetric electromagnetic modes.

### 6.1.2 Governing equations and boundary conditions

The three-dimensional model shares the same governing equations, the same plasma chemical reactions and most common boundary conditions as the two-dimensional model in chapter 4. For both types of MPTs, the wave excitations on the input ports are characterized by the wave port boundary condition in COMSOL with consideration of the PMC boundary. For the Helmholtz equation, the plane-symmetry is achieved by the PMC boundary, as follows:

$$\vec{n} \times \vec{H} = 0 \tag{6.1}$$

For the Navier-Stokes equations, the plane-symmetry is characterized as follows:

$$\begin{aligned} &\vec{u}\bullet\vec{n}=0 \\ &\overrightarrow{K_n}-\left(\overrightarrow{K_n}\bullet\vec{n}\right)\vec{n}=0 \\ &\overrightarrow{K_n}=\mu(\nabla\vec{u}+(\nabla\vec{u})^T)\vec{n} \end{aligned} \tag{6.2}$$

For the energy conservation equations for heavy species and electron temperatures, the plane-symmetric boundaries are given as follows:

$$\begin{aligned} &\vec{n}\bullet\left(-k_h\nabla T\right)=0 \\ &\vec{n}\bullet(\frac{5}{2}K_B T_e\overrightarrow{\Gamma_e}-k_e\nabla T_e)=0 \end{aligned} \tag{6.3}$$

For mass conservation equations (density continuity equations for each species), the plane-symmetric boundaries are as follows:

$$\vec{n}\bullet\left(-D_k\nabla n_k\right)=0 \tag{6.4}$$

In order to simplify the model and get a better convergence performance, The transport coefficients of the ions and the excited atoms in the pure argon plasma are neither from the classic $f(E/N)$ relation based on experiments [111] as in our first paper [51] nor from the more general but complicated Binary gas mixture theory as in our second paper [69] and chapter 5. In this chapter, we followed reference [67] to calculate the free mobility of ions and the diffusivity of excited atoms in a much simpler way as follows:

$$\begin{aligned} &\mu_{i1}=\frac{10100T}{273.16p}\times 1.52\times 10^{-4}[m^2\bullet V^{-1}\bullet s^{-1}] \\ &\mu_{i2}=1.2\mu_{i1} \\ &D_s=D_p=\frac{1.16\times 10^{20}}{N_n}\left(\frac{T}{300}\right)^{0.5}[m^2\bullet s^{-1}] \end{aligned} \tag{6.5}$$

$\mu_{i1}\ and\ \mu_{i2}$ are the free mobility of atomic argon ion (Ar+) and molecular argon ion ($Ar_2$+) respectively. The corresponding diffusivity of ions ($D_{f,i1}\ and\ D_{f,i2}$) are obtained via the well-known Einstein relation with the mobility in equation (6.5). $P$ is the gas pressure obtained from the Navier-Stokes equations. This much simpler way to obtain the transport coefficients greatly improves the convergence performance of the three-dimensional model, making it possible to model MPTs in three dimensions with our current calculation capability.

### 6.1.3 Implementation of the numerical calculations

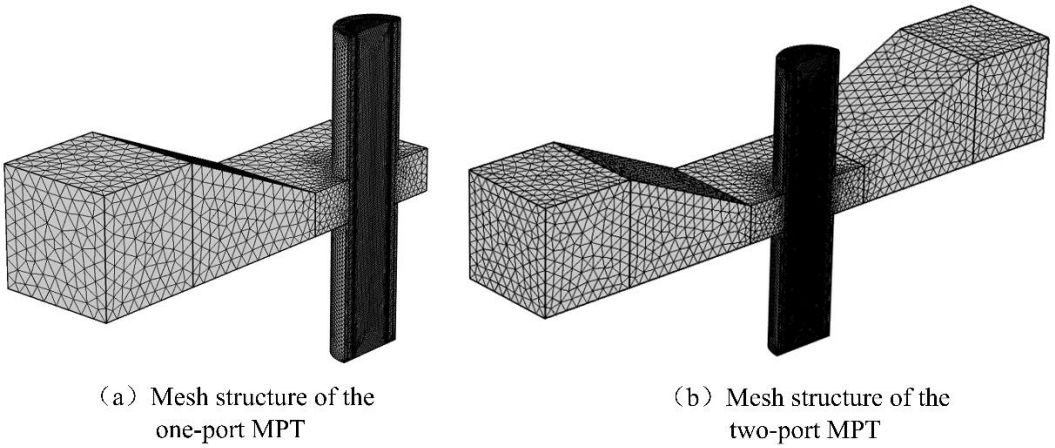


**Figure 6.2** Mesh structures of the two types of MPTs.

The numerical calculations are implemented in COMSOL Multiphysics as well. The calculation procedure and convergence criterion keep the same as for the two-dimensional model in chapter 4. The mesh structures for the two types of MPTs are shown in Figure 6.2.

The total number of mesh cells for the one-port MPT is 580867, while the number for the two-port MPT is 603337. The three-dimensional calculations are implemented on a computer which has 2 CPUs with 32 cores (Intel Xeon CPU E5-2630V3) and 72 GB of RAM memories. It takes approximately 10 days to complete a calculation of the one-port MPT and approximately 14 days to complete a calculation of the two-port MPT.

## 6.2 Results and discussion

### 6.2.1 Non-axisymmetric discharge properties and wave propagation in the one-port MPT

The results in section 6.2.1 are obtained under a total input microwave power of 300 W and a gas inflow rate of 1 L•min$^{-1}$.

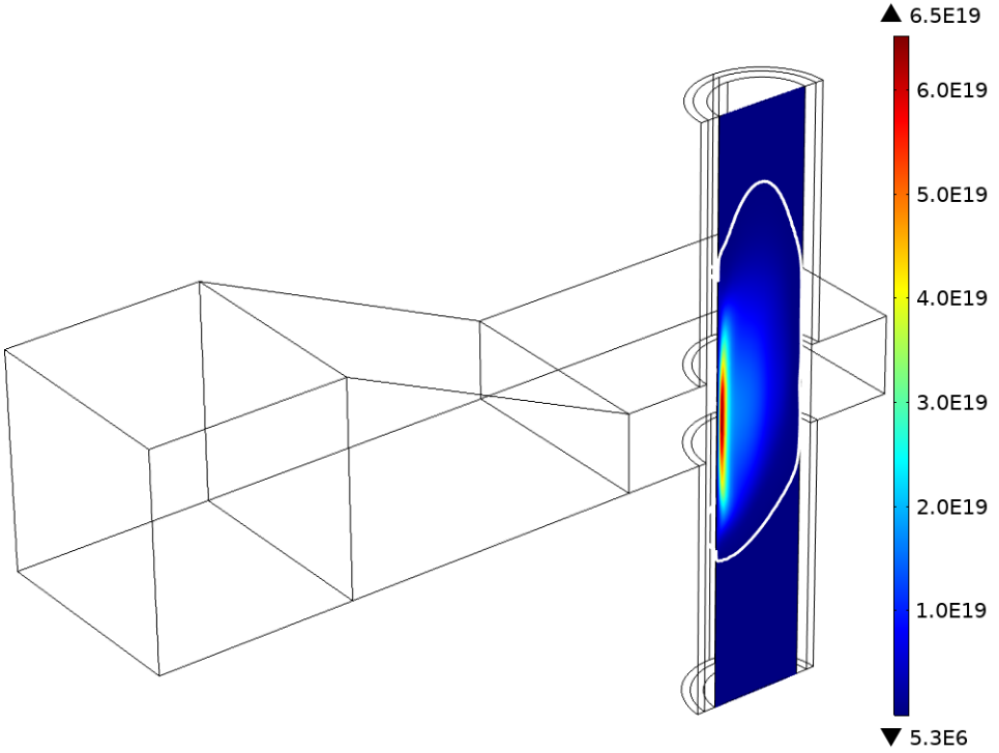


**Figure 6.3** Electron number density distribution in the one-port MPT with a 3-mm-wall-thickness glass tube (unit: $1/m^3$).

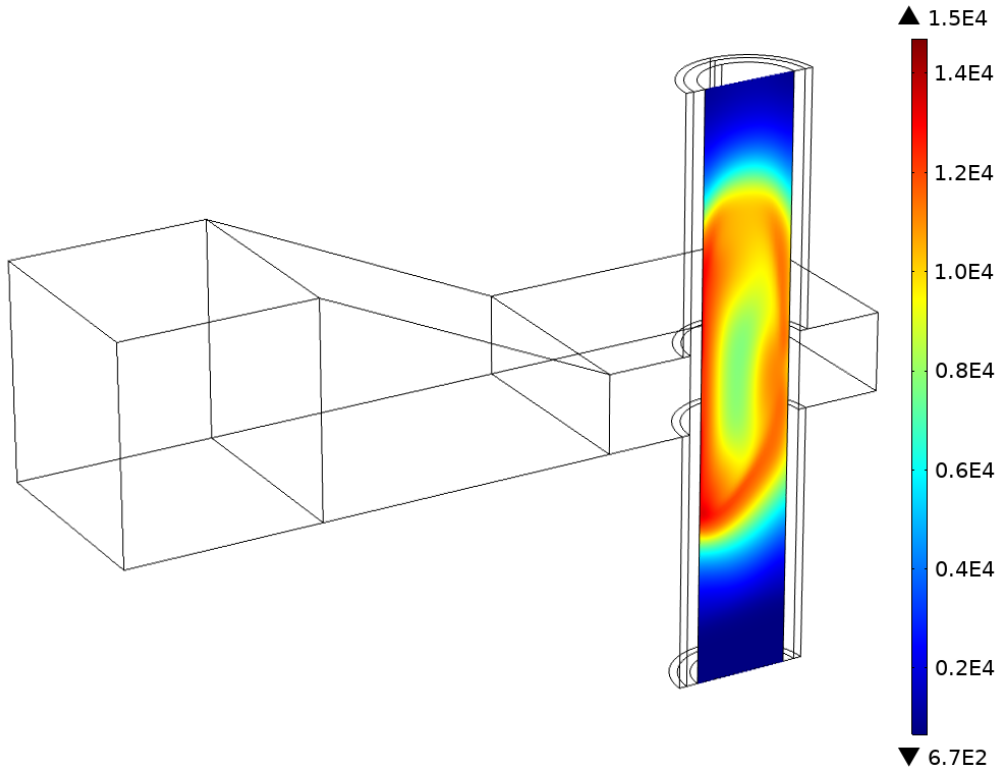


**Figure 6.4** Electron temperature distribution in the one-port MPT with a 3-mm-wall-thickness glass tube (unit: Kelvin)

Figure 6.3 shows the distribution of electron number density on the plane-symmetric surface of the plasma column in the one-port type MPT. It can be seen that the electron number density distribution is not axisymmetric any more. The distribution has a higher-value part that is close to the tapered rectangular waveguide and a lower-value part near the short-circuited end. The white curve is a contour corresponding to the critical electron number density of $7.6 \times 10^{16}\ m^{-3}$, which indicates the profile of the plasma column.

Accordingly, Figure 6.4 gives the electron temperature distribution of the plasma column on the symmetric plane in the one-port MPT. Its distribution profile matches that of electron number density distribution in Figure 6.3. The electron temperature value is lower than 2 eV (1eV=11602 Kelvin). The values of both electron number density and temperature are in the same orders as those in other numerical studies [66, 67, 82].

It is worth noting that the glass tube in the cylindrical metallic enclosure has a wall thickness of 3 mm and an inner radius of 12 mm. Besides, the relative permittivity of the glass tube material is set to be 3.5, which corresponds to quartz glass. According to our previous analysis in chapter 2 (Figure 2.5), the travelling wave in the cylindrical discharge tube is not able to propagate in pure azimuthally symmetric (in cylindrical coordinate) TEM mode with such a glass tube. Instead, the travelling microwave in the discharge tube will propagate in hybrid $TE_{11}$ and TEM modes. Because of the non-axisymmetric $TE_{11}$ mode, the discharge properties of plasma column (electron number density, electron temperature and heavy species temperature) will become non-axisymmetric any more.

With a mirror presentation skill, the obtained results can be shown in a complete MPT as shown in Figure 6.5. It presents the distributions of the microwave electric field intensity in the one-port MPT. It demonstrates that the input microwave indeed entered and propagated in the cylindrical discharge tube. Combined with the plasma column profile in Figure 6.3, it can be observed that the travelling microwave propagated along the plasma column towards both ends of the glass tube. However, when the plasma column has an electron number density that lower than the critical density $7.6 \times 10^{16}\ m^{-3}$, the microwave stopped propagating.

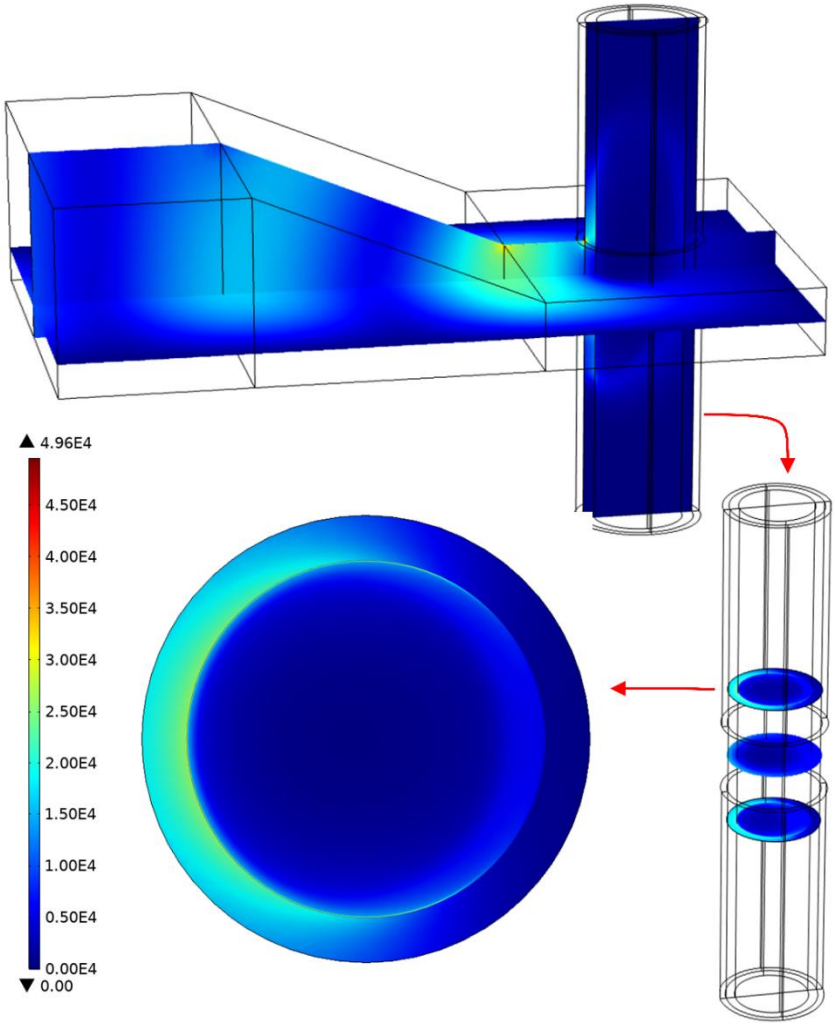


**Figure 6.5** Distributions of the microwave electric field intensity in the one-port MPT with a 3-mm-wall-thickness glass tube (unit: V/m)

Furthermore, Figure 6.5 proves that the microwave in the discharge tube propagate in hybrid TEM and $TE_{11}$ modes, because of the azimuthal non-symmetric (in cylindrical coordinate) distribution of the microwave electric field at a cross section of the discharge tube.

### 6.2.2 Axisymmetric discharge properties and wave propagation in the one-port MPT

According to our analysis in chapter 2, when the wall thickness of a quartz glass tube (Relative permittivity is 3.5) is larger than 10 mm, the input microwave is able to propagate in azimuthally symmetric TEM mode in the discharge tube, even for the one-port MPT. Therefore, in this section, a three-dimensional modelling of the one-port MPT with a 12-mm-wall-thickness glass tube is implemented to investigate the

discharge properties and wave propagation characteristics. The results are obtained under a total input microwave power of 100 W and a gas inflow rate of 0.1 L•min$^{-1}$.

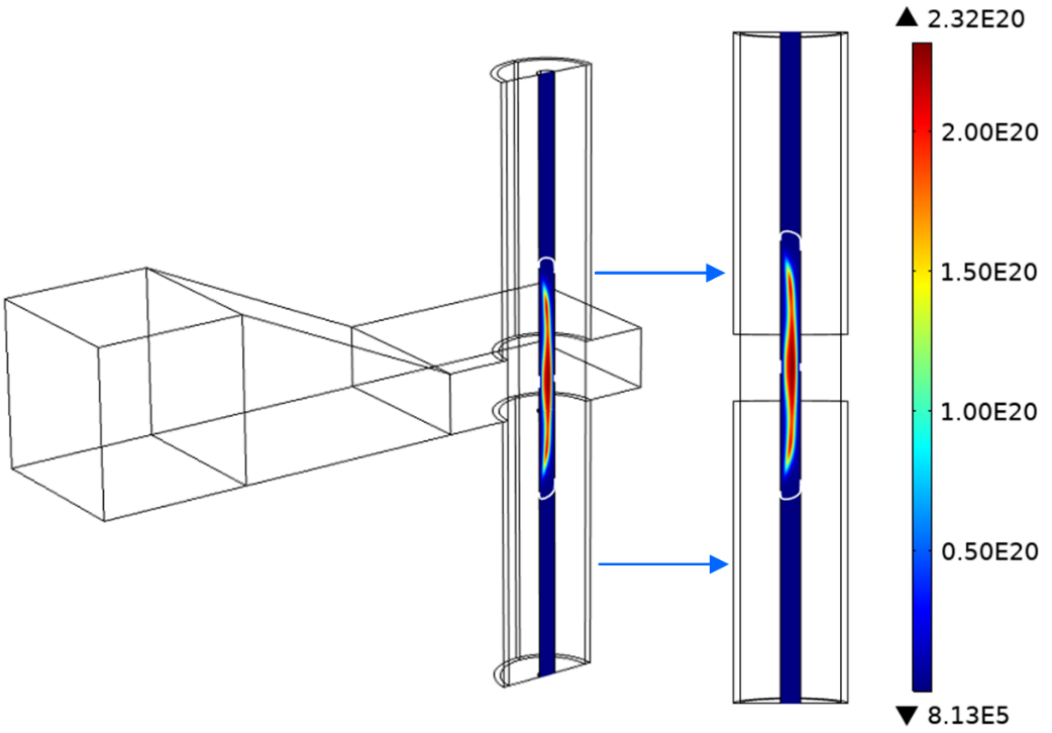


**Figure 6.6** Electron number density distribution in the one-port MPT with a 12-mm-wall-thickness glass tube (unit: 1/m$^3$)

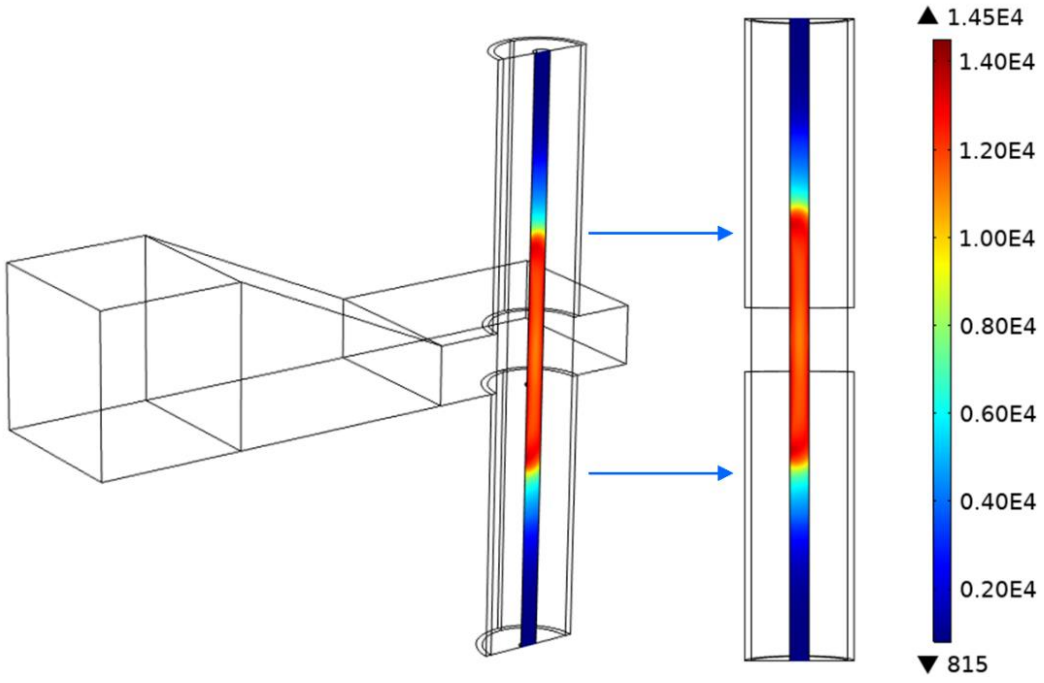


**Figure 6.7** Electron temperature distribution in the one-port MPT with a 12-mm-wall-thickness glass tube (unit: Kelvin)

Figure 6.6 presents the electron number density distribution of the plasma column on the symmetric plane in the one-port MPT with a 12-mm-wall-thickness glass tube. Unlike the discharges in the MPT with the glass tube having a much smaller wall thickness (Figure 6.3), the plasma column in Figure 6.6 has an approximately axisymmetric electron number density distribution. Higher-value parts of the electron number density distribution occur in the centre of the plasma column. Besides, the electron number density is even much higher than that in Figure 6.3 with a much lower input microwave power (300 W). Figure 6.7 shows the corresponding electron temperature distribution, which demonstrated a much better axially symmetry than the electron number density distribution in Figure 6.6.

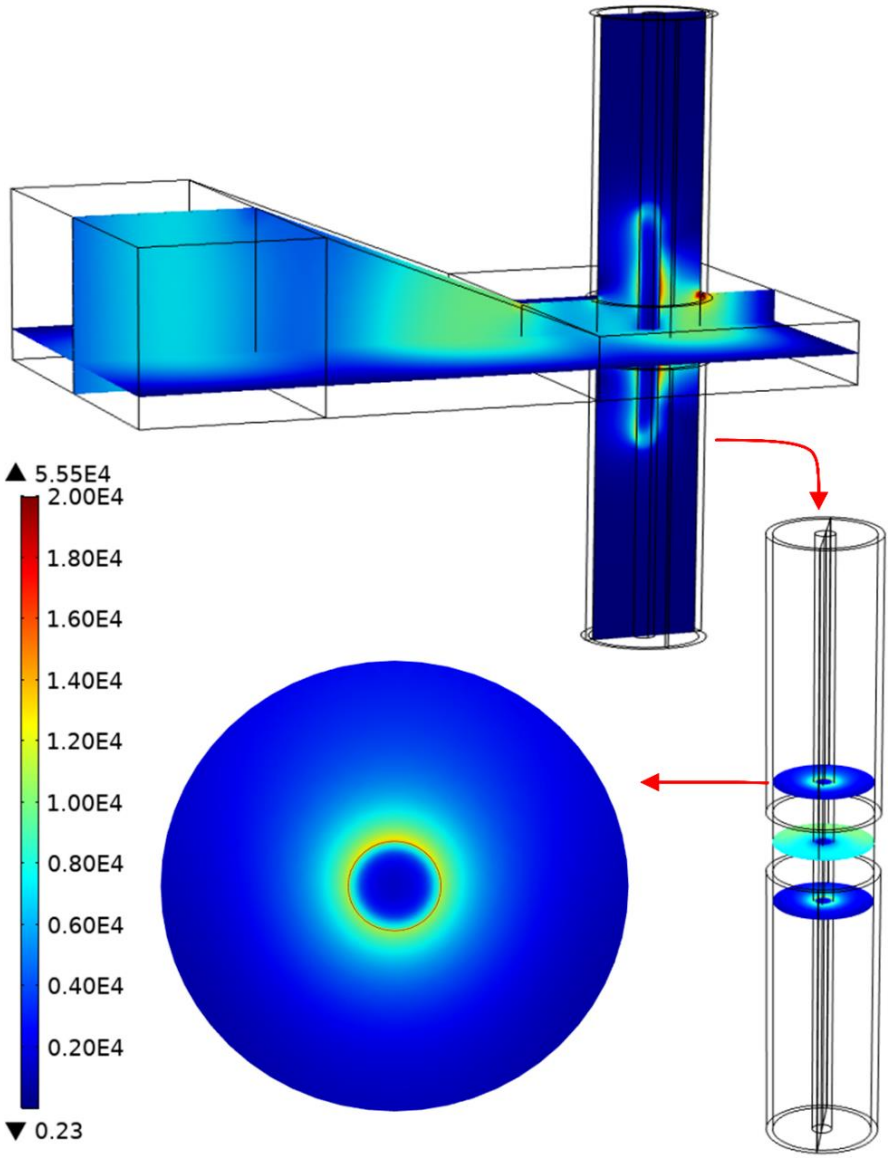


**Figure 6.8** Distribution of the microwave electric field intensity in the one-port MPT with a 12-mm-wall-thickness glass tube (unit: V/m).

Figure 6.8 gives the distribution of the microwave electric field intensity in the one-port MPT with a 12-mm-wall-thickness glass tube. It can be seen that the input microwave entered and propagated in the cylindrical discharge tube as well. However, the microwave field distribution characteristics have demonstrated great difference than that in Figure 6.5, which has a more axisymmetric distribution. Its microwave field distribution characteristics on the cross section of the discharge tube in the metallic enclosure can prove that the microwave propagates in TEM mode. In this case, it is reasonable to simplify the discharge tube of the one-port MPT in two dimensions with the axisymmetric approximation, as we analysed in chapter 4 and done in chapter 5.

### 6.2.3 Discharge properties and wave propagation in the two-port MPT with microwave excitations from both ports

In chapter 2, we have analysed the effects of the energy-input ways on the electromagnetic mode of the microwave in the discharge tube. It was concluded that the microwave can propagate in TEM mode in the discharge tube of the two-port MPT, providing that the microwave energy comes from both ports with the same power, phase and frequency. In chapter 4 and 5, we have established a two-dimensional model to numerically investigate discharge properties and wave propagation characteristics in the two-port MPT.

However, the conclusion was made in chapter 2 without consideration of the dynamic discharge having assumed a constant electron number density and collision frequency. The numerical investigations in chapter 5 were done in two dimensions with the axisymmetric simplification. These previous works can not strongly prove that the microwave will definitely propagate in TEM mode in the two-port MPT, even the microwave energy comes from both ends.

Therefore, a three-dimensional modelling of the two-port MPT is conducted in this section to diagnose the effects of the energy-input ways and validate the analysis in our previous works. The glass tube has a wall thickness of 3 mm (relative permittivity is set to be 3.5), allowing the existence of the non-axisymmetric higher-order $TE_{11}$ mode in this case.

The following results in this section (Figure 6.9-6.11) are obtained under a total input microwave power of 300 W (150 W for each port) and a gas inflow rate of 1 L•min$^{-1}$.

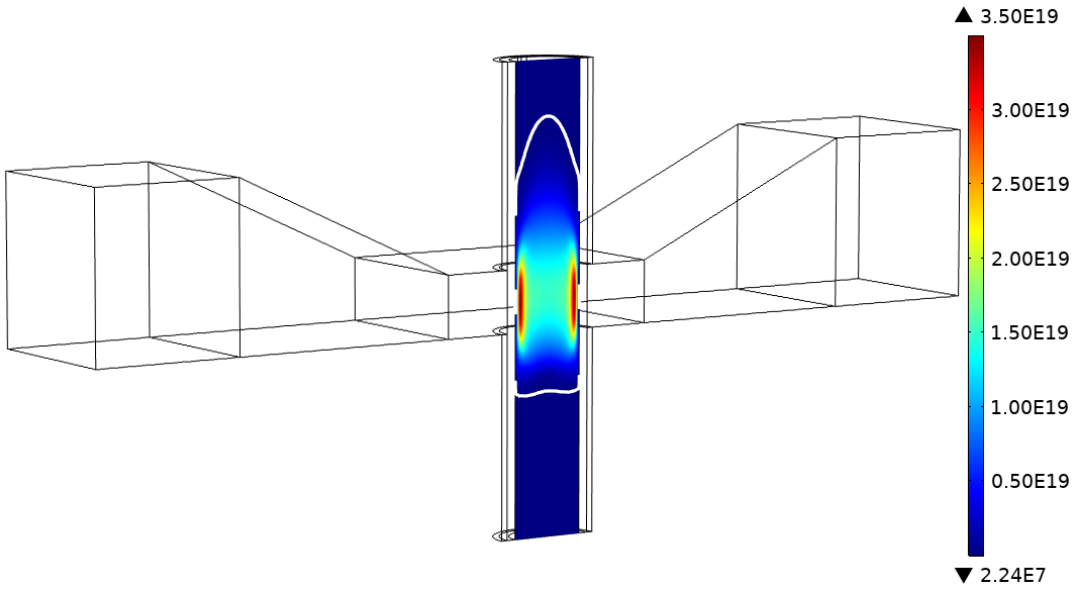


**Figure 6.9** Electron number density distribution in the two-port MPT (unit: $1/m^3$).

Figure 6.9 shows the electron number density distribution of the plasma column on the symmetric plane in the two-port MPT. It can be observed that the distribution is relatively axisymmetric to the axis in the centre of the plasma column.

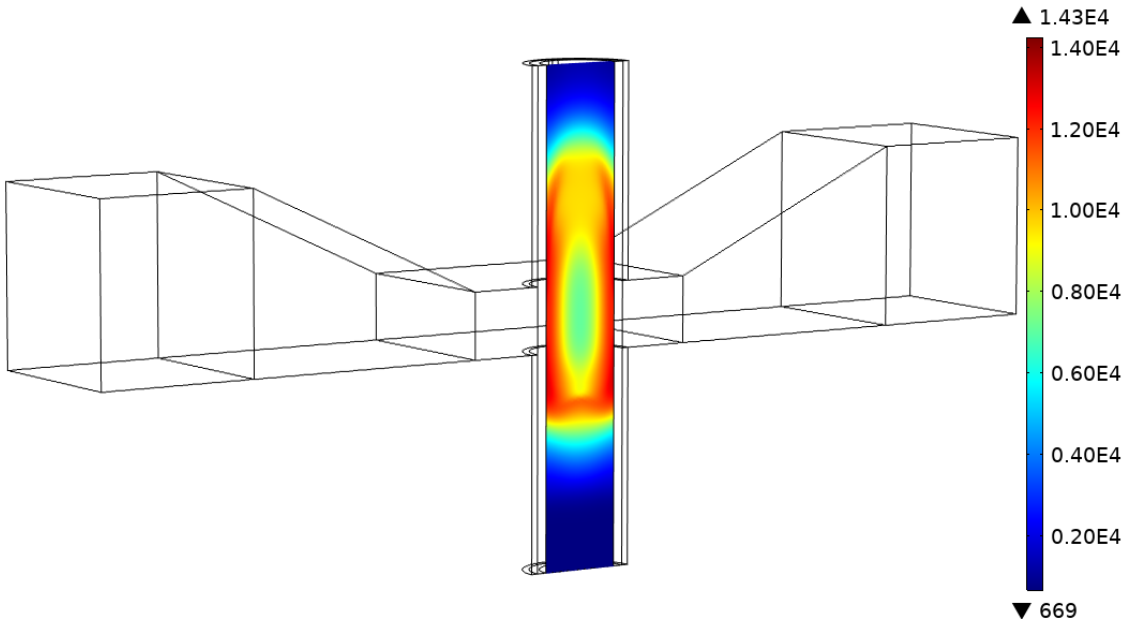


**Figure 6.10** Electron temperature distribution in the two-port MPT (unit: Kelvin).

Figure 6.10 presents the electron temperature distribution of the plasma column on the same surface as in Figure 6.9. The distribution characteristics also have demonstrated a good symmetry to the axis in the centre of the plasma column.

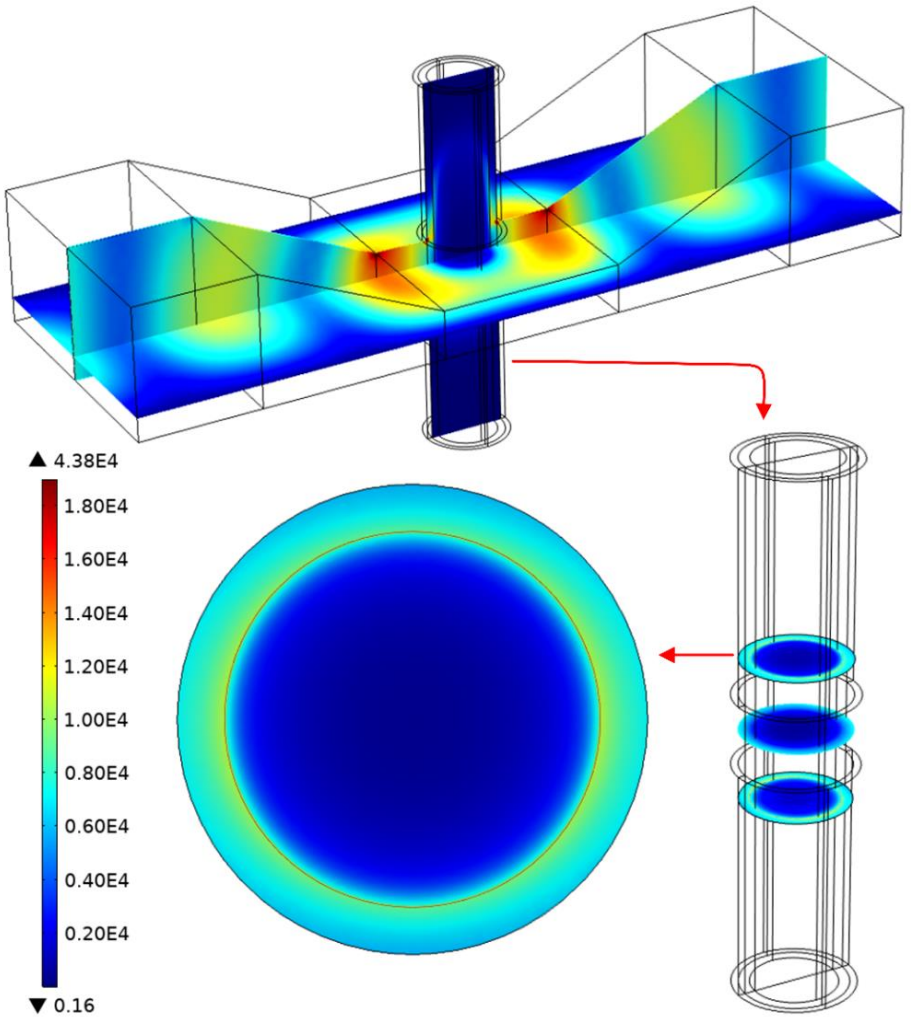


**Figure 6.11** Distribution of the microwave electric field intensity in the two-port MPT (unit: V/m).

Figure 6.11 shows the distribution of the microwave electric field intensity in the two-port MPT. The microwave electric field distribution in the discharge tube, that is axisymmetric to the axis in the center of the plasma column, demonstrates that the microwave indeed propagates in TEM mode. The non-axisymmetric higher-order mode $TE_{11}$ was successfully suppressed. It is valid to simplify the discharge tube in two dimensions for the two-port MPT even with a glass tube having a small wall thickness.

### 6.2.4 Comparison of the results from two-dimensional axisymmetric modelling and three-dimensional plane-symmetric calculation

Although the two-dimensional simulations in chapter 5 provided important and meaningful numerical insights about the discharge and wave propagation characteristics in MPTs, they have been conducted with the simplification of calculation domain and the assumption that microwave in the discharge tube and around

the glass tube in the rectangular waveguide part are axially symmetric. People may wonder how much difference is there between the results from three-dimensional calculation and simplified two-dimensional modelling.

Figure 6.12-6.15 present the comparison of results from two-dimensional axisymmetric modelling and three-dimensional plane-symmetric calculation. The two-dimensional results are obtained under a total plasma-absorbed microwave power of 300 W and a gas inflow rate of 1 L•min$^{-1}$. The three-dimensional results are obtained under a total input microwave power of 300 W (150 W for each port) and a gas inflow rate of 1 L•min$^{-1}$ as well. The glass tubes in both models have the same wall thickness of 3 mm.

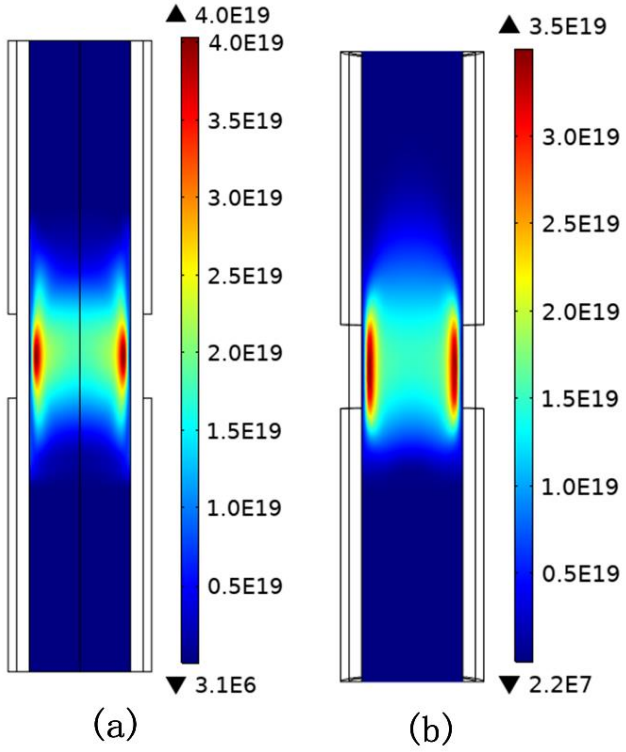


**Figure 6.12** Electron number density distributions of the plasma column in the two-port MPT with a 3-mm-wall-thickness glass tube (unit: 1/m$^3$). (a) Result from the two-dimensional simulation (b) Result from the three-dimensional simulation.

Figure 6.12 shows the electron number density distributions of the plasma column from both the two-dimensional simulation and the three-dimensional modelling. The two-dimensional result is shown with a mirror presentation skill (Figure 6.12 (a)). The black line in the centre of the plasma column in Figure 6.12 (a) is symmetric axis. The three-dimensional result (Figure 6.12 (B)) is the electron number density distribution on the plane-symmetric surface of the plasma column, which is the same as in Figure

6.9. The following Figures 6.13-6.15 present the obtained results in the same way as in Figure 6.12.

It can be seen that the electron number density distributions are considerably similar in general. They have similar profile, distribution characteristics and magnitudes of value. In conclusion, Figure 6.12 shows a negligible difference between the results from two-dimensional and three-dimensional calculations.

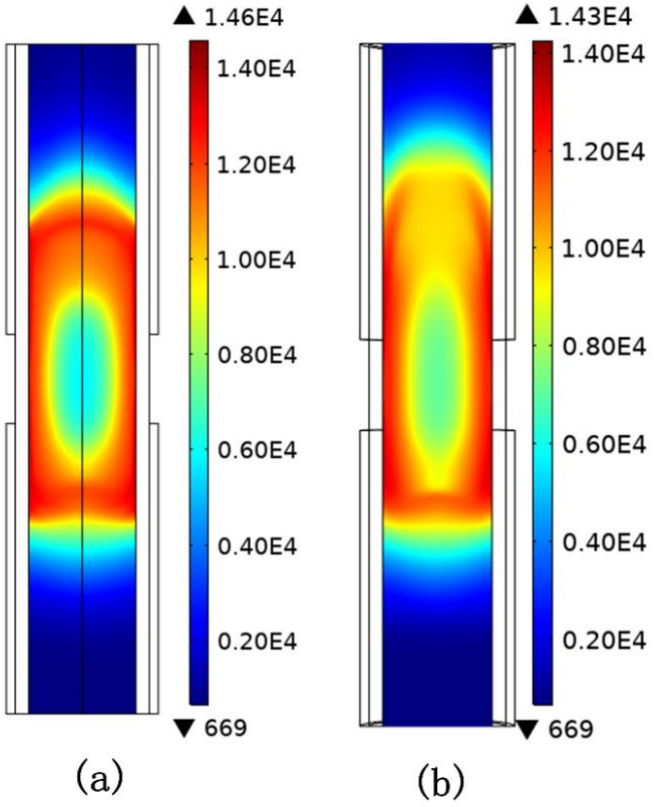


**Figure 6.13** Electron temperature distributions of the plasma column in the two-port MPT with a 3-mm-wall-thickness glass tube (unit: Kelvin). (a) Result from the two-dimensional simulation (b) Result from the three-dimensional simulation.

Figure 6.13 gives the electron temperature distributions of the plasma column in the two-port MPT from both the two-dimensional simulation and the three-dimensional modelling. The two obtained electron temperatures have the same minimum value (669 Kelvin), highly similar distributions and considerably close maximum value.

Figure 6.14 shows the temperature distributions of the plasma column and Figure 6.15 presents the distributions of the microwave electric field intensity from both the two-dimensional simulation and the three-dimensional modelling. In general, Figure 6.14 and 6.15 have shown a very small difference between the distributions of the computed parameter from two-dimensional and three-dimensional calculations.

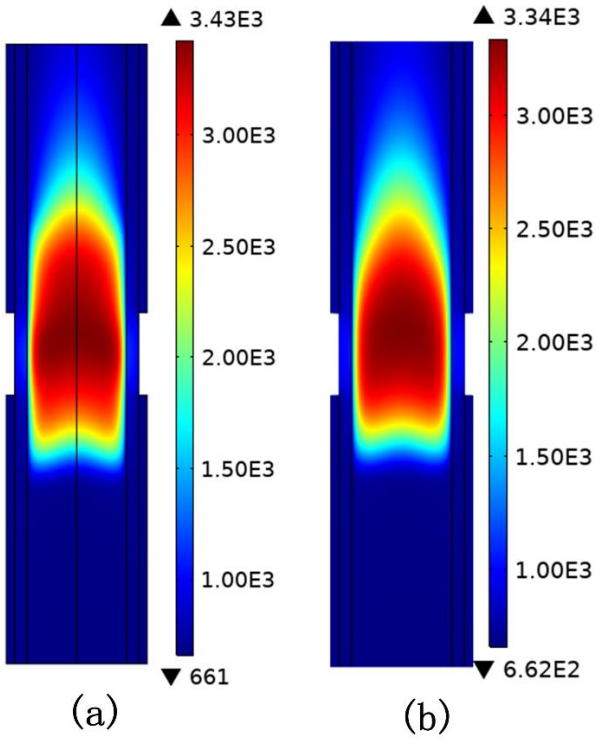


**Figure 6.14** Heavy species temperature distributions of the plasma column in the two-port MPT with a 3-mm-wall-thickness glass tube (unit: Kelvin). (a) Result from the two-dimensional simulation (b) Result from the three-dimensional simulation.

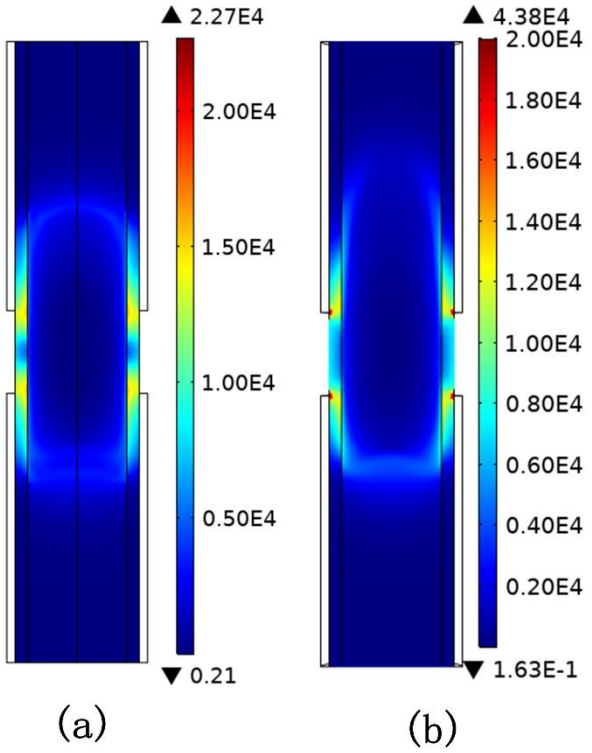


**Figure 6.15** Distributions of the microwave electric field intensity of the plasma column in the two-port MPT with a 3-mm-wall-thickness glass tube (unit: V/m). (a) Result from the two-dimensional simulation (b) Result from the three-dimensional simulation.

It is found that the maximum values from the two-dimensional simulation are higher than those from three-dimensional modelling in Figure 6.12-6.14. However, the microwave electric field intensity from the three-dimensional modelling is a little higher than that from two-dimensional simulation, as shown in Figure 6.15. Besides, the highest values from three-dimensional modelling occur on the edges of the interaction part between the rectangular waveguide and the glass tube.

Compared with the two mathematical models, these minor difference may be introduced by the following impacts:

(1) Different transport properties applied in the three-dimensional modelling for better convergence performance.

(2) The microwave power of 300 W in the two-dimensional modelling is assumed to be totally absorbed by the plasma without considering the power reflection. However, 300 W are the input microwave power in the three-dimensional calculation and part of the input microwave power is reflected. Actually, the microwave power coupling efficiency is approximately 82% $((123.5\ \mathrm{W} \times 2) \div (150\ \mathrm{W} \times 2))$. It can explain why the values from two-dimensional simulation are higher than those from three-dimensional modelling in Figure 6.12-6.14.

(3) Sharp corners can lead to singularities in solving Helmholtz equation using finite element method, resulted in overestimation of the microwave electric field intensity. In the two-dimensional modelling, the transition edges of the rectangular waveguide to the cylindrical discharge tube (sharp corners) were neglected. Therefore, the microwave electric field intensity from the three-dimensional modelling is higher than that from two-dimensional simulation in Figure 6.15.

However, despite these negligible differences, the numerical results from both two-dimensional simulation agree well with the results from three-dimensional modelling. The consistency proves that it is valid to simplify the calculation domain of the two-port MPT with microwave excitations from both ports in two dimensions and it will not introduce too much errors.

## 6.3 Conclusions

In this chapter, we have proposed a three-dimensional model to investigate the discharge properties and wave propagation characteristics in the MPTs, based on the plane-symmetric simplification of the calculation domain.

With this model, we have numerically modelled the steady-state argon discharges under atmospheric pressure in both the one-port MPT and the two-port MPT with two different glass tubes. Besides, we have compared the results about the two-port MPT from the two-dimensional simulation with the axisymmetric simplification and the three-dimensional modelling with the plane-symmetric simplification. The main conclusions can be summarized as follows:

(1) When the wall thickness of the glass tube in the one-port MPT is small, the plasma column will have higher values of electron number density and temperature near the tapered waveguide facing the energy-input port. The plasma properties are not axisymmetric and the microwave propagates in hybrid electromagnetic modes in the discharge tube.

(2) It is numerically proved that input microwave can propagate in the azimuthally symmetric (in cylindrical coordinate) TEM mode even in the one-port MPT.

(3) When the microwaves come from both ports with the same power, phase and frequency, the two-port MPT will have axisymmetric distributions of plasma properties and wave propagation characteristics in the discharge tube. In this energy-input way, non-axisymmetric higher-order electromagnetic modes can be restrained.

(4) Even the discharge tube of the two-port MPT allows higher-order electromagnetic modes to exist, the two-dimensional axisymmetric simplification is valid, when the microwaves energy is input from both ports with the same power, phase and frequency.

Besides the limitations introduced by the ambipolar diffusion approximation detailed in chapter 4, the three-dimensional steady-state model in this chapter can not be used to simulate the instant the ignition process and model the filamentary discharge.

# Chapter 7 Conclusions and future works

## 7.1 Conclusions

The objective of this dissertation is to better understand the discharges and the microwave propagation in MPTs. To achieve this goal, the following works have been conducted:

(1) The waveguide structure change of the discharge tube with metallic enclosure in the MPTs has been discussed and a new criterion is proposed to determine this waveguide structure transition. The propagating electromagnetic modes of the travelling microwave in the discharge tube with metallic enclosure in MPTs and the existence conditions of these modes have been theoretically investigated and numerically validated.

(2) Experiments have been conducted to explore the glass tube effects on the power coupling efficiency of a waveguide-based MPT under different operational conditions (different pressures, microwave input powers and gas inflow rates).

(3) A two-dimensional fluid model based on ambipolar diffusion approximation and axisymmetric simplification of the calculation domain is proposed to numerically model the argon discharges in the MPTs under atmospheric pressure.

(4) Numerical simulations based on the proposed two-dimensional model are conducted to investigate the mechanism of plasma column length variation, glass overheating problem, changes of discharge properties and wave propagation characteristics under different microwave powers and gas inflow rates.

(5) A three-dimensional model based on our previous two-dimensional model is proposed based on a plane-symmetric simplification of the calculation domain of the MPTs. With this three-dimensional model, we have numerically modelled the discharges sustained by pure azimuthally symmetric TEM mode and by hybrid non-axisymmetric modes in MPTs. Besides, regarding modelling the two-port

MPT, the two-dimensional simulation results have been compared with the results obtained from the three-dimensional modelling.

After these works, we have made some conclusions, which can be summarized as follows:

1. The waveguide structure of the discharge tube with metallic enclosure in the MPTs can change with variation of the plasma column properties. When the plasma skin depth is larger than the diameter of the plasma column, the discharge tube remains to be a one-conductor circular waveguide filled with a multiple-layer medium. While the plasma skin depth is smaller than the radius of the plasma column, the plasma column, the glass tube and the metallic enclosure will form a two-conductor-like coaxial waveguide, allowing the input microwave to enter the discharge tube and propagate along the plasma column. The cylindrical discharge tube is no longer cut-off for the input microwave any more.
2. In a MPT with a metallic enclosure that bounds the glass tube, the m=0 mode of the travelling microwave in the discharge tube can be TEM mode as well, when the discharge tube becomes a two-conductor-like coaxial waveguide.
3. The wall thickness and the dielectric permittivity of the glass tube are able to determine the microwave propagating modes allowed to exist in the two-conductor-like discharge tube. For the one-port MPT in this chapter, the glass tube is even able to determine whether the travelling wave propagates in a pure TEM mode or in hybrid modes in the discharge tube. It indicates that it is possible to control the propagating electromagnetic modes of the travelling microwave in the discharge tube of MPTs for different purposes by choosing a proper glass tube with particular wall thickness and dielectric property.
4. The non-axisymmetric $TE_{11}$ can be restrained in the two-port MPT, when the microwave energy is supplied from both ports with the same frequency, phase and power. In this case, the two-port MPT will have axisymmetric distributions of plasma properties and wave propagation characteristics in the discharge tube, even the discharge tube of the two-port MPT allows non-axisymmetric higher-order electromagnetic modes to exist.

5. Increasing the thickness of the glass tube wall is able to improve the power coupling efficiency under both low pressures and atmospheric pressure. Furthermore, when the input microwave power becomes different, this efficiency-improving method is still valid.
6. A power coupling efficiency around 90% can be achieved by simply choosing a proper glass tube with its wall thickness in particular range rather than using external tuning measures like the movable short-circuit ending plunger or the three-stub tuner. For the MPTs having a metallic enclosure with the inner diameter of 30 mm, the wall thickness should be 5.5-9 mm.
7. Besides the cylindrical metallic enclosure that bounds the glass tube, the argon plasma column under atmospheric pressure is able to act as another conductor, changing the discharge tube to a two-conductor-like coaxial waveguide. It removes the limitation of cut-off frequency and allows the input microwave to propagate in the discharge tube towards both the gas inlet and outlet. In this way, the input microwave supplies energy to the discharge, being able to sustain a long plasma column.
8. The plasma column length extension in the discharge tube with the increase of microwave power is actually driven by the travelling microwave in the discharge tube. The length of the plasma column is determined by the propagation distance of the microwave in the discharge tube under a low gas inflow rate.
9. Increasing the gas inflow rate will decrease the propagation distance of the travelling wave in the discharge tube, especially in the gas inlet direction.
10. Apart from the particle loss introduced by the increasingly strong gas flow convection, the shortening of plasma column length with an increase in the gas inflow rate is reinforced by the consequent decrease of the surface wave propagation distance. At a high enough gas inflow rate, the discharge instability and extinction are caused by the disappearance of the travelling wave in the cylindrical discharge tube.
11. For a MPT operated with only axial gas flow, increasing the gas inflow rate can not solve the glass overheating problem. It is mainly due to the microwave shielding capability of the plasma column, which restricts the microwave

heating within a small depth of the plasma column from surface and close to the inner glass tube wall.

12. When the wall thickness of the glass tube in the one-port MPT is small, the plasma column will have higher values of electron number density and temperature near the tapered waveguide facing energy-input port. The plasma properties are not axisymmetric and the microwave propagates in hybrid electromagnetic modes in the discharge tube.

13. It is valid to simplify the calculation domain of the discharge tube in two-dimensions with the axisymmetric simplification, when the microwave in the discharge tube propagates in azimuthally symmetric modes (TEM mode for example). For the two-port MPT with microwave excitations on both ports with the same power, phase and frequency, negligible difference has been found in the results from two-dimensional simulation and three-dimensional modelling.

## 7.2 Future works

This thesis has investigated the gas discharge phenomena and the wave propagation characters in MPTs by theoretical analysis, experimental exploration and numerical simulation. Although we have obtained some results and conclusions in this thesis, some problems still remain unsolved due to the limited time and they will be our future works.

A. Development of new models to simulate the discharges in MPTs under low pressures.

The plasma fluid modelling in this thesis only involved the argon discharges under atmospheric pressure. When the gas pressure is low, the discharges are very different from the discharges under atmospheric pressure. Therefore, it is necessary to develop a new model to investigate the discharges in the MPTs under low pressures.

B. Development of three-dimensional models for the MPT operating with other kinds of gases, such as helium, nitrogen, oxygen, hydrogen, carbon dioxide and their mixtures.

For the popular applications of MPTs such as the hydrogen production and the carbon dioxide elimination, it requires a fast, efficient and accurate model that can be used to simulate the discharges with other types of gases especially the gas mixtures.

C. Direct comparison of the computed parameters with experimental results.

Due to the lack of plasma diagnostic measures, we have only compared the value orders and the variation trends of the computed parameters in this thesis with those from other numerical studies and experimental observations. Therefore, a direct comparison of the computed parameters with experimental data is required in the future.

D. Investigation of other kinds of MPTs and development of new MPTs.

# Reference


[1] J. A. Bittencourt, “Fundamentals of Plasma Physics” 3rd ed, New York, USA: Springer, 2004, pp.1–9. pp.122–138.

[2] F. F Chen, “Introduction to plasma physics and controlled fusion” 2ed ed, New York, USA: Plenum Press, 1984, pp.1. pp. 116.

[3] C. M. Ferreira and M. Moisan, “Microwave discharges: fundamentals and applications,” 1st ed, New York, USA: Springer, 1993.

[4] J. H. Kim, Y.C. Hong, H. S. Kim and H. S. Uhm, “Simple microwave plasma source at atmospheric pressure,” *J. Koren Phys. Soc.*, vol. 42, pp. S876-S879, Feb. 2003.

[5] S. R. Wylie, A. I. Al-Shamma’a and J. Lucas, “Microwave plasma system for material processing,” *IEEE Trans. Plasma Sci.*, vol. 33, no. 2, pp. 340-341, Apr. 2005.

[6] A. I. Al-Shamma’a, S. R. Wylie, J. Lucas and C. F. Pau, “Design and construction of a 2.45 GHz waveguide-based microwave plasma jet at atmospheric pressure for material processing,” *J. Phys. D: Appl. Phys.*, vol. 34, no. 18, pp. 2734–2741, Sept. 2001.

[7] L. Su, R. Kumar, B. Ogungbesan and M. Sassi, “Experimental investigation of gas heating and dissociation in a microwave plasma torch at atmospheric pressure,” *Energy Convers. Manage.*, vol. 78, pp. 695-703, Feb. 2014.

[8] K. M. Green, M. C. Borrás, P. P. Woskov, G. J. Flores, III, K. Hadidi, and P. Thomas, “Electronic excitation temperature profile in an air microwave plasma torch,” *IEEE Trans. Plasma Sci.*, vol. 29, no. 2, pp. 399–406, Apr. 2001.

[9] R. Rincon, A. Marinas, J. Munoz and M. D. Calzada, “Experimental research on ethanol-chemistry decomposition routes in a microwave plasma torch for hydrogen production,” *Chem. Eng. J.*, vol. 284, pp. 1117-1126, Jan. 2016.

[10] E. Tatatova, J. P. Henriqus, E. Felizardo, M. Lino da Silva, C. M. Ferreira and B. Gordiets, “Microwave plasma source operating with atmospheric pressure air-water mixtures,” *J. Appl. Phys.*, vol. 112, no. 9, pp. 093301-1–093301-14, Nov. 2012.

[11] M. Moisan, Z. Zakrzewski and P. Leprince. “A waveguide-based launcher to sustain long plasma columns through the propagation of an electromagnetic surface wave,” *IEEE Trans. Plasma Sci.*, vol. PS-13, no. 3, pp. 203-214, Apr. 1984.

[12] H. S. Uhm, Y. C. Hong, and D. H. Shin, “A microwave plasma torch and its applications,” *Plasma Sources Sci. Technol.*, vol. 15, no. 2, pp. S26–S34, Apr. 2006.

[13] M. Moisan, C. Beaudry, P. Leprince, “A small microwave plasma source for long column production without magnetic field,” *IEEE Trans. Plasma Sci.*, vol. PS-3, no. 2, pp. 55-59, Jun. 1975.

[14] Q. H. Jin, C. Zhu, M. W. Border and G. M. Hieftje, “A microwave plasma torch assembly for atomic emission spectrometry,” *Spectrochim. Acta. Part B: At. Spectrosc.*, vol. 46, No. 3, pp.417-430, 1991.

[15] M. Moisan, M. Chaker, Z. Zakrzewski and J. Paraszczak, “The waveguide surfatron: a high power surface-wave launcher to sustain large-diameter dense plasma columns,” J. Phys. E: Sci. Instrum., vol. 20, no. 11, pp. 1356-1361, May. 1987.

[16] https://www.sairem.com/microwave-radio-frequency-rf-products/microwave-plasma/microwave-plasma-sources

[17] Y. Mitsuda, T. Yoshida and K. Akashi, “Development of a new microwave plasma torch and its application to diamond synthesis,” *Rev. Sci. Instrum*, vol. 60, no. 2, pp. 249-252, Feb. 1989.

[18] J. H. Kim, Y. C. Hong and H. S. Uhm, “Synthesis of oxide nanoparticles via microwave plasma decomposition of initial materials,” *Surf. Coa. Technol*., vol. 201, no. 9, pp. 5114-5120, Feb. 2007.

[19] J. Lee, H. Sun, S. Im, and M. S. Bak, “Formation of nitrogen oxides from atmospheric electrodeless microwave plasmas in nitrogen–oxygen mixtures,” *J. Appl. Phys.*, vol. 122, no. 8, pp. 083303-1-083303-10, Aug. 2017.

[20] J. Henriques, E. Tatarova and C. M. Ferreira, “Microwave N2-Ar plasma torch. I. Modeling,” *J. Appl. Phys*., vol. 109, no. 2, pp. 023301-1–023301-11, Jan. 2011.

[21] W. Lai, H. Lai, S. P. Kuo, O. Tarasenko and K. Levon, “Decontamination of biological warfare agents by a microwave plasma torch,” *Phys. Plasmas*, vol. 12, no. 2, pp. 023501-1–023501-6, Feb. 2005.

[22] Y. Kabouzi, M. Moisan, J. C. Rostaing, C. Trassy, D. Guérin, D. Kéroack, and Z. Zakrzewski, “Abatement of perfluorinated compounds using microwave plasmas at atmospheric pressure,” *J. Appl. Phys*., vol. 93, no. 12, pp. 9483-9496, Jun. 2003.

[23] G. S. J. Sturm, A. N. Muñoz, P. V. Aravind, and G. D. Stefanidis, “Microwave-driven plasma gasification for biomass waste treatment at miniature scale,” *IEEE Trans. Plasma Sci*., vol. 44, no. 4, pp. 670-678, Mar. 2016.

[24] H. S. Uhm, H. S. Kwak and Y. C. Hong, “Carbon dioxide elimination and regeneration of resources in a microwave plasma torch,” *Environ. Pollut*., vol. 211, pp. 191-197, Apr. 2016.

[25] G. Chen, T. Silva, V. Georgieva, T. Godfroid, N. Britun, R. Snyders, M. P. Delplancke-Ogletree, “Simultaneous dissociation of CO2 and H2O to syngas in a surface-wave microwave discharge,” *Int. J. Hydrogen Energy*, vol. 40, no. 2, pp. 3789-3796, Mar. 2015.

[26] R. Snoeckx and A. Bogaerts, “Plasma technology – a novel solution for CO2 conversion?,” *Chem. Soc. Rev*. vol. 46, pp. 5805-5863, Jan. 2017.

[27] T. Silva, N. Britun, T. Godfroid and R. Snyders, “Optical characterization of a microwave pulsed discharge used for dissociation of CO2,” *Plasma Sources Sci. Technol*. vol. 23, no. 2, pp.025009-1-025009-13, Mar. 2014.

[28] B. Hrycak, D. Czylkowski, R. Miotk, M. Dors, M. Jasinski, and J. Mizeraczyk, “Application of atmospheric pressure microwave plasma source for hydrogen production from ethanol,” Int. J. Hydrogen Energy, vol. 39, no. 26, pp. 14184-14190, Sep. 2014.

[29] M. Jasinski, M. Dors and J. Mizeraczyk, “Production of hydrogen via methane reforming using atmospheric pressure microwave plasma,” *J. Power Sources*, vol. 181, no. 1, pp. 41-45, June. 2008.

[30] B. Ogungbesan, R. Kunar, L. Su and M. Sassi, “Experimental validation of local thermal equilibrium in a MW plasma torch for hydrogen production,” *Int. J. Hydrogen Energy*, vol. 38, no. 35, pp. 15210-15218, Nov. 2013.

[31] J. Henriques, N. Bundaleska, E. Tatarova, F. M. Dias, and C. M. Ferreira, “Microwave plasma torches driven by surface wave applied for hydrogen production,” *Int. J. Hydrogen Energy*, vol. 36, no. 1, pp. 345-354, Jan. 2011.

[32] M. Jasinski, D. Czylkowski, B. Hrycak, M. Dors, and J. Mizeraczyk, “Atmospheric pressure microwave plasma source for hydrogen production,” *Int. J. Hydrogen Energy*, vol. 38, no. 26, pp. 11473-11483, Aug. 2013.

[33] E Tatarova, N Bundaleska, F M Dias, D Tsyganov, R Saavedra, and C M Ferreira, “Hydrogen production from alcohol reforming in a microwave 'tornado'-type plasma,” *Plasma Sources Sci. Technol*., vol. 22, no. 6, pp. 065001-1-065001-9, Oct. 2013.

[34] G. Wattieaux, M. Yousfi and N. Merbahi, “Optical emission spectroscopy for quantification of ultraviolet radiations and biocide active species in microwave argon plasma jet at atmospheric pressure,” *Spectrochim. Acta. Part B: At. Spectrosc.*, vol. 89, pp. 66-76, Nov. 2013.

[35] D. Zhu, W. Jin, B. W. Yu, Y. W. Ying, H. X. Yu, J. Shan, Y. W. Yan, C. Xu, B. L. Wang and Q. H. Jin, “Development of a Novel Kilowatt Microwave Plasma Torch Source for Atomic Emission Spectrometry,” *Chem. Res. Chin. Univ.*, vol.33, no. 5, pp. 709—713, Sept. 2017.

[36] E. Tatarova, F. M. Dias, E. Felizardo, J. Henriques, M. J. Pinheiro, C. M. Ferreira, and B. Gordiets, "Microwave air plasma source at atmospheric pressure: experiment and theory," *J. Appl. Phys.*, vol. 108, no. 12, pp.123305-1–123305-18, Dec. 2010.

[37] M. Moisan and H. Nowakowska, "Contribution of surface-wave (SW) sustained plasma columns to the modeling of RF and microwave discharges with new insight into some of their features. A survey of other types of SW discharges," *Plasma Sources Sci. Technol*. vol. 27, no. 7, pp. 073001-1-073001-43, Jul. 2018.

[38] S. Ramo, "Space Charge and Field Waves in an Electron Beam", *Phys. Rev*. vol. 56, p. 276-283, Aug. 1939.

[39] A. W. Trivelpiece and R. W. Gould, "Space Charge Waves in Cylindrical Plasma Columns", *J. Appl. Phys*. Vol.30, no.11, p.1784-1793, Feb. 1959.

[40] J. Margot and M. Moisan, "Characteristics of surface-wave propagation in dissipative cylindrical plasma columns," *J. Plasma Physics*., vol. 49, no. 3, pp. 357-374, Mar. 1993.

[41] M. Moisan and Z. Zakrzewski, "Plasma sources based on the propagation of electromagnetic surface waves," *J. Phys. D: Appl. Phys.*, vol. 24, no. 7, pp. 1025-1048, Jul. 1991.

[42] I. Zhelyazkov and E. Benova, "Modeling of a plasma column produced and sustained by a traveling electromagnetic surface wave," *J. Appl. Phys.*, vol. 66, no. 4, pp. 1641-1650, Aug. 1989.

[43] E. Benova and I. Zhelyazkov, "Theoretical study of the influence of a metal enclosure on the parameters of a plasma column sustained by a travelling electromagnetic surface wave," *Physica Scripta.*, vol. 43, no. 1, pp. 68-73, Nov. 1991.

[44] E. Benova, I. Ghanashev and I. Zhelyazkov, "Theoretical study of a plasma column sustained by an electromagnetic surface wave in the dipolar mode," *J. Plasma Physics*, vol. 45, no. 2, pp. 137-152, Apr. 1991.

[45] E. Benova and I. Zhelyazkov, "Conditions for sustaining low-pressure plasma columns by travelling electromagnetic UHF waves," *Physica Scripta.*, vol. 56, no. 4, pp. 381-387, 1997.

[46] A. Sola, A. Gamerc, J. Cotrino and V. Colomer, "Reexamination of recent experimental results in surface-wave-produced argon plasmas at 2.45 GHz: Comparison with the diffusion-recombination model results," *J. Appl. Phys.*, vol. 64, no. 7, pp. 3419-3423, Oct. 1988.

[47] C. M. Ferreira, "Theory of a plasma column sustained by a surface wave," *J. Phys. D: Appl. Phys.*, vol. 14, no. 10, pp. 1811-1830, Oct. 1981.

[48] M. Zethoff and U. Kortshagen, "Dispersion characteristics and radial field distribution of surface waves in the collisional regime," *J. Phys. D: Appl. Phys.*, vol. 25, no. 11, pp. 1574-1582, Nov. 1992.

[49] W. Q. Li, G. Wang, D. Xiang, and X. B. Su, " Propagation and attenuation characteristics of azimuthal symmetric surface waves in un-magnetized plasma column," *Phys. Plasmas*, vol. 23, no. 11, pp. 113302-1- 113302-7, Nov. 2016.

[50] J. Margot-Chaker, M. Moisan, M. Chaker, V. M. M. Glaude, P. Lauque, J. Paraszczak and G. Sauvé, "Tube diameter and wave frequency limitations when using the electro magnetic surface wave in the m=1 (dipolar) mode to sustain a plasma column," *J. Appl. Phys.*, vol. 66, no. 9, pp. 4134- 4148, Nov. 1989.

[51] W. C. Zhang, J. W. Tao, K. M. Huang and L. Wu, "Numerical investigation of the surface wave formation in a microwave plasma torch," *IEEE Trans. Plasma Sci*., vol. 45, no. 11, pp. 2929-2939, Oct. 2017.

[52] E. Benova, I. Zhelyazkov and I. Ghanashev, "Low-pressure plasma columns sustained by traveling electromagnetic surface waves in the dipolar (m=1) mode," *J. Appl. Phys.*, vol. 71, no. 2, pp. 1026-1028, Jan. 1992.

[53] S. Nonaka and Y. Akao, "Mode conversion and its utilization of degenerating surface wave modes on a plasma column," *J. Appl. Phys*., vol. 54, no. 7, pp. 3798-3806, Jul. 1983.

[54 ] M. A. Lieberman and A. J. Lichtenberg, Principles of Plasma Discharges and Materials Processing (John Wiley & Sons, Inc, Hoboken, 2005).

[55 ] D. M. Pozar, Microwave engineering (John Wiley & Sons, Inc, Hoboken, 2012), p.10, p.19, P.99, P.212.

[56 ] E. S. Weibel, "Anomalous Skin Effect in a Plasma," *Phys. Fluids*. vol. 10, no. 4, pp. 741-748, Apr. 1967.

[57 ] V. I. Kolobov and D. J. Economou, "The anomalous skin effect in gas discharge plasmas," *Plasma Sources Sci. Technol.* vol. 6, no. 2, pp. R1–R17, May. 1997.

[ 58 ] M. Moisan and J. Pelletier, Physics of Collisional Plasmas: introduction to high-frequency discharges (Springer Science & Business Media, New York, 2012), p.451-454.

[59] S. F. Adam and H. Packard, Microwave theory and applications (Courtesy of Agilent Technologies, Inc., 1969), p.42.

[60] T. Naito, S. Yamaura, Y. Fukuma and O. Sakai, "Radiation characteristics of input power from surface wave sustained plasma antenna," *Phys. Plasmas,* vol. 23, no. 9, pp. 093504-1-093504-9, Sept. 2016.

[61] E. N. Istomin, D. M. Karfidov, I. M. Minaev, A. A. Rukhadze, V. P. Tarakanov, K. F. Sergeichev, and A. Y. Trefilov, "Plasma asymmetric dipole antenna excited by a surface wave," *Plasma Phys. Rep*. Vol. 32, no. 5, pp. 388–400, May. 2006.

[62] W. Li, G. Wang, D. Xiang and X. Su, "Effect of the sheath thickness of thin inhomogeneous plasma layer on the propagation constant for the surface waves," *Phys. Plasmas,* vol. 24, no. 4, pp. 042103-1-042103-5, Apr. 2017.

[63] José M. Catalá-Civera, Antoni J. Canós, Pedro Plaza-González, José D. Gutiérrez, Beatriz García-Baños, and Felipe L. Peñaranda-Foix, "Dynamic Measurement of Dielectric Properties of Materials at High Temperature During Microwave Heating in a Dual Mode Cylindrical Cavity," *IEEE Trans. Microw. Theory Techn.*, vol. 63, no. 9, pp. 2905- 2914, Sept. 2015.

[64] M. Jasinski, Z. Zakrzewski and J. Mizeraczyk, "Spectroscopic measurements of electron density in atmospheric-pressure surface wave sustained discharge in argon," *Czech. J. Phys*. vol. 56, no. 2, pp. B787–B794, Oct. 2006.

[65] Y. Kabouzi, D. B. Graves, E. Castaños-Martínez, and M. Moisan, "Modeling of atmospheric-pressure plasma columns sustained by surface waves," *Phys. Rev. E*, vol. 75, no. 1, pp. 016402-1–016402-14, Jan. 2007.

[66] H. Nowakowska, M. Jasinski, and J. Mizeraczyk, "Modelling of discharge in a high-flow microwave plasma source (MPS)," *Eur. Phys. J. D*, vol. 67, no. 7, pp. 133-1–133-8, Jul. 2013.

[67] V. Georgieva, A. Berthelot, T. Silva, S. Kolev, W. Graef, N. Britun, G. X. Chen, J. van der Mullen, T. Godfroid, D. Mihailova, J. van Dijk, R. Snyders, A. Bogaerts, Marie-Paule Delplancke-Ogletree, "Understanding microwave surface-wave sustained plasmas at intermediate pressure by 2D modeling and experiments," *Plasma Process Polym*., Vol. 14, no. 4-5, pp.1600185-1-1600185-25, Nov. 2016.

[68] G. J. M. Hagelaar, K. Hassouni, and A. Gicquel, "Interaction between the electromagnetic fields and the plasma in a microwave plasma reactor," *J. Appl. Phys*. vol. 96, no. 4, pp. 1819-1828, Aug. 2004.

[69] W. C. Zhang, L. Wu, J. W. Tao and K. M. Huang, "Numerical investigation of the gas flow effects on surface wave propagation and discharge properties in a microwave plasma torch," *IEEE Trans. Plasma Sci*., vol. 47, no. 1, pp. 271 - 277, Jan. 2019.

[70] R. Miotk, M. Jasinski and J. Mizeraczyk, " Improvement of Energy Transfer in a Cavity-Type 915-MHz Microwave Plasma Source," *IEEE Trans. Microw. Theory Techn.* vol. 66, no. 2, pp. 711-716, Feb. 2018.

[71] T. Fleisch, Y. Kabouzi, M. Moisan, J. Pollak, E. Castanos-Martinez, H. Nowakowska and Z. Zakrzewski, "Designing an efficient microwave-plasma source, independent of operating conditions, at atmospheric pressure," *Plasma Sources Sci. Technol.*, vol. 16, no. 1, pp. 173–182, Feb. 2007.

[72] H. Nowakowska, M. Jasinski, P. S. Debicki and J. Mizeraczyk, "Numerical Analysis and Optimization of Power Coupling Efficiency in Waveguide-Based Microwave Plasma Source," *IEEE Trans. Plasma Sci.* vol. 39, no. 10, pp. 1935 – 1942, Oct. 2011.

[73] R. Miotk, M. Jasinski and J. Mizeraczyk, "Analysis of the tuning characteristics of microwave plasma source," *Phys. Plasmas.* vol. 23, no. 4, pp. 043507-1-043507-4, Apr. 2016.

[74] R. Miotk, M. Jasinski and J. Mizeraczyk, "Electromagnetic optimisation of a 2.45 GHz microwave plasma source operated at atmospheric pressure and designed for hydrogen production," *Plasma Sources Sci. Technol.* vol. 27, no. 3, pp. 035011-1-035011-10, Mar. 2018.

[75] W. C. Zhang, L. Wu, K. M. Huang and J. W. Tao, "Propagating modes of the plasma-sustaining travelling wave in a microwave plasma torch with metallic enclosure," Physics of plasmas. (Minor revision, returned, Ms number: POP18-AR-56861R)

[76] Z. Q. Chen, G. Q. Xia, Q. Y. Zhou, Y. L. Hu, X. L. Zheng, Z. Zheng, L. L. Hong, P. Li, Y. R. Huang and M. H. Liu, "Filamentary streamer discharges in argon at atmospheric pressure excited by surface plasmon polaritons," *Rev. Sci. Instrum*. Vol. 83, no. 8, pp. 084701-1-084701-5, Jul. 2012.

[77] H. Nowakowska, D. Czylkowski, B. Hrycak and M. Jasiński, "Characterization of a novel microwave plasma sheet source operated at atmospheric pressure," *Plasma Sources Sci. Technol*. vol. 27, no. 8, pp. 085008-1-085008-16, Aug. 2018.

[78] Y. Kabouzi, "Etude de la contraction et de la filamentation des decharges micro-ondes entretenues a la pression atmospherique: Application a la detoxication des gaz a effet de serre," Ph.D. thesis (in French), Dept. Phys., Université de Montréal, Montréal, Canada, 2003.

[79] G. J. M. Hagelaar, "*Modelling methods for low-temperature plasmas*" HDR. Thesis, Laboratoire Plasma et Conversion d'Energie (LAPLACE), Université Paul Sabatier, Toulouse, France, 2008. pp. 7-8.

[80] J. van Dijk, K. Peerenboom, M. Jimenez, D. Mihailova and J. van der Mullen, "The plasma modelling toolkit Plasimo," *J. Phys. D: Appl. Phys*.,vol. 42, no. 19, pp. 194012-1–194012-14, Oct. 2009.

[81] J. van Dijk, G. M. W. Kroesen and A. Bogaerts, "Plasma modelling and numerical simulation," *J. Phys. D: Appl. Phys*.,vol. 42, no. 19, pp. 190301-1–190301-14, Oct. 2009.

[82 ] M. Baeva, F. Hempe, H. Baierl, T. Trautvetter, R. Foestand and D. Loffhagen, "Two- and three-dimensional simulation analysis of microwave excited plasma for deposition applications: operation with argon at atmospheric pressure," *J. Phys. D: Appl. Phys.*, vol. 51, no. 38, pp. 385202-1- 385202-13, Sept. 2018.

[83] J. Muñoz, R. Rincón, C. Melero, M. S. Dimitrijevic, C. González, and M. D. Calzada, "Validation of the van der Waals broadening method for the determination of gas temperature in microwave discharges sustained in argon–neon mixtures," *J. Quant. Spectrosc. Radiat. Transfer*, vol. 206, pp. 135-141, Feb. 2018.

[84] C. J. Chen, S. Z. Li, J. L. Zhang, and D. P. Liu, "Temporally resolved diagnosis of an atmospheric-pressure pulse-modulated argon surface wave plasma by optical emission spectroscopy," *J. Phys. D: Appl. Phys.*, vol. 51, no. 2, pp. 025201-1-025201-11, Dec. 2017.

[85] S. Ashida, C. Lee and M. A. Lieberman, "Spatially averaged (global) model of time modulated high density argon plasmas," *J. Vac. Sci. Technol. A*, vol. 13, no. 5, pp. 2498–2507, May. 1995.

[86] M. Baeva, M. Andrasch, J. Ehlbeck, D. Loffhagen, and K.-D. Weltmann, "Temporally and spatially resolved characterization of microwave induced argon plasmas: Experiment and modeling," J. Appl. Phys., vol. 115, no. 14, pp. 143301-1–143301-13, Apr. 2014.

[87] D. A. Benoy, "Modelling of thermal argon plasmas," Ph.D. thesis, Eindhoven Univ. Technol., Eindhoven, The Netherlands, 1993.

[88] J. Jonkers, M. van de Sande, A. Sola, A. Gamero, A. Rodero and J. van der Mullen, "The role of molecular rare gas ions in plasmas operated at atmospheric pressure," Plasma Sources Sci. Technol., vol. 12, no. 3, pp. 464–474, Jul. 2003.

[89] G. L. Rogoff, “Ambipolar diffusion coefficients for discharges in attaching gases,” J. Phys. D: Appl. Phys., vol. 18, no. 8, pp. 1533–1545, Aug. 1985.

[90] B.M. Wunderer, “Ambipolar diffusion in a nonuniform plasma containing different positive ion components,” *IEEE Trans. Plasma Sci*., vol. 6, no. 4, pp. 406 - 416, Dec. 1978.

[91] M. Jimenez-Diaz, E. A. D. Carbone, J. Van Dijk and J. J. A. M. van der Mullen, “A two-dimensional plasimo multiphysics model for the plasma-electromagnetic interaction in surface wave discharges: the surfatron source,” J. Phys. D: Appl. Phys., vol. 45, no. 33, pp. 335204-1–335204-17, Aug. 2012.

[92] L. L. Zhong, X. H. Wang, M. Z. Rong, Y. Wu and A. B. Murphy, “Calculation of combined diffusion coefficients in SF6-Cu mixtures”, Phys. Plasmas, vol. 21, no. 10, pp. 103506-1-103506-9, Oct. 2014.

[93] K. Kutasi, V. Guerra, and P. Sa, “Theoretical insight into Ar–O2 surface-wave microwave discharges,” J. Phys. D: Appl. Phys., Vol. 43, no. 17, pp. 175201-1-175201-14, Apr. 2010.

[94] B. E. Poling, J. M. Prausnitz and J. P. O'connell, , “The properties of gases and liquids,” Fifth Edition, New York: McGraw-Hill, 2004, pp. 11.5.

[95] P. D. Neufeld, A. R. Janzen, and R. A. Aziz, “Empirical Equations to Calculate 16 of the Transport Collision Integrals Ω (l, s)* for the Lennard-Jones (12-6) Potential,” J. Chem. Phys., vol. 57, no. 3, pp. 1100-1102, Mar. 1972.

[96] G. J. M. Hagelaar, F. J. de Hoog, and G. M. W. Kroesen, “ Boundary conditions in fluid models of gas discharges,” *Phys. Rev. E*, vol. 62, no. 1, pp. 1452-1454. Jul. 2000.

[97] Y. A. Cengel, “Heat transfer: a practical approach,” Second Edition, New York: McGraw-Hill, 2002, pp. 28, pp. 884.

[98] A. Bejan and A. D. Kraus, “Heat transfer handbook” New Jersey: John Wiley & Sons, Inc, 2002, pp. 546.

[99 ] S. Z. Li, X. Zhang, C. J. Chen, J. L. Zhang, Y. X. Wang and G. Q. Xia, “Role of discharge tube in determination of operating mode in waveguide-based atmospheric-pressure microwave-induced plasma,” IEEE Trans. Plasma Sci.,vol.42, no.10, pp.2776-2777, Oct. 2014.

[100 ] M. Moisan, A. Shivarova and A. W. Trivelpiece, “Experimental investigation of the propagation of surface waves along a plasma column”, Physics of Plasmas. Vol.24, no.11, p.1331-1400, Feb. 1982.

[101 ] Moisan M, Zakrzewski Z and Pantel R, “The theory and characteristics of an efficient surface wave launcher (surfatron) producing long plasma columns”, J. Phys. D: Appl. Phys. vol. 12, no.2, pp. 219-237, Feb. 1979.

[102 ] Z. Zakrzewski, M. Moisan, V. M. M. Glaude, C. Beaudry and P. Leprince, “Attenuation of a surface wave in an unmagnetized RF plasma column”, Physics of Plasmas. vol. 19, no. 2, pp. 77-83, Feb. 1977.

[103 ] M. Moisan, M. Chaker, Z. Zakrzewski and J. Paraszczak, “The waveguide surfatron: a high power surface-wave launcher to sustain large-diameter dense plasma columns,” J. Phys. E: Sci. Instrum., vol. 20, no. 11, pp. 1356-1361, May. 1987.

[104 ] J. Martínez, E. Castaños-Martínez, C. González-Gago, R. Rincón, M. D. Calzada and J. Muñoz, “Influence of gas flow on the performance of surface-wave discharges sustained in capillary tubes,” Plasma Sources Sci. Technol., vol. 27, no. 7, pp. 077001-1 – 077001-5, Jul. 2018.

[105 ] D. Czylkowski, M. Jasinski, J. Mizeraczyk, and Z. Zakrzewski, “Argon and neon plasma columns in continuous surface wave microwave discharge at atmospheric pressure,” Czech. J. Phys., Vol. 56, pp. B684–B689, Apr. 2006.

[106 ] A. Gulec, F. Bozduman, and A. M. Hala, “Atmospheric pressure 2.45-GHz microwave helium plasma,” IEEE Trans. Plasma Sci., vol. 43, no. 3, pp. 786-790, Mar. 2015.

[107 ] J. Muñoz, J. Margot, and M. D. Calzadal, “Experimental study of a helium surface-wave discharge at atmospheric pressure,” J. Appl. Phys., vol. 107, no. 8, pp. 083304-1-083304-7, Feb. 2010.

[108] Y. Kabouzi, M. D. Calzada, M, Moisan, K. C. Tran and C. Trassy, “Radial contraction of microwave-sustained columns at atmospheric pressure,” J. Appl. Phys., vol. 91, no. 3, pp. 1008–1019, Feb. 2002.

[109] R. Garg, Analytical and Computational Methods in Electromagnetics (Artech house, Inc., Norwood, 2008), p.9–11, p. 346.

[110] M. Koshiba, K. Hayata and M. Suzuki, “Improved Finite-Element Formulation in Terms of the Magnetic Field Vector for Dielectric Waveguides,” IEEE Trans. Microwave Theory Tech., vol.33, no.3, pp. 227-233, Mar. 1985.

[111] A. V. Phelps, “The diffusion of charged particles in collisional plasmas: free and ambipolar diffusion at low and moderate pressures,” J. Res. Natl. Inst. Stan. Technol., vol. 95, no. 4, pp. 407–431, Aug. 1990.

# List of publications

***Journal papers:***

**W. C. Zhang**, J. W. Tao, K. M. Huang and L. Wu, "Numerical investigation of the surface wave formation in a microwave plasma torch," *IEEE Trans. Plasma Sci.*, vol. 45, no. 11, pp. 2929-2939, Oct. 2017.

**W. C. Zhang**, L. Wu, J. W. Tao and K. M. Huang, "Numerical investigation of the gas flow effects on surface wave propagation and discharge properties in a microwave plasma torch," *IEEE Trans. Plasma Sci*., vol. 47, no. 1, pp. 271 - 277, Jan. 2019.

**W. C. Zhang**, L. Wu, K. M. Huang and J. W. Tao, "Propagating modes of the plasma-sustaining travelling wave in a microwave plasma torch with metallic enclosure," *Physics of plasmas*. vol. 26, no. 4, pp. 042101-1-042101-8, Apr. 2019

**W. C. Zhang**, L. Wu, Z, Liu, K. M. Huang and J. W. Tao, "Experimental investigation of the Role of the glass tube in improving the power coupling efficiency of a microwave plasma torch," *Physics of plasmas*. (Out to reviewers)

***Conference papers:***

W. C. Zhang, J. W. Tao, K. M. Huang and R. Perrussel, "An alternative method to model the mode-stirrers in microwave cavities" *18th International Symposium on ElectroMagnetic Compatibility (CEM 2016)*, Rennes, France, 11-13 Jul. 2016.

# Acknowledgements

This PhD study was accomplished partly in Laboratoire Plasma et Conversion d'Energie (LAPLACE), INPT-ENSEEIHT, Toulouse University under the supervision of Prof. Dr. Junwu TAO in France, and partly in Institute of Applied ElectroMagnetics (IAEM), College of Electronics and Information Engineering, Sichuan University under the supervision of Prof. Dr. Kama HUANG in China.

Firstly, I would like to thank Sichuan University and University of Toulouse to receive my PhD study. Besides, I would like to thank China Scholarship Council for the financial support to my PhD study in Toulouse.

Secondly, I would like to address my sincere gratitude particularly to my supervisors, Prof. Junwu TAO and Prof. Kama Huang. Thank you very much for your support, help and advice in my study. Thank you so much for guiding me in the research. To be honest, self-doubt has always followed me during the entire study. Thank you for having not given me up. Thank you for encouraging me when I encountered failure and felt deeply depressed. Your erudition, patience, modesty and strict attitudes towards academic research greatly impressed me and set good examples to me. It is a great honor to be your student.

Besides, my deep appreciation also goes to the teachers and the researchers in IAEM and LAPLACE. Thank you for delivering wonderful courses to me and having helpful discussions during my study.

I also want to thank my friends and my colleagues both in China and in France: Li WU, Zhuang LIU, Jie YU, Cheng CHEN, Shaopeng WAN, Fang LEI, Xiaoyan MA, Tianyi LIU, Linlin ZHONG, Jingyi WANG, Issa Mohammad and Kuhler Lucille. Thank you for your help in my daily life and research.

Particularly, I want to thank Dr. Li WU for her kind help in doing experiments, revising the papers and discussing about the research. Without her assistance, I would encounter more problems and failures. Thank you so much for encouraging me during my study.

I want to take this opportunity to thank my family. All credit and honor belong to you. I want to thank particularly my mother Mingzhi Li. Thank you for your

unconditional love and support. I am sorry for my late PhD defense. Now, I finally graduate anyway and become capable to live on my own. Do not warry for me anymore. May you be free from pain and disease in heaven. I also want to thank my uncle: Hongxiang Li, my elder sisters: Qiongfen ZHANG, Cuifen, ZHANG, Huanfen ZHANG, Wenxi ZHANG and my brothers-in-law: Jiashun MA, Wengang YANG, Caihua GUO. Thank you so much for your love and support. It is the power source for me in my life.

Finally, I want to thank my beloved wife Jinhan LIU. Thank you for keeping accompany with me all the time and sharing all the pressure, happiness and pain with me. Thank you for your comfort when I was depressed. Thank you for your insistence in our long-distance love. Thank you for your trust when I lost the self-confidence. I am a lucky person.